FACULDADE DE ENGENHARIA DA UNIVERSIDADE DO PORTO

Improve Energy Efficiency and Sustainability of the Thermal Reconditioning System - Annealing Process

Raquel Luckow Ferreira

Master in Environmental Engineering

President of the Jury: Prof. Dr. Adrián Manuel Tavares Silva

Member of the Jury: Dr. Mariana Garcia Domingos

Supervisor: Prof. Dr. José Carlos Magalhães Pires

Company Supervisor: Dr. Paulo Jorge da Cunha Gomes

July 31, 2023

Abstract

In the quest to reduce energy consumption, the glass industry has shown an increasing interest in optimising glass heat treatment processes due to the urge to fight climate change and the volatility of natural gas prices in 2022, since most treatment processes rely on natural gas combustion. This research focuses on the optimisation of an annealing lehr of a glass manufacturer. It counts on the development of an algorithm that predicts the temperature profile of the glass container throughout the tempering process. The aim is that this algorithm behaves as a digital twin to the process and accurately models the temperature distribution of the air inside the annealing lehr and within the glass container.

The motivation is to enhance the overall performance of the lehr and improve the quality of the glass containers produced, as well as prevent the emission of CO_2 in the sense of energy saving. An energy balance was conducted, considering various factors such as the bottles' mass, the lehr's geometric properties, and the material characteristics of the specific type of glass and lehr. This analysis adopts a conservative way since radiation heat transfer was not considered in the calculations, and it plays a significant role in transferring heat within the containers.

The results show that the models strongly depend on the accuracy in estimating the heat transfer coefficient h. The heat loss estimation is circa 60 kW, whilst the average energy power input of the lehr is 140 kW. The analyzed annealing lehr is operating at an almost optimal performance level. However, the digital twin and its user interface developed in this research play a crucial role in decision-making processes by providing real-time predictions of temperature variations in response to changes in setpoint temperatures. This is particularly relevant when changing the type of glass container, its design, or geometric parameters, such as thickness.

The digital twin must be adapted to be connected to the annealing lehr control panel and improved to provide a more accurate analysis of transfer phenomena. With that, the digital twin enables long-term optimisation and enhances the heat treatment processes of the glass container manufacturing industry.

Keywords: Annealing, annealing lehr, digital twin, glass, glass container, heat treatment.

Resumo

Com o objetivo de reduzir o consumo de energia, a indústria vidreira tem demonstrado um interesse crescente na otimização dos processos de tratamento térmico do vidro, devido à necessidade de combater as alterações climáticas e à volatilidade dos preços do gás natural em 2022, uma vez que a maioria dos processos de tratamento depende da combustão de gás natural. Esta investigação centra-se na otimização de um forno de recozimento de um fabricante de vidro. Conta com o desenvolvimento de um algoritmo que prevê o perfil de temperatura da embalagem de vidro ao longo do processo de recozimento. O objetivo é que este algoritmo se comporte como um *digital twin* do processo e modele com precisão a distribuição da temperatura do ar no interior da arca de recozimento e na parede interior da garrafa.

A motivação para este estudo é aumentar o desempenho da arca de recozimento e melhorar a qualidade das embalagens de vidro produzidas, bem como diminuir a emissão de CO_2 no sentido da poupança de energia. Foi realizado um balanço energético, considerando vários fatores como: a massa das garrafas, as propriedades geométricas da arca e as características do material do tipo específico de vidro e lehr. Esta análise adota uma forma conservadora, uma vez que a transferência de calor por radiação não foi considerada nos cálculos, e esta desempenha um papel significativo na transferência de calor nas garrafas.

Os resultados mostram que os modelos dependem fortemente da exatidão da estimativa do coeficiente de transferência de calor h. A estimativa da perda de calor é de cerca de 60 kW, enquanto a entrada média de potência energética do forno é de 140 kW. A arca de recozimento analisada está a funcionar a um nível de desempenho quase ótimo. No entanto, o *digital twin* e a sua interface de utilizador desenvolvidos nesta investigação desempenham um papel crucial nos processos de tomada de decisão, fornecendo previsões em tempo real das variações de temperatura em resposta a alterações nas temperaturas de referência. Isto é particularmente relevante quando se altera o tipo de garrafa, o seu design ou parâmetros geométricos, como a espessura.

O *digital twin* deve ser adaptado para ser ligado ao painel de controlo da arca de recozimento e aperfeiçoado para fornecer uma melhor análise dos fenómenos de transferência. Deste modo, o *digital twin* permite uma otimização a longo prazo e melhora dos processos de tratamento térmico da fábrica de vidro.

Palavras-chave:: Arca de recozimento, embalagem de vidro, gémeo digital, perfil de temperatura, recozimento do vidro, tratamento térmico

Acknowledgments

I conclude this stage of my life with this work, which challenged me as a student and future professional. The development of this work was only possible with the collaboration of special people to whom I offer my sincere gratitude.

To my mother, who taught me what true and unconditional love is, I thank her for giving me the freedom to take wings, but also for always having her arms wide open for when I flew higher than I could. Thank you for allowing me to be who I am.

I thank my aunt Karin for the precious support in these 5 years away from home, for believing in my education, and for being a source of inspiration on returning to medical school after being a mother of three.

I thank Prof. Dr. José Carlos Pires for his exceptional dedication in following my work and for supporting me whenever I needed it. We were fortunate students to have him as a teacher, especially for the commitment with which he taught and oriented us.

I thank Dr. Paulo Gomes for trusting in my potential, collaborating with the enrichment of my work and for his ability to open paths and create necessary connections for the evolution of his team. I hope to continue our work together.

To the BA Glass team, I appreciate the companionship and help provided so that I could fruitfully develop this work. A special acknowledgement to Gustavo, who was my right-hand man on this project and advised me in the algorithm development.

I'm thankful to my beloved friends, who were my beacon in this academic journey, especially those who actively assisted in my study. To Pedro, for sharing life with me, encouraging me to be my best version, and bringing me clarity in foggy moments. I'm happy we did this together. To Carolina, for being my safe harbour in this foreign continent and an endless source of good laughs. At last, I thank Griep and Agostini for being my inspiration to study abroad.

Finally, I thank all those who materially contributed to my stay in this country. Without them, I would not have finished my graduation.

Raquel Luckow Ferreira

Funding
Dr. José Carlos Magalhães Pires, supervisor of this dissertation, is an integrated member of LEPABE – Laboratory for Process Engineering, Environment, Biotechnology and Energy, financially supported by LA/P/0045/2020 (ALiCE), UIDB/00511/2020 and UIDP/00511/2020 (LEPABE), funded by national funds through FCT/MCTES (PIDDAC).

“O Brasileiro é o Português -
dilatado pelo calor.”

Eça de Queiroz

Contents

List of Figures

List of Tables

Nomenclature

Acronyms

CFD	Computational Fluid Dynamics
MAPE	Mean Absolute Percentage Error
UI	User Interface

Constants

σ	Stefan-Boltzmann constant, $5.67 \cdot 10^8$ $W \cdot m^{-2} \cdot K^{-4}$

Math Operators

$\cdot$	Dot product operator

Greek Symbols

α	Thermal diffusivity $[m^2 \cdot s^{-1}]$
α_r	Reflectivity
ε	Emissivity
ε_b	Thickness [m]
ζ_1	One-term approximate solution coefficient
η_1	Glass viscosity [Poise]
λ	Wavelength [m]
μ	Dynamic viscosity $[kg \cdot m^{-1} \cdot s^{-1}]$
μ_b	Dynamic viscosity at bulk temperature $[[kg \cdot m^{-1} \cdot s^{-1}]$
μ_w	Dynamic viscosity at wall temperature $[kg \cdot m^{-1} \cdot s^{-1}]$
π	Pi
ρ	Density $[kg \cdot m^{-3}]$
ρ_r	Absorptivity
τ_r	Transmissivity
ω	Radiation heat transfer coefficient $[W \cdot m^{-2} \cdot K^{-4}]$
Ω	Thermal conductivity resistance $[K \cdot W^{-1}]$
Ω_c	Thermal resistance for convection cold side $[K \cdot W^{-1}]$
Ω_h	Thermal resistance for convection hot side $[K \cdot W^{-1}]$
ϕ	General coefficient of upper annealing point
ϕ_i	Coefficient of component i

Roman Symbols

A_b	Bottle's surface area [m^2]
A_w	Lehr's wall surface area [m^2]
Bi	Biot number
C_1	One-term approximate solution coefficient
c_p	Specific heat capacity [$J \cdot kg^{-1} \cdot K^{-1}$]
D_b	Bottle's outer diameter [m]
D_{bn}	Bottleneck's outer diameter [m]
e	Nepper number
$E(T)$	Emissive power [$W \cdot m^{-2}$]
E	Thermal radiation energy [$W \cdot m^{-2}$]
$\dot{E}_{annealing}$	Power consumption in the annealing process [kW]
Fo	Fourier number
h	Convective heat transfer coefficient [$W \cdot m^{-2} \cdot K^{-1}$]
h_b	Bigger cylinder's height [m]
h_{bn}	Smaller cylinder's height (bottleneck) [m]
h_c	Truncated cone's height [m]
h_{out}	Convective heat transfer coefficient of outside air [$W \cdot m^{-2} \cdot K^{-1}$]
h_{short}	Convective heat transfer coefficient by Deissler correlation's [$W \cdot m^{-2} \cdot K^{-1}$]
H_d	Hydraulic diameter [m]
k	Thermal conductivity [$W \cdot m^{-1} \cdot K^{-1}$]
k_w	Lehr's wall thermal conductivity [$W \cdot m^{-1} \cdot K^{-1}$]
L_c	Characteristic length [m]
n	Number of cycles
n_{max}	Maximum number of cycles considering Fo restriction
N_b	Number of bottles at the stacker bar
p_i	Percentage of chemical compost i
$\dot{Q}$	Heat transferred per unit of time [W]
$\dot{Q}_w$	Heat loss flux through lehr's wall [W]
R_b	Bottle's outer radius [m]
R_{bn}	Bottleneck's outer radius [m]
r_b	Bottle's inner radius [m]
r_{bn}	Bottleneck's inner radius [m]
t	Time [s]
$t_{annealing}$	Annealing time [min]
$T_{annealing}$	Upper annealing point [°C]
V_b	Bottle's volume [m^3]
v	Velocity [$m \cdot s^{-1}$]
V_{gas}	Natural gas volume input in the annealing process [Nm^3]

Chapter 1

Introduction

This study is a thesis for a Master's degree in Environmental Engineering at the Faculty of Engineering, University of Porto. The work had five months long, starting in February 2023 and ending in June 2023, and was developed for the Data Science and Analytics unity of BA Glass headquarters, located in Vila Nova de Gaia, Portugal.

1.1 Glass Industry

The production of glass is a complex process that has been a vital component of modern society since 4000 years B.C. Although glass has not given its name to any historical period, such as the Stone Age, the Bronze Age, and the Bronze Age, it has been present in all of them and has accompanied humans combining utility and beauty until now (Navarro, 2003).

Regarding the usage of glass as a container, it still maintains a vast potential for innovation. The chemical properties of glass yield benefits in terms of contamination of the packaged material and sustainability since it is an inert material 100% recyclable. In other words, the absence of chemical reactions makes glass the perfect container for the packaging of food, beverage and medicines since it preserves the chemical and organoleptic characteristics of its contents (Vellini and Savioli, 2009). Furthermore, the malleability in production and design, together with the above reasons, enables glass to fight a fierce battle with its competitors, such as plastic and tetra-pack containers.

There are several different types of glasses and considering the type produced, it is possible to characterize the glass industry into five sectors (National Renewable Energy Lab., 2002):

- Flat glass: windows, automobile windshields, and picture glass;
- Container glass: bottles, jars, and packaging;
- Pressed/Blown glass: light bulbs, scientific and medical glassware, flat panel display glass;
- Glass fibre: fibreglass, optical fibres;

- Products from purchased glass: items assembled from intermediate glass products, such as aquariums, mirrors, and table tops.

The one process in common to all glass manufacturers is the melting process of glass. This takes place in a furnace at around 1500 °C and can be done in batches, semi-continuous, or continuous production. As regards glass container production, the entire process is done in continuous mode and the process can be divided into two stages: hot-end and cold-end. The hot-end is the phase when the container is formed, characterized by batch preparation, melting, conditioning, forming, and annealing. The cold-end is everything that happens after the container is cooled down and involves procedures such as quality control, packaging and shipment. Figure 1.1 represents the chain of processes in a glass container manufacturing plant.

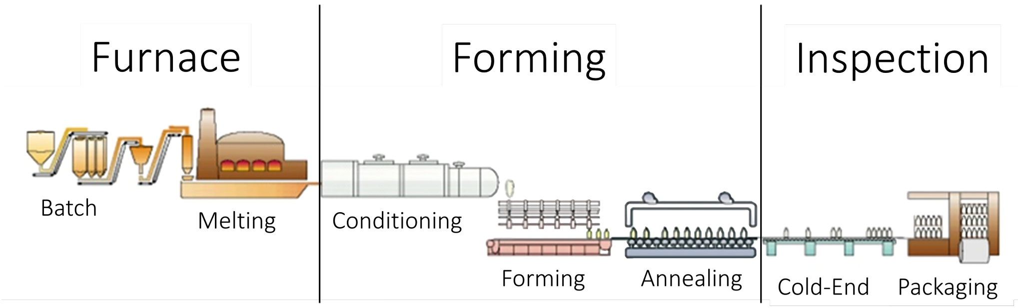

Figure 1.1: Glass container production process, adapted from BA Glass (2022).

In the beverage sector, containers are usually made with soda-lime-silica glass, with the addition of other oxides to adjust chemical resistance, brilliance, and colour. The structure of this type of glass is composed of tetrahedra mutually linked in a regular hexahedral lattice (Vellini and Savioli, 2009). Table 1.1 presents the percentage range of components of soda-lime-silica glass in its most common forms: container, float, and domestic glass.

Table 1.1: Soda-lime-silica glass composition range, adapted from Bingham (2010)

Weight (wt%)	Container	Float	Domestic
SiO_2	70–73	70–74	70–74
Al_2O_3	1–2	0–1	1–2
Na_2O	12–15	12–14	12–14
K_2O	0–1	0–0.5	0–2.5
MgO	0.5–2	2–4	1–2
CaO	10–12	7–10	7–9
Fe_2O_3	0–1	0–1	0–0.05
SO_3	0–0.5	0–0.5	0–0.5
Cr_2O_3	0–0.3	0–0.3	0

Regarding its composition, glass is in a framing limbo of the physical states of matter. The term glass is usually referred to high-viscosity substances that do not have enough mobility during solidification and yield an intermediate meta-stable stage with the formation of an amorphous solid. In other words, from the point of view of the non-deformability of glass at room temperature, it could be considered as a solid. However, considering its structural disorder, glass shows more similarity to liquids. Thus, it is said that glass belongs to a vitreous state, a state that will impart peculiar characteristics to matter (Navarro, 2003).

In the modern glass industry, the production of glass has high-quality standards and hence requires precision and attention to detail in order to meet these standards. One of the most vital steps in the manufacture of glass is the annealing process. It is the process responsible to relieve the internal stress of the glass body and ensure the reliability and durability of the product.

After the glass has acquired its form, it is in an unstable condition: the surface layers begin to harden and solidify, while the inner layers remain in a hot and malleable state for longer. Thus, mechanical stresses are produced within it, for the uneven cooling along the glass body. Hence the glass should be heated again until a sufficiently high temperature and then slowly cooled (Navarro, 2003). Without the annealing, the glass is not able to withstand the stresses of shipping, handling, and use and can break or shatter at any moment. This can lead to economic loss and, above all, safety implications.

In the case of the glass container manufacture, between the moment when the liquid glass is cut into gobs and it is found at the entrance of the annealing process, there is a temperature drop of almost 800 °C in a fleeting time of about 10 to 30 seconds. This fast cooling is essential to obtain a well-shaped container, however, it is responsible for generating internal stress that weakens the container. Therefore, the goal of the annealing is to pass the container from a plastic state to a rigid one slowly enough to relax uniformly its structure and acquires the same volume at all points (Navarro, 2003).

Since glass viscosity is a function of temperature, there are four viscosity points that are important in the glass-forming process as they determine the suitability of the glass for certain processes. These points indicate the temperature of these processes and are shown in Figure 1.2. They are:

- Working point: temperature that determines the suitability of the glass for the forming process;
- Softening point: temperature of a natural deformation of glass at a rate of 1 mm/min;
- Annealing point: temperature that the glass should reach for a certain time to eliminate its stress;
- Strain point: temperature at which the relief of internal stress is virtually impossible.

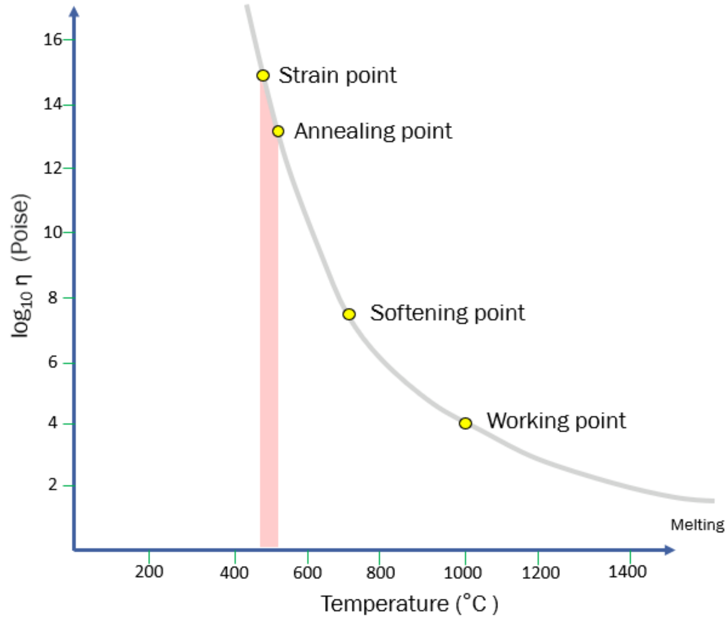

Figure 1.2: Viscosity of glass, adapted from Bingham (2010).

The annealing point, the main focus of this work, is also known as the upper annealing point, whereas the strain point is known as the lower annealing point. The annealing process happens in the temperature range between the upper and the lower annealing point. Depending on the glass composition and geometry, a certain time in the upper annealing point is required. For a glass container, the duration of this stage is usually between the range of 5 to 15 minutes (BA Glass, 2022). Nevertheless, it is possible to anneal the glass in the strain point, but it would take more than 16 hours, which would compromise the production efficiency (Littleton and Roberts, 1920).

Therefore, the annealing of glass is a process that happens in a relatively narrow range of temperatures, which brings the challenge of discovering the optimal temperature profile for each glass container, for different articles with different shapes and compositions will have different thermal behaviour and a different annealing curve (Navarro, 2003). For example, a beer bottle usually needs only 20 minutes inside the annealing chamber, whereas a champagne bottle will need around 60 minutes.

1.1.1 Company Background

Originally under the name of Barbosa & Almeida, BA Glass is a Portuguese glass container manufacturing company. Its headquarters are in Avintes, Portugal, and ensures an annual production of more than 11 billion containers distributed to over 80 countries worldwide. However, the company did not start its trajectory as a manufacturer. In 1912, when it was founded, it was dedicated only to the commercialization of glass bottles. It was in 1930 that the company positioned itself as a glass manufacturer (Alves, 2003).

The company started its internalization in the 90's, which strongly contributed to maintaining its domain in the Portuguese glass industry. Nowadays, the company owns 12 factories distributed in the following countries by order of plant acquisition: Spain, Poland, Germany, Greece, Bulgaria, and Romania. The international footprint allowed the company to produce more than 20 million units a day. Furthermore, the company operates with almost 4000 employees and has a turnover of more than 900 million euros (BA Glass, 2023).

1.2 Motivation

Due to the high temperature required for melting the raw materials, the glass industry operates as an energy-intensive industry (Schmitz et al., 2011). Wherefore, glass manufacturers appear as major consumers of energy and, consequently, are responsible for significant amounts of CO_2 emissions. Much effort is put into optimising the energy consumption of furnaces among glass manufacturers. However, sometimes it is not possible to reduce the input of natural gas because there are temperature limitations for the glass to remain molten. In this way, the annealing process, which also requires natural gas, presents itself as another contributor to overall emissions and energy consumption that needs optimising. The strategy for optimising the annealing can follow three paths: finding the temperature profile with the minimum values for the set points necessary for a successful process, carrying out the process below the strain point, but for a longer time, or reducing heat loss from the lehr. The second option would drastically reduce the natural gas input but would slow the production and create a bottleneck in the processes chain. The third option would not change the duration of the annealing time but would call for new equipment and, therefore, a costly investment. Thus, the best option for this scenario will be the heat transfer analysis from the lehr to the container's body.

In this sense, it becomes important to reduce energy consumption not only for monetary reasons but also from the perspective of climate change. By implementing energy-efficient machinery in the processes, the factory can reduce its carbon footprint and help to maintain its good sustainability performance among competitors.

1.3 Objectives

This study aims to analyse the energy consumption of an annealing lehr and explore strategies for optimising the process, by studying heat transfer phenomena in glass bottles. The main goal is to develop a digital twin model that can simulate and predict the temperature profile of the bottles. This prediction is crucial in determining the minimum setpoint temperature required for successfully annealing a specific bottle. By finding this optimal temperature, it is possible to ensure the bottles undergo the necessary duration of heat treatment. Furthermore, the objective is to use the digital twin as a tool to simulate different scenarios and test the impact of different operational parameters on the temperature profile. In the end, this analysis should contribute to providing valuable insights for enhancing the process efficiency and sustainability of the company.

1.4 Thesis Outline

This document is composed of 5 chapters. Chapter 1 describes the main objectives and motivation of the project and the history of the glass industry and company background. Chapter 2 provides a literature review of the heat transfer phenomena, their relevance in tempering furnaces, and the importance of annealing in the glass manufacturing process. Chapter 3 contains the methodological description of the digital twin as well as the parameters, tools, and materials used in this study. Chapter 4 explores the results and discusses them. Finally, Chapter 5 presents the conclusion of this analysis and proposes future improvements to be developed.

Chapter 2

State-of-the-art

2.1 Annealing of Glass

2.1.1 Annealing Process

Glass cooling can be controlled when it is in a plastic-viscous state. However, beyond its softening point, when glass becomes soft enough to be deformed under its own weight, rapid cooling can cause nonuniform heat dissipation throughout the body due to the glass's low calorific conductivity. This creates a temperature gradient within the glass, with the outer layers cooling faster and reaching rigidity before the inner layers, which will stay hot and in a plastic state for longer (Navarro, 2003).

The inner layers start to contract whilst the thermal gradient disappears. Nevertheless, they are already constrained by the rigid superficial layers that hinder them. That is, they are hampered from reaching the dimensional equilibrium required by their coefficient of expansion when they cool down. Consequently, when the temperature gradient equalizes, residual stress remains inside the bottle. The surface experiences compression forces, while the inner wall faces tensile stresses, in opposition to the initial thermal gradient where the deep layers were subjected to compression and the outer layers to tension (Navarro, 2003).

This stress caused above the strain point is characterized as permanent stress, whilst the stress acquired below the strain point is called temporary stress. Therefore, it is necessary to subject the glass to a heat treatment process in order to eliminate as much as possible or as wanted the permanent stress within the bottle. An ideal heating process would be one in which the heat transfer rate to glass is the same via the top and bottom of a glass container in order to generate a symmetrical temperature profile thickness-wise.

These processes are also important in shaping the mechanical and thermal properties of glass products, and different types of heat treatment processes are employed to achieve distinct outcomes. For example, the annealing process involves the rapid heating of the product until a specific temperature, followed by a slow and controlled cooling, whereas the tempering process involves rapid cooling of the glass surface while maintaining the core at a higher temperature.

This causes tempered glasses to endure many times more load and sustain steeper temperature gradients than annealed glass.

Considering the manufacturing of glass containers, the heat treatment process to which the containers are subjected is annealing. Two variables govern the process: time and temperature. The slower the elimination of the thermal gradient, the more effectively the stress is eradicated. Hence, each glass piece requires a specific temperature curve for the annealing chamber based on its chemical composition, geometry (shape and critical thickness), and desired outcome.

The process can be divided into four stages: reheating, homogenization, slow cooling, and fast cooling, according to the Corning Method (BA Glass, 2022). The annealing phases of glass containers are described in Figure 2.1.

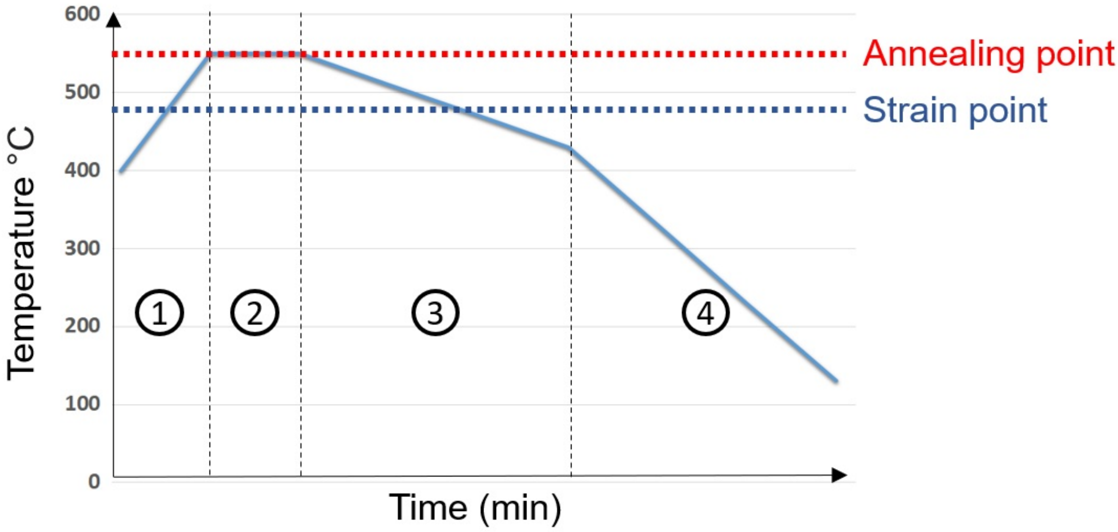

Figure 2.1: Stages of an annealing process.

1. Reheating: the container is reheated until the annealing point temperature that ranges between 540 and 565 °C.

2. Homogenization: the container then remains at the annealing point during the relaxation time.

3. Slow cooling: considering the cooling rate constraint, the container suffers a controlled cooling until it reaches the strain point, in which the temperature ranges between 485 and 500 °C.

4. Fast cooling: since no permanent stress can be generated below the strain point, the glass can now be cooled without speed limitation. The container cools down until the annealing lehr outlet is.

The annealing temperature is the constant and uniform temperature of a particular glass type at which stresses are allowed to relax. The range of temperature where the process happens is narrow, as shown in Figure 1.2. If the temperature is too high, the glass can start deforming or changing its character. If the temperature is too low, the stress relaxation will be too slow. The initial cooling must be slow and accurately controlled until the strain point. Therefore, the main goal is to have a process as slow as necessary but also as fast as possible in order to save energy.

2.1.2 Annealing Lehr

The annealing process happens inside a long chamber called lehr. It is a type of tempering furnace in the glass industry processes. The heating is based on thermal radiation exchange between resistors and glass and on forced convection from air to glass. There are two different types of technologies to implement convection in tempering furnaces: external air convection and circulated air convection (Rantala, 2019).

- External air convection furnace: blows pressurizes fresh air coming from the outside towards the glass through holes in convection pipes. In this case, the same amount of air blown into the furnace is also blown out of the furnace.
- Circulating air convection furnace: operates with fans inside it that draw air and guide it to blowing holes that will blow it toward the glass. There is no external air feed into the furnace, and the convection rate is controlled by changing the rotation speed of the fan impeller, which will change the blowing pressure.

Air temperature control is more complex in circulating air convection tempering furnaces than in external air. The air temperature drops strongly at the beginning of the heating and is much more stable when air is forced to flow through the resistors. The heat is transferred first to the air and then from the air to the glass.

The lehr contains a temperature-controlled conveyor belt that slowly moves the glass through different temperature zones. The cooling rate is carefully controlled to prevent thermal shock and ensure uniform cooling throughout the container's walls (BA Glass, 2022). The chamber is controlled by a programmable logic controller and the human-machine interface is ensured by a touch panel. In order to be able to control the interface, the annealing cabinet is divided into a certain number of zones, in which, generally, 60 % correspond to heating modules and 40 % to cooling modules. Figure 2.2 shows the cross-sectional lateral view of a lehr and its components.

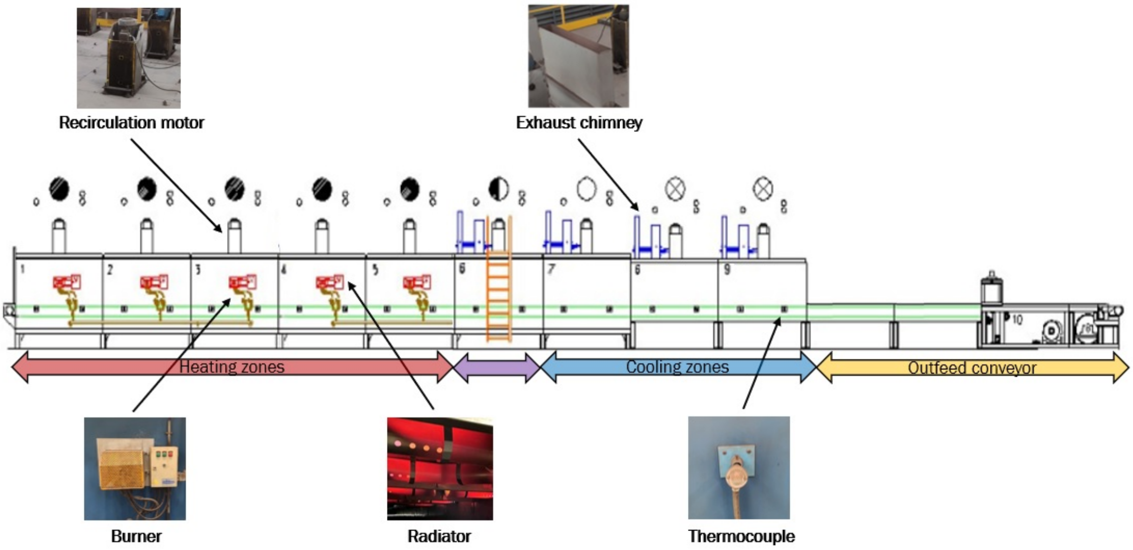

Figure 2.2: Cross-sectional lateral view of an annealing lehr and its components.

Each zone with forced convection has the following elements:

- External body;
- Internal body forming the chamber tunnel and the air circulation pipeline;
- Recirculation impellers;
- Burners;
- Resistor;
- Isolation.

The burners are responsible for providing the required heat for the annealing of glass containers and can operate with natural gas or propane. The gas is burned inside heat exchanger tubes built into the side walls, which allows maintenance without interrupting the regular operation of the equipment. Normally, the first one or two zones are equipped with two burners, one on each side, and the rest of them have only one burner per zone. They can be automatically controlled by comparing a sensor signal with the set point temperature. Good combustion is obtained by regulating the gas pressure and the Venturi air inlet regarding the air-gas mixture.

The resistors radiate heat directly towards glass containers, whereas the radiation heat transfer path to glass on the bottom side is the one resistors radiate to the conveyor belt and it radiates to the glass. The hot surfaces present inside the lehr, such as resistors, conveyor belt, and walls, radiate heat to glass, and the rate of heat transfer does not represent much variation considering the materials but their relative surface area.

Forced convection inside the chamber is carried out using centrifugal fans with impellers made of refractory stainless steel. Then, it aims to standardize the temperature in each zone of the lehr and accelerate thermal exchanges with the bottles. There are recirculating ducts alongside the lehr's walls where air flows from the fans to the conducts from bottom to top. These fans are a monobloc type, built in a way that allows a quick replacement, and the stopping of any recirculator fan immediately stops the burners in that area and activates the light alarms.

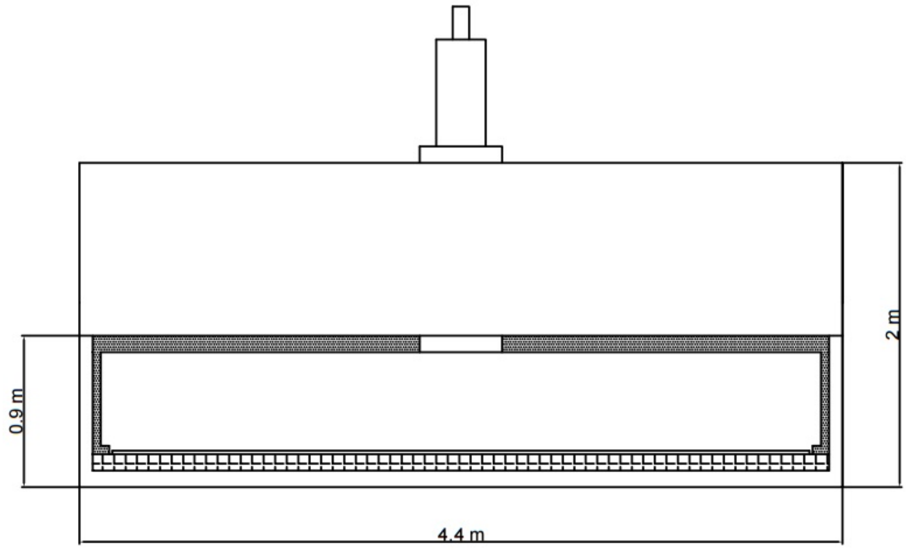

Figure 2.3: Drawing of the cross-sectional view of an annealing lehr.

Figure 2.3 is an example of a cross-sectional view of the inside of a lehr, in which the painted area represents the air recirculation ducts and the conveyor belt. The outlet of the ducts is in the side walls at the same height as the bottom of the glass containers. The impeller is represented at the top of the lehr.

2.1.3 Stress Measurement

Stress measurement is crucial to ensuring the production of high-quality glass products after the annealing process. Although manufacturers desire perfect annealing, it is not always required. Different glass applications tolerate certain levels of residual stress without affecting their functionality and safety. For instance, tempered glass retains stress to enhance its strength and glass containers can tolerate stress if well-distributed along its area.

The way to measure the efficiency of the annealing process is to evaluate the level of internal stress of the glass. The procedure to do so is to put container samples under a polariscope. This equipment produces a polarized light that allows seeing the internal stress intensity in the container. If a glass container is exposed to a polarized light beam, interference becomes coloured, and its stresses can be observed (BA Glass, 2022).

One of the characteristics of the vitreous state is isotropy, in which physically homogeneous glasses behave like an empty medium and light rays can propagate in them with the same velocity in all directions. Therefore, when exposed to polarized light, they do not exert any action unless they have tensions because a glass subjected to the action of mechanical forces loses its isotropic character (Navarro, 2003).

The polariscope has a set of strain disks that can be overlapped, in which the first polarizing filter is characterized as the ”polarizer” and the second as the ”analyser”. The more discs overlapped to get a similar image of the container bottom, the higher internal stresses are present. Figure 2.4 illustrates an example of a polariscope with its filters, and Figure 2.5 displays a set of the strain disks used in a polariscope. The more discs overlapped to get a similar image of the container bottom, the higher internal stresses are present.

Figure 2.4: Polariscope with polarizer and analyser filters, adapted from BA Glass (2023).

Figure 2.5: Set of strain disks of a polariscope, adapted from BA Glass (2023).

Considering the level of rigour, the annealing is particularly critical for optical glass or glass manufactured for thermometers, where the security standards are higher. For flat and hollow glass, the relaxation required is less rigorous, and certain residual stress is tolerable, provided they do not exceed $0.2 \cdot 10^7\ \mathrm{N \cdot m^{-1}}$ and $0.4 \cdot 10^7\ \mathrm{N \cdot m^{-1}}$, respectively.

To ensure compliance with stress levels, standard test methods must be employed. Manufacturers must collect sample bottles at regular intervals and examine them using the polariscope.

According to the Standard Test Methods for Polariscopic Examination of Glass Containers, three sample bottles must be collected every 4 hours to be examined, one from the left, one from the center, and the other from the right side of the lehr. Figure 2.6 presents a flowchart of the sample collection according to *C148 - Standard Test Methods for Polariscopic Examination of Glass Containers* (2022).

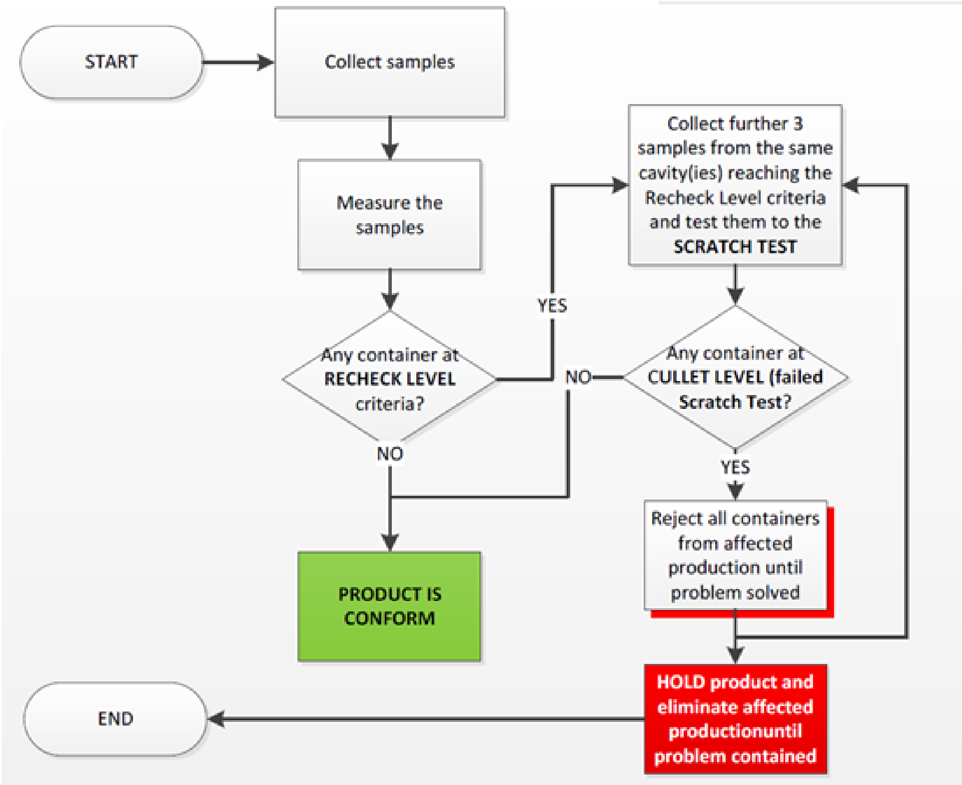

Figure 2.6: Flowchart of sample testing in glass containers.

The method is to view the bottom of the container (critical thickness) through the neck and compare the maximum broad colour pattern in the bottom with the maximum colour generated by 1, 2, 3, 4, or 5 strain standard disks (*C148 - Standard Test Methods for Polariscopic Examination of Glass Containers*, 2022). If the samples fail the acceptable stress level, another 3 sample bottles with the same cavity must be collected. If they fail again, then all containers from the affected production must be rejected.

In Table 2.1, the limits of the polariscope test are presented, in which the target level, minimum acceptable level, and recheck level are the number of used disks in the test.

Table 2.1: Polariscope test limits

Container's thickness (mm)	Target level	Minimum acceptable level	Recheck level
$1.7 \leq \varepsilon_b \leq 2.0$	1	-	≤ 2
$2.0 \leq \varepsilon_b \leq 3.0$	1	2	≤ 3
$3.0 \leq \varepsilon_b \leq 5.0$	2	3	≤ 4
$\varepsilon_b \geq 5.0$	2 - 3	4	5

Hence it is possible to conclude that a perfect annealing process is not always necessary and good quality standards levels could be reached since achieving the minimum acceptable level will not cause the breakage of the container. It is possible to produce quality glass containers if the stress tolerance is considered and the annealing process is optimized accordingly. The goal is to balance the necessity of optimal stress relief and the achievement of the specific requirements of stress levels of different glass applications.

2.2 Literature Review

The glass manufacturing industry is growing interested in optimising heat treatment processes to reduce energy consumption. Table 2.2 presents a summary of relevant studies on the topic. The reviewed articles presented focus predominantly on the broad theme of thermal process in the industry, with a specific concentration on the tempering process of glass. The studies focused on annealing techniques, temperature control methods, and stress relief optimisation. In general, their objectives revolve around enhancing the understanding of thermal processes and optimising various parameters to improve product quality and process efficiency, minimize defects and find the optimal tempering furnace design.

Table 2.2: Previous studies about heat treatment processes

Title & Author	Methodology	Findings	Limitations
Numerical Analysis of the Radiant Heating Effectiveness of a Continuous Glass Annealing Furnace, Altun and Başol (2022)	• Creation of a detailed 3D model of the annealing lehr. • Computational fluid dynamics simulations.	• Impact assessment in the process of lehr design, material properties, and operating conditions. • Optimising the process with changes in the arrangement of heating elements.	• Simplifications and assumptions to facilitate numerical simulations. • Generalization of the results to other tempering furnaces is not possible.

Continued on next page

Table 2.2 – continued from previous page

Title & Author	Methodology	Findings	Limitations
Computation of Foam Glass Thermal Field in the Annealing Process, Grushko (2018)	• Creation of a 3D model of a foam glass sample. • Finite element analysis.	• Understanding of stress relief mechanisms that occur during annealing in foam glass and how to mitigate it. • Identification of the optimal annealing parameters to achieve the desired glass properties.	• Lack of experimental validation of the numerical results. • Results are specific to annealing conditions of foam glass.
Thermal Radiation and Forced Convection in Flat Glass Tempering Furnaces, Rantala (2019)	• Experimental set up of flat glass tempering furnace with sensors to measure temperature profiles. • Temperature data collection from various points on the glass surface • Computational fluid dynamics simulations.	• Thermal radiation and forced convection play crucial roles in determining the temperature distribution of glass during tempering. • Manufacturers can minimize defects and increase production efficiency by adjusting parameters based on heat transfer mechanisms. • Insights into the optimal design and configuration of flat glass tempering furnaces.	• Study is limited to the particular tempering furnace used in experiments. • Study did not consider the effect of conduction or quenching rate. • Variation of glass thickness and composition or transient operational conditions were not considered.

Continued on next page

Table 2.2 – continued from previous page

Title & Author	Methodology	Findings	Limitations
Heat Transfer and Temperature Control in Annealing Lehr for Float Glass, Chui (1977)	• Collection of experimental data from sensors and thermocouples to validate simulations. • Finite element analysis.	• Temperature profile across the glass surface during the process. • Proposal of different temperature control strategies.	• Study did not consider variations of the glass composition. • Generalization of the results to other tempering furnaces is not possible.
Adaptative Temperature Control for Simulated Annealing: A Comparative Study, Azizi and Zolfaghari (2004)	• Experimental evaluation to compare the performance of different simulated annealing methods. • The performance of the algorithms is compared in terms of convergence speed and solution quality.	• Adaptative temperature control techniques lead to improved convergence rates compared to traditional fixed-temperature simulated annealing. • The algorithm finds better solutions in a shorter time when adjusting the temperature parameter dynamically during the optimization process. • The algorithm can explore the search space broadly in the early stages and focus on exploiting promising regions as it converges.	• Effectiveness of adaptive control depend on the specific case characteristics. • Adaptive temperature control introduces additional computational overhead compared to fixed temperature control. • The choice of benchmark problems may be influential in the study's conclusion

Continued on next page

Table 2.2 – continued from previous page

Title & Author	Methodology	Findings	Limitations
Modelling of Internal Stresses in Sheet Glass during the Cooling, Benbahouche et al. (2011)	• Characterization of thermal expansion coefficients, elastic properties, and viscosity. • Computational fluid dynamics simulations with different cooling scenarios.	• Distribution and magnitude of internal stresses within the sheet glass during cooling. • Identification of optimal cooling rate to minimize stress-induced defects.	• Generalization of the model to other glass types requires further validation. • Study did not consider non-uniform cooling rates or transient conditions.
Application of simulated annealing in a rectangular fin with variable heat transfer coefficient, Das and Ooi (2013)	• Creating an algorithm for simulated annealing in metallurgy. • Performing multiple iterations and updating the design parameters to reach the optimal solution.	• Efficiently optimising the design of a rectangular fin. • Achieving the highest heat dissipation with consideration of variable heat transfer coefficient.	• Assumptions made in the simulation. • Generalization of the model to annealing of glass requires further validation.

Continued on next page

Table 2.2 – continued from previous page

Title & Author	Methodology	Findings	Limitations
IR-Annealing Technology for Glass Products, Tyutyunnik and Guloyan (2000)	• Establishment of a IR-annealing setup and experiments with different annealing methods. • Computational fluid dynamics simulations.	• Results in the effectiveness of IR-annealing technology in comparison to traditional annealing methods. • Enhanced mechanical strength and better optical quality of products annealed with IR radiation.	• Results are specific to the particular IR-annealing system. • Lack of consideration of potential challenges in scaling up the IR-annealing technology to industrial production.
Optimization of a glass annealing process: a statistical and materials science approach to a glass container manufacturing case application Franco et al. (2018)	• Statistical and materials science to optimize the process. • Data collection to identify the most influential factors in the quality. • Mechanical testing.	• Identification of key factors that significantly affect the quality and energy efficiency of the process.	• Variability in operating conditions impacts the applicability of the proposed optimisations.

The majority of the studies discussed have employed Computational Fluid Dynamics (CFD) simulations and experimental validations to comprehend temperature distribution and stress relief mechanisms during annealing. These simulations assess the impact of design changes in tempering furnaces, material properties, and operating conditions. The limitations of these studies restrict the generalization of results to other furnaces. Furthermore, the studies that have done experiments to validate the numerical results show more reliable findings.

While the application of numerical simulations is a common method among these studies, the specifics of the research, the particularities of the design and the material properties distinguish from one another. The research of Tyutyunnik and Guloyan (2000) stands out as it experiments with a particular technology and shows comparative effectiveness. The study of Das and Ooi (2013) shares commonalities with the work of Azizi and Zolfaghari (2004) by applying simulated annealing, but they diverge when the first study concentrates on optimising the design of a rectangular fin with variable heat transfer coefficient.

The work of Rantala (2019) - which is a continuation of the previous work done in *Heat Transfer Phenomena in Float Glass Heat Treatment* -, Grushko (2018), Chui (1977), and Altun and Başol (2022) emphasize the modelling and simulation of different heat treatment processes of glass and their impacts, but each one considers unique features to focus on, such as thermal radiation and forced convection or internal stresses during cooling. The study of Azizi and Zolfaghari (2004) showed interesting results regarding algorithm use. It used simulated annealing, a heuristic algorithm for solving complex optimisation problems in metallurgy. The study aimed to enhance the algorithm's efficiency by introducing adaptative temperature control strategies. The temperature would be dynamically adjusted during the optimisation process. Then, different adaptive control techniques were evaluated over the fixed control method.

In conclusion, the studies focused on comprehending and improving thermal processes, mainly in the glass industry. However, they differ regarding their research aims, chosen academic framework, and research problem.

Chapter 3

Materials and Methods

The Materials and Methods chapter introduces the methodology followed to perform the predictions and data analysis of the annealing process and explains the tools used. This chapter also describes how the temperature measurement experiment was performed and the materials used in it.

The mechanism of heat being transferred is rather complex, yet it is possible to divide it into three types: convection, conduction, and radiation. It is mentioned in Chapter 3.1.3 and in Equation 3.40, radiation is an important factor in glass heat treatment processes. However, glass radiative properties are quite complex and could hardly be integrated into this study analytically. CFD simulations would be necessary to consider radiation in this heat analysis, and the time required to solve it depends on the size and complexity of the simulation domain. The computational time can be extended for complex simulations involving intricate flow and heat phenomena. Therefore, the development of CFD simulations was out of the scope of this work due to high-performance computing resources and time requirements. The idea was to develop an algorithm that could instantaneously provide information about the bottle's temperature.

3.1 Heat Transfer in Glass Containers

Heat transfer phenomena are the energy transfer process between material bodies that happens as a result of temperature differences and play a pivotal role in various fields of engineering and science. Although it is generally related to mechanical engineering, heat transfer problems are also relevant in chemical and environmental engineering, in which important work has also been done.

The analysis of heat transfer problems is essential to design systems such as heat exchangers, boilers, refrigeration systems, and power plants and to predict the performance of these systems. The science behind these analyses is based upon foundations comprising both theory and experiment. The theoretical part is composed of four general laws that are valid to any medium under consideration (Kakaç et al., 2013).

1. The law of conservation of mass;
2. The law of conservation of energy;
3. The law of conservation of entropy;
4. The law of conservation of momentum.

In addition, other general laws were addressed, such as Fourier's law of heat conduction, Newton's law of cooling, and the Stefan-Boltzmann law of radiation.

In the case of heating systems using natural gas as a heat source, e.g. a furnace, understanding the principles of heat transfer could be critical in optimising the required amount to achieve the desired heating effect. Hence natural gas is a finite and valuable resource, the efficient use of it becomes not only crucial for saving energy, and thus, costs, but also for reducing greenhouse gas emissions. Therefore, it is possible to improve efficiency, reliability, and safety of engineering systems.

3.1.1 Transient Conduction

When a solid is subjected to a change in environment, a determined time must elapse until a condition of temperature equilibrium prevails in this body. The equilibrium state is defined as the steady state, and the process that happens in the interim period before this state is established is defined as the unsteady or transient state. Since the change in the internal energy of the body must be taken into account, the boundary conditions of the heat transfer problem must be accordingly adjusted (Holman, 2010).

In the real world, most heat transfer phenomena involve transient behaviour and have a substantial practical interest in industrial applications, since there is a large number of heating and cooling processes that must be calculated. In this scenario, the temperature of a body varies not only with time but with position as well. Moreover, this temperature variation generally happens in multidimensional systems, not only as one-dimensional transfer phenomena. In these complex systems, numerical simulations are the most detailed solution for modelling heat transfer and fluid flow. Generally, the method used is finite difference or finite element and the advantage it provides is it can be applied to irregular geometries regardless of its boundary condition complexity (Behera, 2009).

Nevertheless, numerical simulations such as CFD require sound computational resources and expertise. Also, the simulation quality depends crucially on the quality of the input data and the modelling assumptions. However, to avoid the use of these resources, it is possible to implement a simplified analysis when certain criteria are met. In this study, considering the type of sensors and data available and the lack of a historical profile, an analytical approach will be adopted to calculate the bottle's temperature, that is, it is wished to calculate the convection and conduction heat transfer with the aid of mathematical analysis, empirical data, and industry best practices.

3.1.1.1 Lumped Heat Capacitance

A common and simplistic way of solving transient conduction problems analytically is the lumped capacitance method. The most typical conduction in a solid is initiated by convection from an adjoining fluid. This method assumes that the temperature of the solid is spatially uniform at any instant during the transient process. In other words, there will be no temperature gradient within the solid and the temperature along this solid will only vary with time. Then, the thermal system is reduced to a number of discrete "lumps" and the temperature difference inside each lump becomes negligible (Incropera, 2006).

The heat transferred by convection can be expressed as in Equation 3.1 and is known as Newton's law of cooling (Kakaç et al., 2013).

$$\dot{Q} = hA(T_\infty - T) \tag{3.1}$$

In this Equation, $\dot{Q}$ is the heat transferred per unit of time [W], h is the heat transfer coefficient of the fluid [$W \cdot m^{-2} \cdot K^{-1}$], A is the area of the body in contact with the fluid [m^2], T is the temperature at the body's surface, and T_{inf} is the fluid's temperature [K], in which heat is being transferred from the fluid to the solid.

Nevertheless, to be able to assume the lumped heat capacitance, the dimensionless Biot number must be small enough. The Biot number represents the ratio between the resistance to conduction within the solid to the resistance to convection between the solid and its surrounding fluid. If the Biot number is small, it means that there is more resistance to convection compared to conduction within the body. This happens in cases of relatively small bodies of highly conductive materials (Çengel, 2002). The Biot number is expressed as:

$$Bi = \frac{hL_c}{k} = \frac{convection\,at\,the\,surface\,of\,the\,body}{conduction\,within\,the\,body} \tag{3.2}$$

where L_c is the characteristic length of the solid [m] and k is the thermal conductivity of the solid [$W \cdot m^{-1} \cdot K^{-1}$]. The characteristic length determines the scale of the system and, for solids of complex shapes, is defined as the ratio of the solid's volume to its surface area. Nonetheless, to adopt a conservative criterion, L_c should be the length scale that corresponds to the maximum spatial temperature difference (Incropera, 2006). In the case of a glass container, this length is the container's bottom, designated critical thickness.

When the Biot number is smaller than 0.1, it means the temperatures within the body relative to its surrounding values remain within 5 % of each other and the lumped capacitance method can be used for the solid's temperature profile, since the variation in space can reasonably be approximated as uniform. Moreover, the smaller the Biot, the more exact the analysis, because a $Bi = 0$ means the thermal resistance of the body to conduction is zero or the thermal conductivity is infinite and the governing phenomena are exclusively convection. Since no such material is known to exist, temperature differences always exist. Therefore, it becomes a cost-benefit issue: accuracy vs convenience (Çengel, 2002). The accuracy provided for infinite series to evaluate the transient conduction may not be worth the wear and tear of the analysis.

However, to evaluate this method's feasibility, it is necessary to have the heat transfer coefficient for forced convection that happens inside the annealing lehr, which can be estimated with empirical equations correlating air velocity and relevant dimensionless numbers, such as Reynolds, Prandtl and Nusselt. It is important to note that h, as well as k, c_p, μ and ρ vary as the temperature varies, and to facilitate this heat transfer analysis, they were considered constant for all the calculations. It is commonly accepted a 20 % uncertainty in the convection heat transfer coefficient and assumed to be constant, even for irregular geometries (Çengel, 2002).

The transient temperature distribution will then be determined by formulating an overall energy balance on the solid. It will be considered that the rate of heat transferred by convection will be the same rate of change in internal energy, which in turn is expressed as:

$$\dot{Q} = mc_p \frac{dT}{dt} \tag{3.3}$$

The necessary heat to produce an elevation of temperature dT in a body is directly proportional to its mass. This differential ratio between the heat input and the increase in temperature experienced in the body is defined as the heat capacity c_p. In the case of glass, due to its vapour pressure being very low even in the molten state, it is considered that its heating process is isobaric (Navarro, 2003). Therefore, the heat supplied is used to increase its enthalpy. The energy balance then takes the following form:

$$hA(T_\infty - T) = mc_p \frac{dT}{dt} \tag{3.4}$$

$$-hA(T - T_\infty) = mc_p \frac{dT}{dt} \tag{3.5}$$

$$\frac{-hA}{mc_p} dt = \frac{dT}{(T - T_\infty)} \tag{3.6}$$

$$\int_0^t \frac{-hA}{mc_p} dt = \int_{Ti}^{T(t)} \frac{dT}{(T - T_\infty)} \tag{3.7}$$

$$\frac{-hAt}{mc_p} - 0 = ln(T - T_\infty) - ln(T_i - T_\infty) \tag{3.8}$$

$$\frac{-hAt}{mc_p} = ln\frac{T - T_\infty}{T_i - T_\infty} \tag{3.9}$$

$$e^{-\frac{hAt}{mc_p}} = \frac{T - T_\infty}{T_i - T_\infty} \tag{3.10}$$

Solving in order of the temperature at an instant t:

$$T(t) = e^{-\frac{hAt}{mc_p}} \cdot (T_i - T_\infty) + T_\infty \tag{3.11}$$

3.1.1.2 One-Dimensional Transient Conduction

In the case of moderate to large values of the Biot number, it is not possible to consider that the temperature in the solid remains nearly uniform as it reaches the surrounding temperature. The temperature gradients within the solid become relevant and $T = T(x,y,z,t)$. Since the lumped capacitance method is no longer appropriate, alternative approaches must be used to solve the inner wall temperature (Incropera, 2006). Transient conduction in multidimensional analysis can be expressed in its general form by the heat diffusion equation, Equation 3.12. Its solution provides the variation of temperature with regard to both time and spatial coordinates x, y, and z (Incropera, 2006).

$$\frac{\partial}{\partial x}\left(k\frac{\partial T}{\partial x}\right) + \frac{\partial}{\partial y}\left(k\frac{\partial T}{\partial y}\right) + \frac{\partial}{\partial z}\left(k\frac{\partial T}{\partial z}\right) + \dot{q} = \rho c_p \frac{\partial T}{\partial t} \tag{3.12}$$

In this Equation, each partial differential term is the net conduction heat flux into the control volume for x, y or z coordinate, $\dot{q}$ is the volumetric rate of thermal energy generation, and the term on the right side is the rate of change of internal energy of the volume. However, if the x direction of the solid is small compared to its y and z direction, it is realistic to assume a one-dimensional analysis of the problem. With regards to a glass container, since its thickness is considerably smaller compared to its height and diameter, the internal temperature will mainly vary in only one spatial coordinate. If it is considered only one spatial coordinate (x), a constant thermal conductivity k, and no internal energy generation, Equation 3.12 can be reduced to:

$$\frac{\partial^2 T}{\partial x^2} = \frac{1}{\alpha}\frac{\partial T}{\partial t} \tag{3.13}$$

where α is the thermal diffusivity. The thermal diffusivity illustrates a measure of thermal inertia and is expressed in $[\mathrm{m}^2 \cdot \mathrm{s}^{-1}]$.

$$\alpha = \frac{k}{\rho c_p} \tag{3.14}$$

In addition, Equation 3.15 describes the surface condition experienced in the case of heat transfer of a solid immersed in a fluid.

$$-k\frac{\partial T}{\partial x} = h\left[T(x,t) - T_\infty\right] \tag{3.15}$$

However, the temperature in the solid depends not only on x and t, but also depend on a number of physical parameters: $x, L, t, k, \alpha, h, T_i$, and T_∞. To reduce the number of these parameters, dimensionless quantities can be defined. The dimensionless time, called the Fourier number, is indicated in Equation 3.16, and the dimensionless length is illustrated in Equation 3.17.

$$Fo = \frac{\alpha t}{L^2} = \frac{\alpha t}{\varepsilon_b^2} \tag{3.16}$$

The Fourier number represents the ratio between the heat conducted through the solid and the heat stored. Hence the larger the Fourier number, the faster the propagation of heat within the solid, α is the thermal diffusivity $[\mathrm{m}^2 \cdot \mathrm{s}^{-1}]$, t is the time [s], and L is the length where the diffusion occurs $[m]$ and corresponds to the bottle thickness ε_b. The dimensionless length x^* represents the distance from the center and is expressed as:

$$x^* = \frac{x}{L} \tag{3.17}$$

The functional dependence may now be expressed as $T(x,t) = f(x^*, Fo, Bi, T_i, T_\infty)$. The foregoing problem can be solved numerically or analytically. For simplified geometries, like a plane wall, cylinder, and sphere, the determination of the one-dimensional temperature distribution results in infinite series presented in Equation 3.18 that can be solved using advanced mathematical techniques. However, the terms in the infinite series rapidly converge with increasing time. Generally, for values of $Fo > 0.2$, it is reasonable to keep only the first term and obtain an error under 2 % (Çengel, 2002). The one-term approximation can then be used to determine the temperature anywhere in the x direction of the body in the transient conduction analysis (Schneider, 1955).

$$\frac{T(x,t) - T_\infty}{T_i - T_\infty} = \sum_{n=1}^{\infty} C_n e^{-\zeta_n^2 Fo} \cdot \cos(\zeta_n \cdot x^*) \tag{3.18}$$

$$\frac{T(x,t) - T_\infty}{T_i - T_\infty} = C_1 \cdot e^{-\zeta_1^2 Fo} \cdot \cos(\zeta_1 \cdot x^*) \tag{3.19}$$

$$T(x,t) = C_1 \cdot e^{-\zeta_1^2 Fo} \cdot \cos(\zeta_1 \cdot x^*) \cdot (T_i - T_\infty) + T_\infty \tag{3.20}$$

In these Equations, C_1 and ζ_1 are functions of Bi and are evaluated from Equation 3.21 and 3.22. There are tables with listed values for the three geometries for extended Bi values and a table is shown in Appendix A.

$$C_n = \frac{4\sin(\zeta_n)}{2\zeta_n + \sin(2\zeta_n)} \tag{3.21}$$

The discrete values of ζ_n are positive roots of Equation 3.22:

$$\zeta_n \tan \zeta_n = Bi \tag{3.22}$$

Although this approximate solution may not capture all the intricacies of the real temperature distribution, it is suitable for simple cases where the temperature changes are relatively small and occur over short periods. Considering the simplified geometries and the models of containers produced, it is reasonable to apply the approximate solution for a plane wall since the containers' thickness is relatively small compared to their diameter.

3.1.2 Forced Convection

The mechanism for convective heat transfer can be divided into two types: natural and forced convection. Natural convection happens when the fluid is moved by differences in density that cause buoyancy forces. On the other hand, forced convection is when the motion of the fluid is generated by an external source, that is, it is when convection is induced artificially by an internal source such as fans, impellers, or pumps (Bird et al., 2002). Therefore, this analysis will consider the transport mechanism of forced convection since the air is pulled through a conduit alongside the lehr's sidewalls by an impeller located at the top.

Furthermore, heat and mass transfer in nearly every operation of fluid transport involves the flow of a viscous fluid in some form of closed conduit (Kakaç et al., 2013). This internal flow regime depends on variables such as the duct geometry, flow inlet velocity, temperature profiles, wall temperature, and heat flux boundary conditions (Shah and London, 1978). In this sense, dimensionless numbers of fluid mechanics and empirical correlations can be used to determine the flow regime and estimate the heat transfer coefficient for forced convection.

Reynolds number, *Re*, is used to determine the flow regime of a fluid. It is defined as the ratio of inertial forces to viscous forces within a fluid flow and provides a quantitative measure for differentiating laminar to turbulent flow. When *Re* is below a critical point, the flow is described as laminar, where motion happens in a smooth and orderly way. However, when *Re* is above this threshold, the flow is described as turbulent, with chaotic and irregular patterns. The Reynolds number is defined as (Munson et al., 2012):

$$Re = \frac{\rho\, v\, H_d}{\mu} \tag{3.23}$$

where ρ is the air density [$\mathrm{kg \cdot m^3}$], v is the air velocity [$\mathrm{m \cdot s^{-1}}$], and H_d is the hydraulic diameter [m]. In turn, H_d is defined as (Munson et al., 2012):

$$H_d = \frac{4A}{P} \tag{3.24}$$

where A is the cross-sectional area of the flow in [$\mathrm{m^2}$] and P is the wetted perimeter in [m].

3.1.2.1 Forced Convection in Internal Laminar Flow

For laminar flow and for *Re* above the critical, the Nusselt number can be described with the Sieder and Tate correlation (Welty et al., 2014):

$$Nu = 1.86 \left(Pe \frac{D}{L} \right)^{1/3} \cdot \left(\frac{\mu_b}{\mu_w} \right)^{0.14} \tag{3.25}$$

where Pe is the Peclet number, D is the equivalent diameter, L is the conduit's length [m], μ_b is the dynamic viscosity of the fluid at bulk temperature [$\mathrm{kg \cdot m^{-1} \cdot s^{-1}}$], and μ_w is the dynamic viscosity evaluated at the wall temperature [$\mathrm{kg \cdot m^{-1} \cdot s^{-1}}$]. However, this correlation involves the knowledge of the fluid viscosity at the wall. It can be approximated assuming that the fluid viscosity at the wall is equal to the average fluid viscosity. This assumption is reasonable for several practical cases. In this case, Equation 3.25 becomes:

$$Nu = 1.86 \left(Pe \frac{D}{L} \right)^{1/3} \tag{3.26}$$

However, to avoid this assumption, other correlations can be used. There are various correlations depending on the aspect ratio of the pipe, or the proportion of width to height. The Gnielinski correlation is one often employed correlation for laminar flow in a fully developed rectangular pipe (Ammar and Park, 2020).

$$Nu = 3.66 + \frac{0.0656 \cdot Re \cdot Pr}{1 + 0.04 \cdot Re^{0.8} \cdot (Pr^{2/3} - 1)} \tag{3.27}$$

The Gnielinski correlation works under the assumption of fully developed flow, that is, the flow has reached a stabilized stage and has a constant velocity profile across the pipe cross-section. Also, the rectangular pipe must have approximate values of length and width.

For a high aspect ratio between the width and height of the duct, the adapted Churchill-Bernstein correlation can be used, in which H is the height and W is the width (Churchill and Bernstein, 1977).

$$Nu = \frac{0.664 \cdot Re^{0.5} \cdot Pr^{0.33} \left(\frac{H}{W}\right)^{0.1}}{\left[1 + \left(\frac{0.04}{Pr}\right)^{0.67} \cdot \left(Re^{0.5} \cdot \left(\frac{H}{W}\right)^{0.1} - 1\right)^{0.33}\right]} \tag{3.28}$$

3.1.2.2 Forced Convection in Internal Turbulent Flow

For internal flow in circular channels, experimental observations conclude that for $Re > 2900$, it is the case of a turbulent flow regime. This result can be generalized to non-circular channels using the hydraulic diameter (Schlichting and Gersten, 2017). The following relations can be used to determine the convective heat transfer coefficient. Firstly, the Prandtl number is defined as the ratio of viscous diffusion and thermal diffusion (Çengel and Cimbala, 2018) and is approximately 0.7 for air.

$$Pr = \frac{c_p \mu}{k} \tag{3.29}$$

Where c_p is the specific heat capacity of the air $[\mathrm{J \cdot kg^{-1} \cdot K^{-1}}]$, μ is the air viscosity $[\mathrm{kg \cdot m^{-1} \cdot s^{-1}}]$, and k is thermal conductivity of the air $[\mathrm{W \cdot m^{-1} \cdot K^{-1}}]$. Finally, the Nusselt number represents the ratio of heat transferred by convection to heat transferred by conduction within a fluid. The larger the Nu, the more intense the convective heat transfer, with high values of Re. When $Nu = 1$, the rate of heat transferred by convection is equal to the rate of heat transferred by conduction and, therefore, the fluid is stationary (Munson et al., 2012).

$$Nu = \frac{\dot{Q}convection}{\dot{Q}conduction} = \frac{hA\Delta T}{kA\frac{\Delta T}{L_c}} = \frac{hL_c}{k} \tag{3.30}$$

In this Equation 3.30, h is the heat transfer coefficient of the air $[\mathrm{W \cdot m^{-2} \cdot K^{-1}}]$, L_c is the characteristic length [m], k is the thermal conductivity of the air in $[\mathrm{W \cdot m^{-1} \cdot K^{-1}}]$. This differs from Bi in Equation 3.2 since convection and conduction are related only to the fluid, whereas Bi relates convection from the fluid to the solid and conduction within the solid. However, depending on the flow regime, different correlations apply to each case: laminar or turbulent. If $Re > 10^4$, the flow falls within a turbulent regime. As a consequence of that, the Dittus-Boelter correlation could be applied, an explicit function for calculating the Nusselt number and one of the most widely quoted and used heat transfer correlations for turbulent flow in ducts (Winterton, 1998). This correlation is valid when $Re > 10000$ and $0.6 < Pr < 100$.

$$Nu = 0.0023 Re^{0.8} Pr^{m} \tag{3.31}$$

.

In this Equation, m is equal to 0.4 if the fluid is being heated or 0.3 if it is being cooled (Dittus and Boelter, 1985). Although this correlation does not consider the change in viscosity as a function of the change in temperature, it is a good approximation in cases where differences between bulk fluid and the solid's surface are not significant. Nevertheless, this correlation is appropriate for long ducts, where the ratio between the length and the diameter is higher than 10. Deissler suggests a modification to account for variable velocity and temperature profiles along the flow axis in short passages (Deissler, 1987).

$$h_{short} = \left(1 + \left(\frac{D}{L}\right)^{0.7}\right) \cdot h \tag{3.32}$$

Therefore, it is possible to estimate the heat transfer coefficient of a phenomenon with convection in a short duct.

3.1.3 Radiation

Thermal radiation is the third mechanism of heat transfer, a form of electromagnetic radiation. It is defined as a process by which heat is transferred, without any intervening medium, from a body by virtue of its temperature (Venkanna, 2010). All objects with a temperature higher than 0 K constantly emit electromagnetic waves that travel in a straight line on the basis of their temperature.

It is characteristically different from convection and conduction, for it does not require the presence of a material medium to take place and occurs not only in solids but also in liquids and gases. Furthermore, heat transfer by radiation can occur between two bodies separated by a medium colder than them. In contrast, heat transfer by convection or conduction can only arise from the high-temperature medium to the lower-temperature one (Çengel, 2002).

It can be categorized based on its wavelength λ, and different λ correspond to distinct energy levels. Since a specific range of λ exhibits varying characteristics, thermal radiation can be classified into various types, such as radio waves, microwaves, infrared radiation, visible light, ultraviolet radiation, X-rays, and gamma rays.

3.1.3.1 Emissivity

The amount of thermal radiation emitted by an object depends on its temperature. The concept of a blackbody becomes relevant: an idealized object that absorbs and emits all radiation incident upon it independently of the wavelength. In reality, surfaces are not perfect blackbodies, and their ability to emit radiation differs from a blackbody. In this sense, the emissivity of a surface compares its ability to emit radiation with a blackbody at the same temperature, assuming values between 0 and 1. The emissivity of a real surface varies as a function of the surface temperature, wavelength, and direction of emitted radiation. When the emissivity is independent of λ, the surface is approximated as grey, whereas when it is independent of direction, the surface is approximated as diffuse for radiation calculations. The total emissive power of a diffuse grey surface can be determined using the emissivity and the Stefan-Boltzmann equation (Musikant, 2003), in which the Stefan-Boltzmann law describes the emissive power of a blackbody (Çengel, 2002).

$$E = \sigma T^4 \tag{3.33}$$

In this Equation, E is the thermal radiation energy $[\mathrm{W \cdot m^{-2}}]$, σ is the Stefan-Boltzmann constant $[\mathrm{W \cdot m^{-2} \cdot K^{-4}}]$, and T is the absolute temperature in the surface in $[K]$. The total emissive power for a diffuse grey surface is obtained from Equation 3.35, where ε is the emissivity of the respective surface. Surface emissivity values can be found in the literature or determined experimentally (Musikant, 2003).

$$E(T) = \varepsilon \sigma T^4 \tag{3.34}$$

Regarding the emissivity of glass, this value depends on glass temperature, wavelength, and thickness. Thicker glass emits more thermal radiation, and higher temperatures shift the emission towards shorter wavelengths. It can be approximated using different wavelength bands and considering that the absorption coefficient remains constant. The total emissive power of a glass surface can be calculated by considering the mean emissivity within each wavelength band and the fraction of radiative energy emitted by a blackbody within those bands. According to Rantala (2015), with the use of three bands, the total emissive power can be expressed as:

$$E(T) = [\varepsilon(0,\lambda_2,T) \cdot Fb(0,\lambda_2,T) + \varepsilon(\lambda_2,\lambda_3,T) \cdot F_b(\lambda_2,\lambda_3,T) + \varepsilon(\lambda_3,\infty,T) \cdot F_b(\lambda_3,\infty,T)] \cdot \sigma T^4 \tag{3.35}$$

where $\varepsilon(\lambda_2,\lambda_3,T)$ is the mean emissivity of a surface between wavelengths λ_2 and λ_3 at temperature T, $F_b(\lambda_2,\lambda_3,T)$ is the fraction of radiation of a black body between the same conditions. To solve it, tabular values from the literature can be used and $F_b(\lambda_i,\lambda_j,T) = F_b(0,\lambda_j,T) - F_b(0,\lambda_i,T)$ (Rantala, 2015). However, emissivity is also a function of angles, and capturing this direction dependence in a heat transfer analysis can get quite complex. Assuming an average emissivity or acknowledging the value correspondent of the normal direction to the surface can simplify it.

3.1.3.2 Absorptivity, Reflectivity and Transmissivity

When an object is exposed to thermal radiation, three scenarios can occur: the waves can be absorbed, reflected, or transmitted if the object is not opaque. The absorptivity α_r, reflectivity ρ_r and transmissivity τ_r sum up to 1 (Rantala, 2015).

$$\alpha_r + \rho_r + \tau_r = 1 \tag{3.36}$$

In the case of a blackbody, ρ_r and τ_r are zero since all incoming radiation is absorbed. However, the majority of objects in daily life are opaque surfaces. Its transmissivity τ_r is zero since radiation does not pass through it. Nonetheless, glass adopts a mixed behaviour: it is partially transparent to a specific λ of radiation, whereas being opaque to others. Soda-lime-silica glass, for example, is an opaque glass when λ is higher than 4.5 μm, and when it is below 2.75 μm, it is transparent. In the range between these two values, it has a relatively high absorption coefficient and adopts a semi-transparent behaviour (Rantala, 2015). The presence of impurities, such as iron oxide, also affects the absorption coefficient. Higher temperatures and higher concentrations of impurities can increase absorption in certain wavelength ranges.

3.1.3.3 View Factor

The way radiation is exchanged between surfaces depends on how the surfaces are positioned relative to one another. The heat flux depends on the shapes and sizes of surfaces and the distances between them. The view factor is a geometric parameter that describes the fraction of radiant energy leaving surface 1 that is incident to surface 2 (Ehrt and Vogel, 1992). In other words, the view factor measures how well one surface sees another and assumes values between 0 and 1. Then, the heat flux between two surfaces can be written as:

$$Q_{1-2} = F_{1-2}\varepsilon_{1-2}\sigma A_1 (T_1^4 - T_2^4) \tag{3.37}$$

where F_{1-2} is the view factor from surface 1 to surface 2, therefore, the reciprocity can be expressed in Equation 3.38. In a closed enclosure, the principle of conservation of energy requires that the radiation emitted from a surface be absorbed, reflected, or transmitted by other surfaces of the enclosure. This means that the sum of the view factors from a surface i to surface j to n surfaces of the enclosure, including itself, must be equal to 1, as expressed in Equation 3.39 (Ehrt and Vogel, 1992).

$$F_{1-2}A_1 = F_{2-1}A_2 \tag{3.38}$$

$$\sum_{j=1}^{n} F_{ij} = 1 \tag{3.39}$$

Calculating view factors generally involves numerical methods and the generation of a view factor matrix. The view factor matrix of n element surfaces involved in radiative heat transfer will be $n \cdot n$.

3.1.3.4 Radiation in Glass

The general form of the heat transfer to be solved in this study takes the form of Equation 3.40, where the first term describes the internal energy change of a glass container, $\frac{\partial}{\partial x}\left(k\frac{\partial T}{\partial x}\right)$ stands for conduction and $\frac{\partial q_r}{\partial x}$ is the net radiation heat transfer inside the glass (Rantala, 2015).

$$\rho c_p \frac{\partial T}{\partial t} = \frac{\partial}{\partial x}\left(k\frac{\partial T}{\partial x}\right) + \frac{\partial q_r}{\partial x} \tag{3.40}$$

Nonetheless, there are numerous factors that are determinants for the calculation of the radiation relative to glass. The amount of radiation emitted, absorbed, reflected by, and transmitted within a glass body does not show constant behaviour and is strongly dependent on temperature conditions, glass composition and geometry, and spatial orientation of it. For example, the net radiation can be defined as the absorption and reflection of short-wave radiation and the incoming and outcoming long-wave radiation and the consideration of internal net radiation inside a molten glass is one of the most complicated problems in the field of radiation heat transfer.

The radiative properties of glass play an important role in its thermal processes, especially in melting, but also in annealing and tempering (in float glass manufacturing). It can also be a determinant factor for the efficiency of a type of glass, for example, the case of solar energy collectors.

The simplest method to take radiation into account would require at least three different absorption coefficients since glass can be opaque, semi-transparent, or transparent with regard to wavelength. In the limit, it is possible to assume that glass is an opaque material and use a constant value of emissivity to take radiation into account in the modelling of heat transfer. In addition, the effect of internal net radiation can be neglected in cases in which glass does not reach temperatures above 700 °C (Rantala, 2015).

3.1.4 Thermal Resistance

To estimate the heat losses in a closed chamber, it is necessary to analyse the thermal resistance, that is, the capacity of a material to resist heat flow. The thermal resistance of heat transfer through a plane wall can be expressed in the same way as the electric resistance. The temperature gradient is the driving function for the heat flow and the combination of thermal conductivity, material thickness, and surface area are the resistance to this flow (Holman, 2010).

$$\dot{Q} = \frac{thermal\ potential\ difference}{thermal\ resistance} \tag{3.41}$$

Therefore, the thermal resistance represents the ratio of the temperature difference across a material or interface to the heat flux passing through it. In the case of a chamber with forced convection inside it, the thermal resistance can be expressed as a sum of resistances: resistance to convection inside the chamber, to conduction through the wall, and to convection in the external wall.

3.2 Digital Twin

The goal of this analysis is to create, from scratch, a model that represents in real-time the temperature profile of the bottles. This model performs as a digital twin, which is a virtual representation of a real process and is used to run simulations. The difference between a digital twin and a model is their level of interactivity with the process. A model becomes a digital twin when it integrates real-time data from sensors or other devices to mimic the behaviour of its physical counterpart. Therefore, a digital twin enables users to interact and control the virtual representation in real-time, whereas a model is a static representation.

The objective of the digital twin is to show, via an easy interface, the temperature profile of a bottle throughout the annealing process in order to help decision-making regarding changes in it. This temperature profile will result from the heat transfer phenomena inside the lehr. In an automated way, any action taken on the set points temperatures in the lehr's controller will cause a response in the temperature profile of the bottle.

Two ways of predicting the bottle's temperature profile will be presented, Model 1 and Model 2. Depending on the value of the Biot number, the assumption of a lumped system could be valid. If $Bi < 0.1$, the bottle's temperature profile will follow the lumped capacitance method, although Model 2 is also valid in this case. If $Bi \geq 0.1$, it will follow the one-term approximate solution for transient conduction. Therefore, the first step is to calculate and analyse all the parameters and dimensionless numbers presented in Chapter 2 that will determine the chosen model.

3.2.1 Tools

The algorithm developed was written in Python, using Visual Studio Code, an open-source code editor created by Microsoft. Several programming languages are supported by it, including Python, which is known for its adaptability and popularity within the field. Python offers a diverse array of libraries and frameworks that greatly benefited this analysis. Libraries are pre-written collections of code that provide functions, modules, and classes to simplify and enhance the development process. Therefore, it enables programmers to take advantage of existing code rather than engage in redundant code creation.

The main libraries used were Pandas, Numpy, Scipy, Matplotlib, and Plotly. Pandas provides data structures that allow handling, indexing, and reshaping data from different sources. Furthermore, it enables the processing of large data sets, making it an essential library for data analysis. Numpy and Scipy are libraries for numerical computing; they provide a collection of mathematical modules, such as integration, interpolation, and linear algebra. Finally, Matplotlib is one of the most used plotting libraries in Python that offers a wide range of visualization options, including 2D and 3D plots, histograms, bar charts, or scatter plots. Furthermore, it is easily integrated with other scientific libraries.

Another Python library, called PyQt5, was used to design the interface. It is built on top of the Qt framework, a library in C++. This library offers an interesting set of customizable widgets, layout managers, and event-handling mechanisms, which creates visually appealing interfaces.

AutoCAD was used to design the lehr's and bottle's drawings. It is a widely used computer-aided design software developed by Autodesk and is used in various industries. It also supports programming languages, such as AutoLISP and Visual Basic for Applications (VBA), which allows the automatization of tasks.

The diagramming tool for the schemes and drawings used was draw.io, as it offers a convenient platform to create visually appealing diagrams and is free and open-source.

3.2.2 Input Data

The scheme presented in Figure 3.1 summarizes the necessary data and the logical chaining of equations followed by the digital twin for choosing the most suitable model.

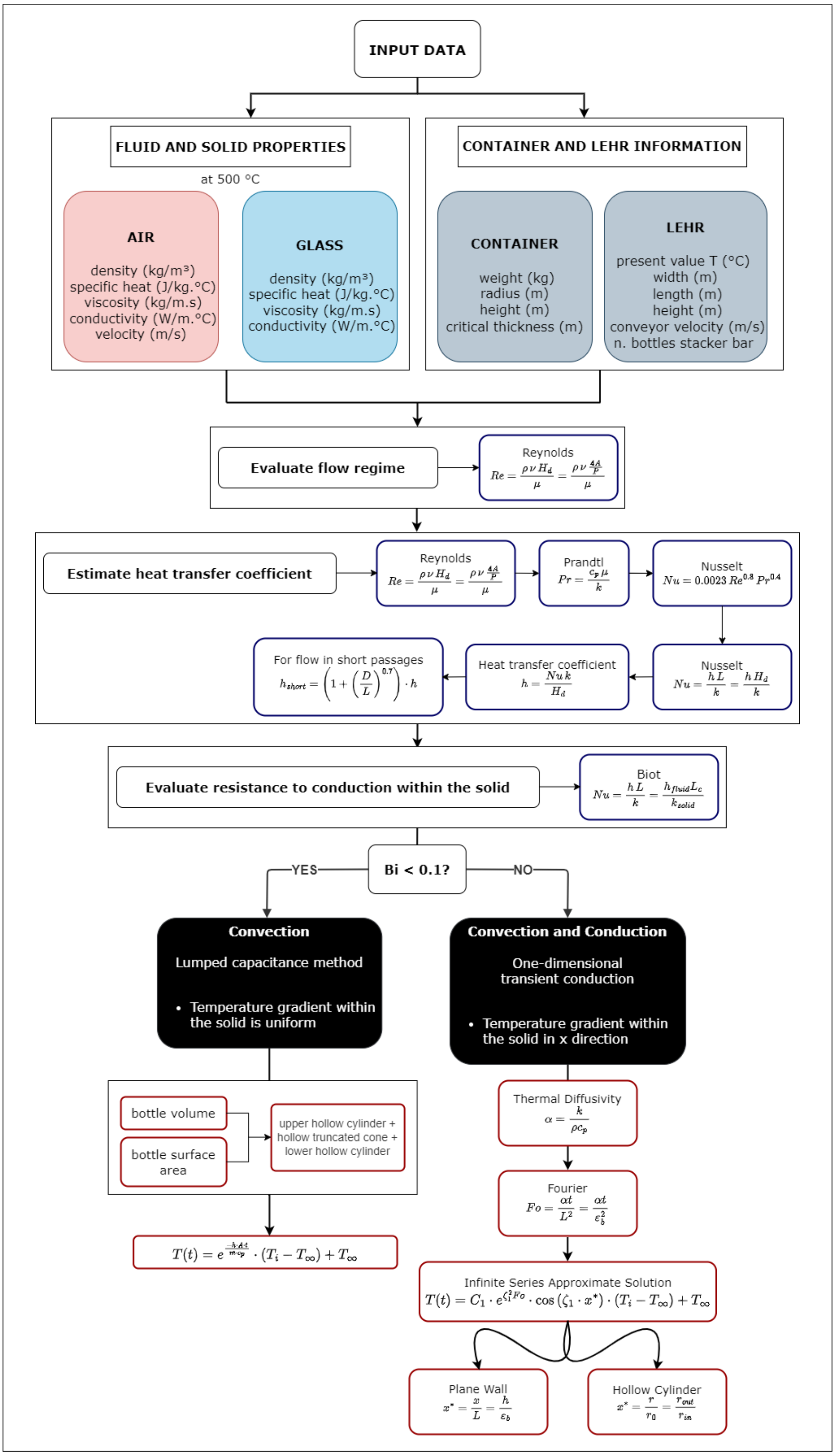

Figure 3.1: Diagram of the digital twin sequence.

As said in the aforementioned description of annealing lehrs, there is no geometry or number of zones common to all. Although they seem very similar, each lehr has its specific width, length, and height and different configuration of burners arranged in its side walls, which will result in distinct zone sets. The model was designed based on a specific lehr, and the glass container analysed corresponded to its current production. Table 3.1 and Figure 3.2 show the dimensions of the studied lehr. The total width and height represent the measurements of the outside points of the lehr's walls. That is, the total height represents the distance between the bottom and the top of the lehr, considering the space for the impellers and bottom structure, and the total width considers the thickness of the wall. The width and height with the smallest values represent the measurements of the inside space where the air and glass containers are located.

Table 3.1: Dimensions of annealing lehr

Dimensions	
Length [m]	20.55
Length zone [m]	2.55
Total Width [m]	4.63
Width [m]	3.6
Total Height [m]	2
Height [m]	0.7

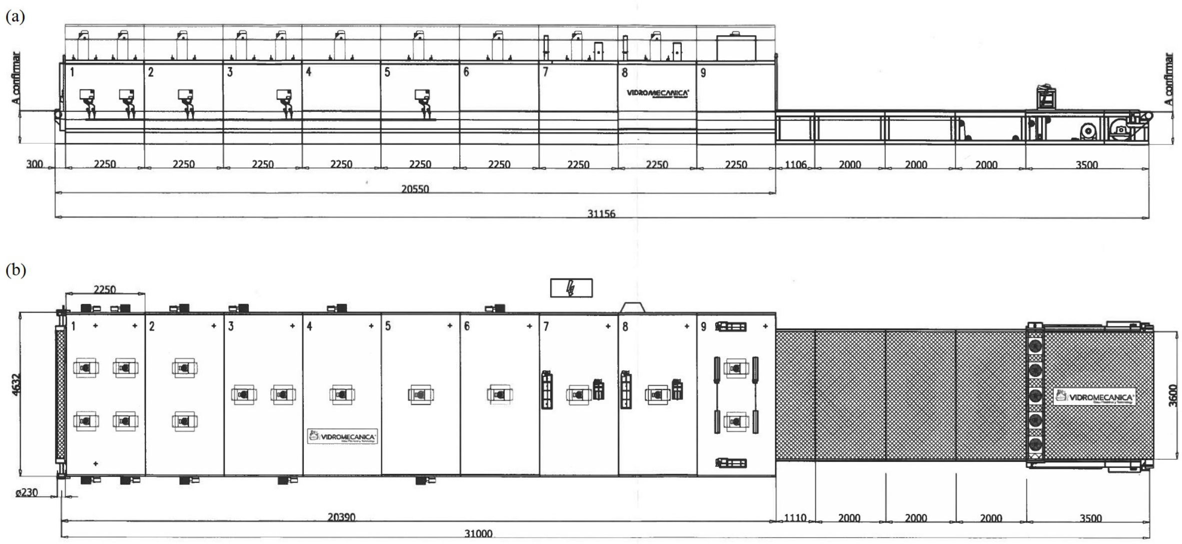

Figure 3.2: Drawing of annealing lehr adapted from Vidromecânica (2019), in which (a) is the side view and (b) is the top view of the machine.

The studied lehr has twelve thermocouples disposed along its length. However, four were in the first zone. For this reason, the first zone will be divided into two and provide two temperature values (the average between the thermocouple on the left and right side), finally getting ten temperature points. Furthermore, it is possible to measure the air temperature at the entrance and exit of the lehr with an infrared thermometer, which will increase the number of available temperature data in two points. Table 3.2 introduces the zones, their setpoint and present value temperature, and their thermocouple position along the lehr's length and time. The time for each data point will be their length divided by the conveyor velocity in m/s. The last digits of the sensible data have been omitted and substituted for "**" for reasons of industrial confidentiality. The inlet and outlet temperatures were measured experimentally with an infrared sensor.

Table 3.2: Setpoint temperature and thermocouples data and their location lengthwise

Zone	Setpoint Temperature [°C]	Present Value Temperature [°C]	Position [m]	Time [min]
Inlet	-	240	0	0
1A	5**	5**	0.75	1.**
1B	5**	5**	1.5	2.**
2	5**	5**	3.38	5.**
3	5**	5**	5.63	8.**
4	5**	5**	7.88	12.**
5	5**	4**	10.13	15.**
6	4**	4**	12.38	19.**
7	3**	3**	14.63	22.**
8	2**	2**	16.88	25.**
9	1**	1**	19.13	29.**
Outlet	-	50	20.55	31.**

The first step was to estimate the temperature profile of the air inside the lehr. The temperature information available is only the one given by the thermocouples located below the burners for each set point. Thus, this information is very spaced out in time and does not convey the actual thermal behaviour, not to mention the bias in it, as the thermocouples do not transmit information about the thermal variation along the width since they are located on the side walls.

Since there are only twelve points of known temperature, linear interpolation is the chosen way to predict the air temperature inside the lehr. If a polynomial trendline were used to estimate it, for example, using the least square method, there would be a risk of overfitting or predicting temperatures higher than the highest one captured by the thermocouples. Hence a conservative approach will be chosen, and the predicted temperature will have a linear profile.

First, two lists for the x-axis and y-axis are created. These lists contain the time values in minutes and corresponding temperature values in °C, respectively. Each list element represents a specific location or a stage in the process.

Then, there will be a chosen n number of times to solve the linear interpolation. In the algorithm in Python, this is solved by a `for loop` in which n is the number of times the loop runs. Each time the loop runs, the letter i will represent the current cycle of the loop. The time step between each cycle will be the total annealing time in minutes divided by n. Based on its position along the x-axis, the time step will be allocated between two known values; that is, for i in n, the predicted temperature y will be the interpolation result of the two nearest known points x_i, y_i and x_{i+1} and y_{i+1}.

Thus, the next step will be to estimate the temperature of the bottle's inner wall since it is the sensible location that must achieve the annealing point. Two approaches can be followed: the lumped capacitance method or the one-dimension transient conduction. As explained previously, if heat is transferred from a fluid to a solid, and if the Biot number is smaller than 0.1, it is possible to assume that the thermal gradient within the solid is uniform.

However, this result will depend on h and k of the air and the glass, respectively. In turn, h will depend on the future estimate of air velocity for Re, and k will depend on the quality of the literature source chosen to obtain it. In addition, although they depend on temperature, it is crucial to emphasize that the following properties were considered constant for air and glass: c_p, k, ρ, μ.

According to Bingham (2010), the specific capacity of glass is more closely an additive function of composition. For soda-lime-silica glasses, Equation 3.42 yields the mean heat capacity with 1 % of error within temperatures from 0 to 1300 °C. This equation was developed by Sharp and Ginther (1951) and improved by Moore and Sharp (1958), resulting in Equation 3.43. The temperature input is in °C and the specific heat is given in $\text{cal} \cdot \text{g}^{-1} \cdot {}^{\circ}\text{C}^{-1}$.

$$c_p = \frac{\sum p_i (f_i T + c_{p,i})}{0.00146T + 1} \tag{3.42}$$

$$c_p = \frac{0.00146T^2 \sum p_i f_i + 2T \sum p_i f_i + \sum c_{p,i}}{(0.00146T + 1)^2} \tag{3.43}$$

In this Equation, p_i is the percentage of component i in the glass composition, f_i is the temperature parameter of component i, and $c_{p,i}$ is the heat capacity of component i. Since there were no parameters of Cr_2O_3 found, and due to its low percentage in the glass composition, its corresponding percentage was added to SiO_2. The conversion factor between c_p [$\text{cal} \cdot \text{g}^{-1} \cdot {}^{\circ}\text{C}^{-1}$] and c_p [$\text{J} \cdot \text{kg}^{-1} \cdot \text{K}^{-1}$] is 4187. Table 3.3 shows the respective percentage, temperature parameters, and heat capacity of components. For confidential reasons, p_i is presented as a range considering the typical composition of a soda-lime-silica glass according to Bingham (2010).

Table 3.3: Component, percentage p_i, temperature parameters f_i and heat capacity $c_{p,i}$ of components

Component	p_i	f_i	$c_{p,i}$
SiO_2	0.70–0.73	0.000468	0.1657
Na_2O	0.12–0.15	0.000829	0.2229
CaO	0.10–0.12	0.000410	0.1709
Al_2O_3	0.01–0.02	0.000453	0.1765
K_2O	0–0.01	0.000445	0.1756
MgO	0.005–0.02	0.000514	0.2142
SO_3	0–0.005	0.00083	0.1890
Fe_2O_3	0–0.01	0.000380	0.1449

Therefore, c_p of glass will be 1214 $J \cdot kg^{-1} \cdot K^{-1}$. However, another important parameter is the thermal conductivity k_g of glass. It plays a pivotal role as well as h in determining the dominant heat transfer mechanism because it is also a determinant factor for Bi value.

It is very difficult to find specific values of k_g in the range of 500 °C. The literature found indicates values from 0.1 to 25 $W \cdot m^{-1} \cdot K^{-1}$. The thermal conductivity of solids depends on many factors that are difficult to measure or predict; hence it should be measured experimentally (Goldsmith, 1962). However, different authors proposed equations for the temperature dependence of k_g. According to Bingham (2010), the conductivity of glass can be expressed as an additive model, defined by Equation 3.44.

$$k_g = \sum A_i \cdot p_i \tag{3.44}$$

In this Equation, A_i is a coefficient for component i, and p_i is the percentage of component i in the glass composition. The values presented for A_i only refer to temperatures above 600 °C, which is above the maximum operating temperature of an annealing lehr for glass containers. Endrys and Turkiz (1985) proposed the following equation, where T is given in °C.

$$k_g = 0.7222 + 0.001583 \cdot T \tag{3.45}$$

The result for 500 °C is $k_g = 1.51$ $W \cdot m^{-1} \cdot K^{-1}$. Table 3.4 presents the data used as input for air and glass properties at 500 °C and for temperature values in the digital twin calculations.

Table 3.4: Input data for air and glass properties and their respective source

Input Data		Source
Air		
ρ	$0.4565\ kg \cdot m^{-3}]$	Çengel (2002)
k	$0.05572\ [W \cdot m^{-1} \cdot K^{-1}]$	Çengel (2002)
c_p	$1093\ [J \cdot kg^{-1} \cdot K^{-1}]$	Çengel (2002)
μ	$3.53\ [kg \cdot m^{-1} \cdot s^{-1}]$	Çengel (2002)
v	$4\ [m \cdot s^{-1}]$	Rantala (2015)
Glass		
ρ	$2540\ [kg \cdot m^{-3}]$	Rantala (2015)
k	$1.51\ [W \cdot m^{-1} \cdot K^{-1}]$	Endrys and Turkiz (1985)
c_p	$1214\ [J \cdot kg^{-1} \cdot K^{-1}]$	Bingham (2010)

3.2.3 Estimated Parameters

In order to decide the governing heat transfer phenomena, it is necessary to estimate h of forced convection inside the lehr. As mentioned before, despite being a parameter that varies with temperature, it will be considered constant throughout the length and width of the entire lehr. For that, Equations 3.23, 3.29, 3.30, 3.31, and 3.32 were used to estimate its value. In chronological order, it was first necessary to calculate *Re* and *Pr* to estimate *Nu* by the Dittus-Boelter correlation further and finally *h*.

Foremost, it is necessary to analyse the flow regime of the forced convection airflow. The air inside the lehr is drawn by an impeller and pulled into pipes that run from the top, passing through the side walls to the bottom of the lehr. The impeller's blades rotation creates a low-pressure region and causes this suction that draws the air towards the impeller. There will presumably be a transition to a more controlled flow within the pipe compared to a high-velocity flow in the impeller's affectation area. After the air flows through these pipes, it is discharged at the height of the conveyor belt. Then, it is possible to consider that the lehr becomes the new conduit for this internal flow.

In this way, it was considered that the air path inside the lehr goes from the side wall to the center since there are analogous pipes on both sides. The air velocity is considered as the same in any outlet point lengthwise. Thus, the length of the cross-sectional area of the airflow will be the length of the lehr. Therefore, the conduit width will be the lehr length, and its length will be the lehr half-width.

The air will flow from a smaller conduit into a larger rectangular region, and dispersion phenomena may occur. As the air moves inside the lehr, the boundary layer changes. Due to the bigger dimensions, it may begin as a laminar boundary layer near the walls and eventually evolve into a turbulent boundary layer. Furthermore, dispersion and turbulence generation may occur. When the air enters the larger rectangular space, the available volume will increase and thus lead to dispersion and mixing of the outlet flow from the pipe with the surrounding air (Çengel and Cimbala, 2018).

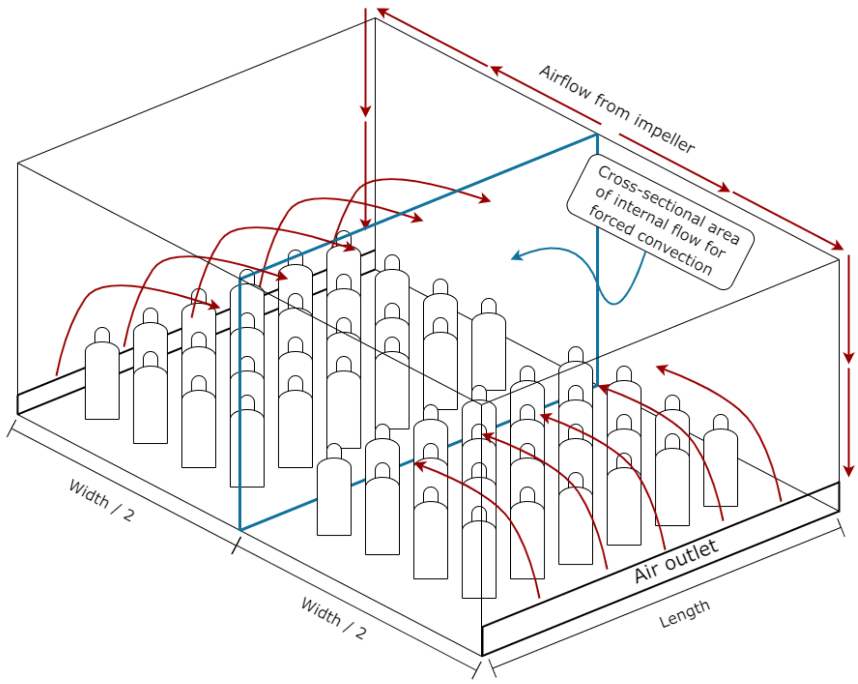

Figure 3.3: Forced convection inside the lehr.

Figure 3.3 demonstrate the forced convection airflow inside the lehr. It is out of scale and illustrates a cut-out of a zone of the annealing lehr. The blue rectangle represents the cross-sectional area of the flow. It is at least the size of the blue rectangle since it is considered a horizontal flow, and a movement from the outlet point to the impeller's point would have a more extensive cross-sectional area.

The actual behaviour of this change in internal flow will depend on parameters such as velocity, geometry, and surface conditions. In this sense, CFD simulations would be required to properly understand it. Since there is a lack of measuring devices and proper conditions to study this air flow due to the physical impossibility of entering the lehr while operating, simpler assumptions will be adopted. The air velocity will also be a determinant parameter to determine the flow regime. The value used is an assumption based on the work of Rantala (2015), which measured the outlet air velocity of the recirculating pipes of forced convection of a tempering furnace in flat glass manufacturing.

Finally, the value of Nu will determine the heat coefficient from Equation 3.30. Knowing h, the Biot number can then be calculated, which will determine the ruling heat transfer mechanism in this case: convection or conduction.

3.2.4 Model 1

Whenever heat conduction within an object is much faster than heat transfer across its boundary, the lumped capacitance model may be used. In this sense, if $Bi < 0.1$, the model used to predict the bottle's temperature will be based on the analysis explained in Subsection 3.1.1.1. However, if Bi is bigger than 0.1, the scenario of the one-dimension transient conduction must be applied and will be explained in Subsection 3.2.5.

The temperature profile of the bottle will be predicted with regard to the temperature profile of the air. Both profiles are discretized in time in n points. For every point in this discretization, the bottle temperature is calculated with Equation 3.46, which represents the application of Equation 3.11 in this analysis.

$$T_b(i) = e^{-\frac{hA_b t}{mc_p}} \cdot (T_b(i-1) - T_{lehr}(i)) + T_{lehr}(i) \tag{3.46}$$

In this equation, $T_b(i)$ is the bottle temperature at time i, $T_b(i-1)$ is the bottle temperature at the previous point, and $T_{lehr}(i)$ is the air temperature inside the lehr at time i. This equation will be solved the same n times used to create the list of predicted air temperature profile. That is, for each predicted temperature in this list, the bottle temperature will be the result of Equation 3.46 after the same time step used in the linear interpolation. Each time the loop runs, a list of the predicted bottle temperature with the lumped capacitance analysis will be updated. Then, this list is used to generate the graphic representation of the bottle's temperature profile and compare it with the lehr's temperature profile. A code snippet for this model is presented below.

```
def lumped_system(heat_transfer_coefficient, surface_area, time, mass, specific_heat, temperature_initial, temperature_inf):
    expo = m.exp(-heat_transfer_coefficient * surface_area * time / (mass * specific_heat))
    temperature_bottle = expo * (temperature_initial - temperature_inf) + temperature_inf
    return temperature_bottle

for temperature_lehr in T_lehr_interpolation_list:
        temperature_t = lumped_system(h, surface_area_bottle, time_step, bottle_weight, cp_glass, temperature_bottle_initial_convection, temperature_lehr)
        temperature_bottle_initial_convection = temperature_t
        T_bottle_convec_list.append(temperature_t)
```

The process starts with the bottle temperature corresponding to its inlet temperature measured experimentally and the temperature at infinity corresponding to the lehr's air temperature estimated by the linear interpolation at time zero. In the second cycle in this loop, the temperature of the bottle becomes the result obtained in the previous cycle, and the lehr's air temperature becomes the one calculated by the linear interpolation at time 2.

This model requires information about the bottle's surface area, mass, and c_p. To facilitate the calculations, it was considered that the bottle is a body composed of two cylinders and a truncated cone. The precision achieved in the results of the surface area and volume calculations would not justify the effort to carry out the integration of the sides of the bottle. Therefore, adopting a conservative approximation, the radius of each cylinder and truncated cone correspond to the biggest radius in the respective zone of the original bottle's geometry. The dimensions and the drawing of the adapted geometry for the container being produced currently are shown in Figure 3.4 and Table 3.5, respectively.

Table 3.5: Bottle's dimensions

Container	Dimensions
Volume [L]	0.75
Weight [kg]	0.390
D_b [m]	0.0743
D_{bn} [m]	0.0305
h_b [m]	0.184
h_c [m]	0.044
h_{bn} [m]	0.073

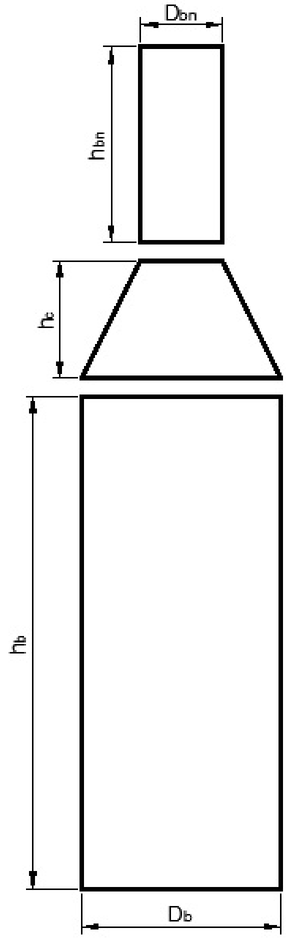

Figure 3.4: Drawing of the adapted bottle's geometry.

The following equations describe the calculations for the surface area and volume of the bottle.

$$A_b = 2\pi \cdot R_b \cdot h_b + 2\pi \cdot R_{bn} \cdot h_{bn} + \pi(R_b + R_{bn}) \cdot \sqrt{(R_b - R_{bn})^2 + h_c^2} \tag{3.47}$$

$$V_{out} = \pi \cdot {R_b}^2 \cdot h_b + \pi \cdot {R_{bn}}^2 \cdot h_{bn} + \pi \cdot h_c({R_b}^2 + R_b \cdot R_{bn} + {R_{bn}}^2) \tag{3.48}$$

$$V_{in} = \pi \cdot {r_b}^2 \cdot h_b + \pi \cdot {r_b}^2 \cdot h_b + \pi \cdot h_c({r_b}^2 + r_b \cdot r_{bn} + {r_{bn}}^2) \tag{3.49}$$

$$V_b = V_{out} - V_{in} \tag{3.50}$$

In these Equations, A_b is the bottle's surface area, V_{out} and V_{in} are the outer and inner bottle's volume, respectively, and V_b is the total bottle's volume. These values will be used in the energy balance and in the characteristic length calculation.

3.2.5 Model 2

If $Bi > 0.1$, the approach to be considered is the one-dimension transient conduction. Applying the one-term approximate solution for a plane wall, Equation 3.20 is modified to Equation 3.51.

$$T_b(\varepsilon_b, i) = C_1 \cdot e^{-\zeta_1^2 Fo} \cdot \cos(\zeta_1 \cdot x^*) \cdot (T_b(i-1) - T_{lehr}(i)) + T_{lehr}(i) \tag{3.51}$$

Again, the bottle temperature will be calculated n times to generate a temperature profile. It will be generated the same way explained in Model 1 in Subsection 3.2.4, where Equation 3.51 is solved in a `for loop` in Python and a list of the bottle's predicted temperature is updated each time the loop runs. For a cycle i in this loop, $T_b(\varepsilon_b, i)$ is the bottle's temperature in its inner wall at time i, $T_b(i-1)$ is the bottle's inner wall temperature at the previous point, $T_{lehr}(i)$ is the air temperature inside the lehr at time i.

However, to obtain the one-dimensional approximate result, Fo and x^* must be previously calculated. Considering that Fo must be higher than 0.2, this constraint will be the one determinant for the maximum number of cycles n_{max} of all predicted temperature lists. A code snippet of this model is presented below.

```
def conduction_plane_wall(c, zeta, fourier, x, L, temperature_initial,
    temperature_inf):
    x_x = x/(L)
    temperature_bottle =
        c*m.exp(-zeta**2*fourier)*m.cos(zeta*x_x)*(temperature_initial -
        temperature_inf) + temperature_inf
    return temperature_bottle

for temperature_lehr in T_lehr_interpolation_list:
        temperature_t = conduction_plane_wall(c1, zeta1, fourier(alpha,
            time_step, bottle_thickness), h_bottle_total,
            bottle_thickness, temperature_bottle_initial_conduction,
            temperature_lehr)
        temperature_bottle_initial_conduction = temperature_t
        T_bottle_cond_list.append(temperature_t)
```

3.2.6 Annealing Validation

Since the annealing point is unique for each type of glass, it can be described as a sum of the products of each component and their respective coefficients. An empirical equation determines the annealing point considering its composition (BA Glass, 2023):

$$T_{annealing} = \sum p_i \cdot \varphi_i + \frac{p_{SiO_2}}{p_{MgO} + p_{CaO}} \cdot \varphi \tag{3.52}$$

where p_i is the percentage of the chemical component i, φ_i is the coefficient of the component i, and φ is a general coefficient of annealing temperature with the value of -2.92. The components used in the formula above are presented in Table 3.6, along with their respective annealing and softening point coefficient. The softening coefficient is only used to calculate the softening point with a similar formula. The percentage is presented as the range proposed in Table 1.1 and the last digits of the annealing and softening coefficients were substituted by "**" due to confidentiality.

Table 3.6: Annealing and softening point coefficients, adapted from BA Glass (2023)

Component	Percentage (%)	Annealing pt. coef.	Softening pt. coef.
SiO_2	70–73	6.**	8.**
Na_2O	12–15	15.**	-1.**
CaO	10–12	7.**	8.**
Al_2O_3	1–2	12.**	16.**
K_2O	0–1	-2.**	-0.**
MgO	0.5–2	5.**	8.**
SO_3	0–0.5	1.**	14.**
Fe_2O_3	0–1	15.**	6.**
Cr_2O_3	0–0.3	0	5.**

In addition, there are several empirical methods to calculate the annealing cycle of glass that present good results in industrial processes. One of the most used in the glass industry is the Corning method. It calculates the time, in minutes, that glass requires above the annealing point as a function of the thickness of the body. However, the relaxation temperature is set at 5 °C above the annealing point.

$$t_{annealing} = \frac{28\varepsilon_b - 3}{100} \tag{3.53}$$

In this Equation, ε_b is the bottle's critical thickness in $[m]$. The bottle's critical thickness will correspond to where residual stresses are most critical. Due to the contact with the conveyor belt, this critical thickness is the bottom wall of the container. Therefore, the thickness is crucial in the relaxation time of a glass container: the bigger the thickness, the greater the required time to eliminate the thermal gradient and the slower the cooling should be.

With the estimated bottle's temperature profile, the next step is to check if the bottle achieve the annealing point for the required time. Using Equation 3.53, it is possible to calculate the time required for a bottle with thickness ε_b to remain above its annealing point. Considering the annealing temperature for the batch and the glass container analysed, the time that the bottles should stay above 547 °C is 11 minutes. Thereafter, the next step is to calculate how long the previously estimated temperature profile of the bottle stays above the annealing point, for Models 1 and 2.

3.2.7 Interface

A user interface (UI) was created to connect the temperature inputs and the temperature profile outputs. The interface allows the input of 10 temperature setpoints, the same number as in the real-life equipment, and the conveyor belt velocity. Currently, the model and interface are designed to work only for the lehr in the study. Adaptation of the interface and algorithm is needed if deploying this tool to other lehrs. It is designed to work only with the studied annealing lehr because every lehr has its own zone designed with different numbers of setpoints. These inputs will generate a comprehensive graph with the calculation explained in SubsSections 3.2.4 and 3.2.5. Therefore, the user can gain valuable insights into the heat distribution and transfer mechanisms that occur during the process. The interface can show the estimated consequences of changing the setpoint temperatures in reality. Due to that, this interface can contribute to optimising the annealing process.

The UI code defines a class that inherits from QWidget class, which is a class from the PyQt library and serves as the base class for all UI elements or widgets. These widgets include buttons, labels, text boxes, and check boxes and can be organized in a hierarchical structure in which one widget can contain another. Subsequently, the widget, the window title, the layout, and the figure plotting are initialized by the `__init__` method. The temperature input fields are created with QLineEdit class and CSS and their values are stored in a list inside the class, and the conveyor velocity input field is added to the layout below the row of temperature input fields and stored as a single variable.

Finally, after the user clicks on the button "Calculate", a graph is created with the aforementioned temperature profiles. When the button is clicked, a method is called and retrieves the conveyor velocity value from the input field and calculates the new annealing time dictionary in minutes and the new annealing present value dictionary based on the user input values. Then, all the related lists and variables are updated with the new input values. The previous plot is cleared, and the new data is added to it.

3.3 Heat Loss

Heat loss, in W, throughout the process, was estimated for the two side walls of the lehr based on Equation 3.41, from which come the following Equations.

$$\Omega_h = \frac{1}{A_w \cdot h} \tag{3.54}$$

$$\Omega_c = \frac{1}{A_w \cdot h_{out}} \tag{3.55}$$

$$\Omega = \frac{\varepsilon_w}{k_w \cdot A_w} \tag{3.56}$$

$$\dot{Q}_w = \frac{\Delta T}{\Omega_h + \Omega_c + \Omega} = \frac{T_{hot} - T_{cold}}{\Omega_h + \Omega_c + \Omega} \tag{3.57}$$

In these Equations, Ω_h is the resistance to heat loss in the hot side (convection inside the lehr), Ω_h is the resistance to heat loss in the cold side (convection in the external air), and Ω is the resistance to heat loss through walls thermal conductivity. The h on the hot side corresponds to the previously estimated heat transfer coefficient, and the h_{out} corresponds to the heat transfer coefficient of the outside air. A value tabulated in the literature for air at 25 °C will be used for it. It is found that h of air ranges between 5 and 20 $\mathrm{W \cdot m^{-2} \cdot K^{-1}}$ for natural convection at this temperature (Kakaç et al., 2013). The chosen value of h is 7 $\mathrm{W \cdot m^{-2} \cdot K^{-1}}$. In addition, the outside air temperature is assumed to be 25 °C.

Heat loss will be calculated in a discretized way, just as the previous temperature profiles explained in Subsections 3.2.2, 3.2.4, and 3.2.4 were calculated. The heat loss flux corresponds to a sum of heat loss fluxes of n wall areas. A time step was calculated previously considering the number of cycles n for the lehr's and bottle's temperature profiles. When multiplied by the conveyor velocity, this time step will generate a length step. Then, the corresponding surface area of this small length will be the length step multiplied by the lehr wall height.

The thickness of the wall and the thermal conductivity of the material need to be determined. The annealing lehr's wall is made mainly of stainless steel and steel St37 in a small portion of its thickness. It is assumed that the wall is made only of stainless steel so that calculations can be simplified since the St37 thickness is not precisely known. According to Davis and Committee (1998), k of stainless steel varies between 15 and 21 $\mathrm{W \cdot m^{-1} \cdot K^{-1}}$ between 25 and 500 °C. The chosen value of k is 18 $\mathrm{W \cdot m^{-1} \cdot K^{-1}}$.

With the parameters set, the thermal conductivity resistance of the wall can be calculated. The result will be stored in a variable called Ω. Thereafter, the heat loss through the wall in kW is calculated by calling a function in a for loop based on the difference between the hot side and the outside air, the surface area of the wall, the heat transfer coefficients for the hot and cold sides, and the thermal resistance of the wall. Each time the loop runs, the temperature of the hot side corresponds to the lehr's temperature estimated by linear interpolation, and the temperature of the cold side, that is, the outside of the lehr, remains constant.

According to Gardon (1982), the lehr's roof and floor can be considered insulated and essentially adiabatic. These components have properties that minimize heat transfer across them. In turn, heat loss through side walls is not negligible. Therefore, only the side walls will be considered in estimating the heat loss, and the heat loss regarding the entrance and exit stages of the process will not also be considered. The result will be multiplied by 2 to represent the heat loss through both side walls. The total heat loss will be the sum of the result in each cycle.

This value can be compared to the energy input of the annealing process. The company keeps a daily record of the energy consumption of natural gas in [Nm^3]. This value can be converted to [kW] to be compared with the estimated loss through the walls with Equation 3.58, where $\dot{E}_{annealing}$ is the power consumption [kW], and V_{gas} is the value of daily input of natural gas in [Nm^3]. V_{gas} needs to be multiplied by the lower heating value of natural gas, which represents the amount of energy released by the complete combustion of the fuel in [kJ]. The lower heating value considers the quality and composition of the mixture of the natural gas used. It is taken from internal company reports and is $LHV = 31736\ \frac{\text{kJ}}{\text{Nm}^3}$. Since the energy consumption value is given in the time-space of one day, it is converted to [kW] when divided by $3600 \cdot 24$ s.

$$\dot{E}_{annealing} = \frac{V_{gas} \cdot 31736}{3600 \cdot 24} \tag{3.58}$$

3.4 Experimental Temperature Data

On April 28, 2023, an experiment was carried out to analyse the temperature variation inside the annealing lehr. The main objective is to evaluate the temperature profile along the lehr's length and, also, along its width. In addition, it is vital to validate the present value measurements of the thermocouples located on the side walls of the lehr.

The experimental setup involves the placement of a mobile thermocouple, a pipe equipped with five thermocouples positioned at equidistant points. These thermocouples were connected to a data acquisition system that recorded temperature readings at regular intervals. Figure 3.5 illustrates a scheme of the mobile sensors being positioned in the real annealing lehr and the five location points for temperature measurement.

The lehr was operated under standard setpoint conditions. However, the experiment took place without any glass container present. Therefore, the absence of glass containers inside the annealing lehr can present an impact on the temperature measurements, as they would act as thermal masses that absorb heat in the first zones and further release heat during the cooling process.

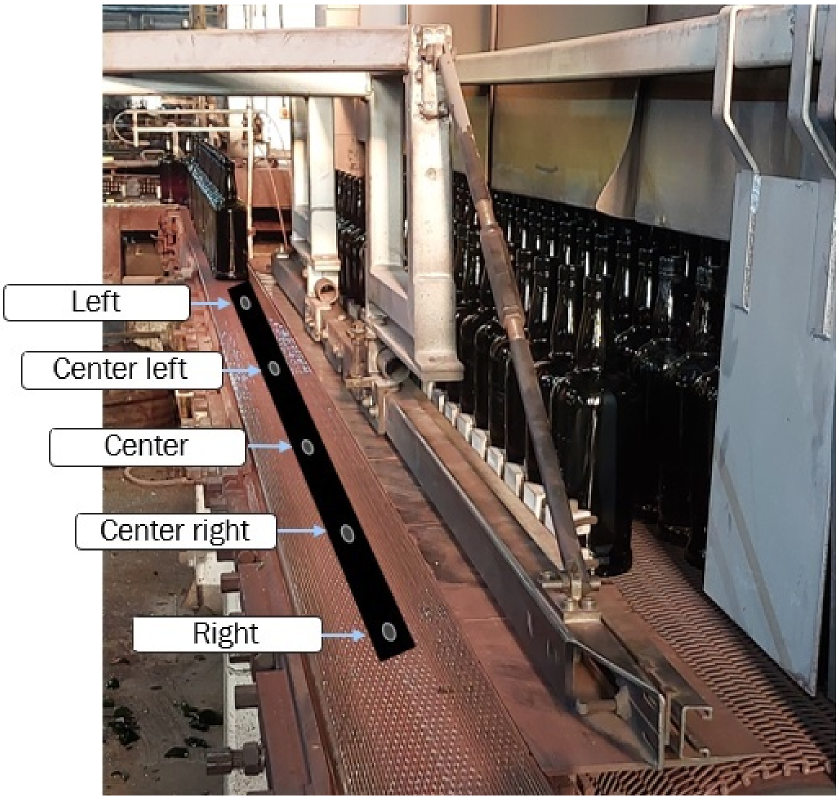

Figure 3.5: Scheme of the experimental data acquisition setup in the conveyor belt.

To have a more precise analysis of the temperature profile, it would be necessary to conduct this experiment concurrently with normal production. However, this could represent a risk for the production. If any bottle fell or jammed during this process, it could result in several minutes or even hours of production stoppage to solve the problem. Therefore, this experiment was conducted during a job change. In other words, the gobs, during this change of moulds, are being constantly rejected, and every process further down the line will be empty during this transitioning time. The annealing lehr and the other machines are functioning with the same conditions as if it was a normal production. Thus, this was the chosen moment to perform the temperature measurement.

The dataset was manipulated from a `.txt` file into a `.csv` file and organized to be manipulated in Python. The code assigns the resulting data from the file to a dataframe and extracts the time column from it. A 2D grid of time and the thermocouples measurements is created. Each series of temperature measurements will be aggregated to form a solid and will be projected to a 3D graph with time as x-axis, temperature as y-axis and series as z-axis.

In addition to the measurement experiment with the sensors, an infrared camera was used to take photographs of the bottles before entering the annealing chamber and at the exit point. These photographs capture the temperature of the object on which it points. The inlet temperature will be used as input for the digital twin and the outlet temperature will be used to validate the temperature profile estimation.

Chapter 4

Results and Discussion

The Results and Discussion presents the results of the Digital Twin explained in Section 3 and discuss their implications, limitations, and significance. In addition, a parallel between the experimental and predicted data is outlined. Appendix B presents the algorithm from which confidential parts have been removed and some data replaced by example values that do not match the ones used to obtain the results presented.

4.1 Digital Twin

The results from the algorithm developed in this work are derived from a series of variables related to the estimation of the bottle's temperature profile. Table 4.1 presents the results obtained for important variables in the heat transfer behaviour that determines the output temperature profile. The calculated Reynolds number, Prandtl number, and Biot number were crucial in deducing the heat transfer coefficient. The significantly low value of Bi is noteworthy because it indicates that the temperature gradient within the glass container is approximately uniform. This uniformity is indicative of the glass's high conductivity and thus validates the employment of Model 1 in this study.

While Model 1 serves as a valid approach, Model 2 required a maximum number of cycles n_{max} of 184 to ensure the Fourier number remained above 0.2. The chosen number of cycles n for both models is 60. The time step, obtained by dividing the total annealing time $t_{annealing}$ by n is 31 s. It should be noted that this time step was consistent with that used in the heat loss estimation.

Table 4.1: Results obtained for heat transfer parameters in the digital twin

Variable	Result
Re	88323
Pr	0.7
h	$11\ \mathrm{W \cdot m^{-2} \cdot K^{-1}}$
Bi	0.036
α	$4.91\ m^2 \cdot s^{-1}$
Fo	0.62
n_{max}	184
n	60
time step	31 s

The temperature estimates for the lehr's air and subsequent results for Model 1 and Model 2 after 60 cycles are depicted in Figures 4.1 and 4.2. In these figures, the air temperature estimated by linear interpolation is denoted by a red line, while the temperature estimated with the corresponding model is indicated by a blue line. To provide a more in-depth analysis of the results, Appendix A presents Tables A.2 and A.3, which offer a discrete overview of the temperature progression across cycles.

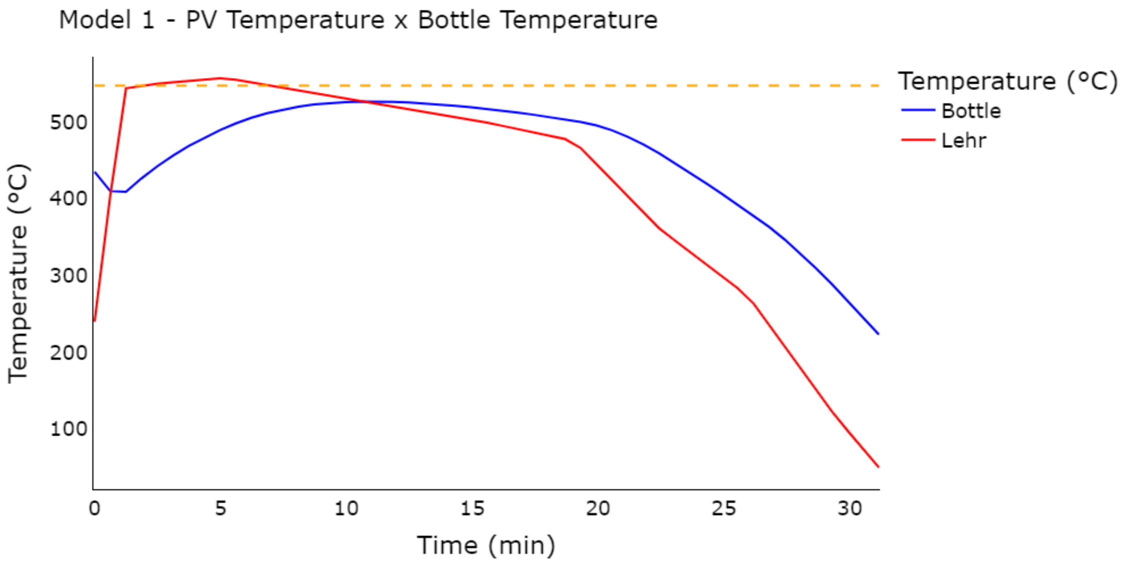

Figure 4.1: Predicted temperature with Model 1.

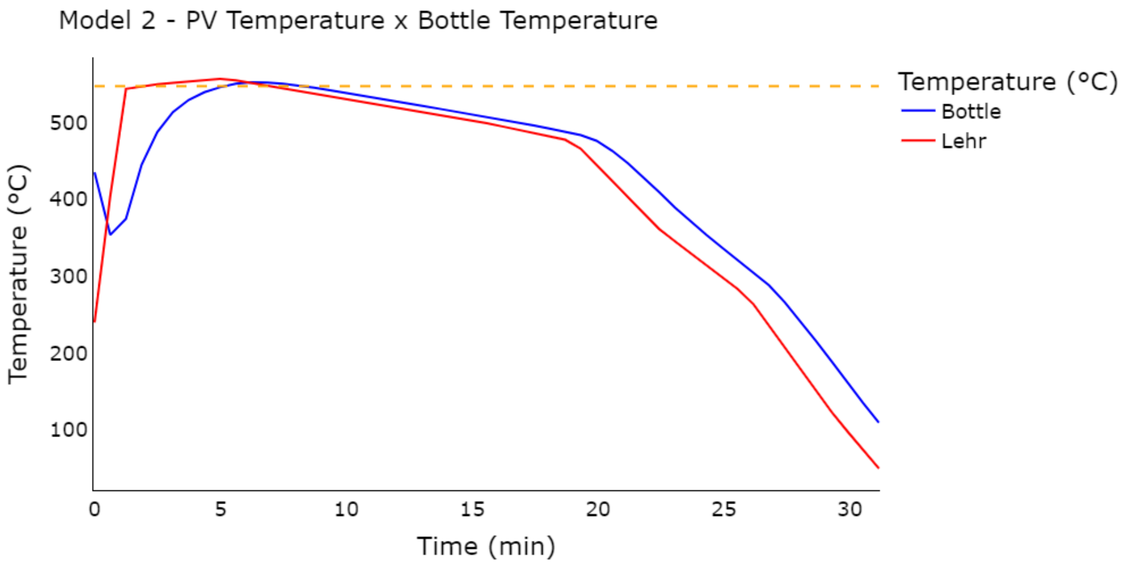

Figure 4.2: Predicted temperature with Model 2.

A key characteristic of Model 1 is its high sensitivity to variations in h values. With an increase in h, the resistance to convection is smaller and the fluid is capable of dispersing heat more rapidly to its surrounding solid. This results in a quicker decrease in the exponential term found in Equation 3.46, leading to a more sharp reduction in the temperature difference between the initial temperature T_i and the lehr temperature T_∞. In other words, a higher heat transfer coefficient makes the bottle's temperature profile increasingly congruent with the lehr's.

In the case of Model 2, the behaviour changes when the number of cycles n in Equation 3.51 is modified. This behaviour is due to the interdependence of the Fourier number with the time step. The time step, in turn, affects the rate at which the bottle's temperature approaches the lehr temperature.

When results from Models 1 and 2 presented in Appendix A are compared, the response of Model 2 is faster, and the temperature of the bottle approaches the air temperature more quickly. This discrepancy can be attributed to the distinct equations used in the models to calculate the temperature at each cycle. Model 1 employs an exponential decay term, whereas Model 2 incorporates an additional cosine term to account for the temperature distribution within the considered plane wall.

4.1.1 Annealing Validation with Experimental Data

Temperature data from the experiment conducted on April 28, 2023, were analysed to understand the temperature distribution width and lengthwise of the annealing lehr. As described in Section 3.4, the experiment was conducted using a mobile thermocouple apparatus, comprised of a tube containing designated spaces for the insertion of five thermocouples, located at the left, center left, center, center right, and right position. This tube enters the lehr and runs through it as if it were a row of glass containers. Unfortunately, erroneous measurements were recorded by the leftmost thermocouple, likely due to physical damage, faulty wiring, or technical issues within the data acquisition system. The same malfunction was detected in experiments repeated on subsequent dates. It was outside the remit of the present work, and its timescale, to fix the issue. Nonetheless, having four thermocouple measurements proved sufficient for the analysis carried out in this work.

Figure 4.3 shows the 3D graph generated with the four valid thermocouple measurements: center left, center, center right, and right.

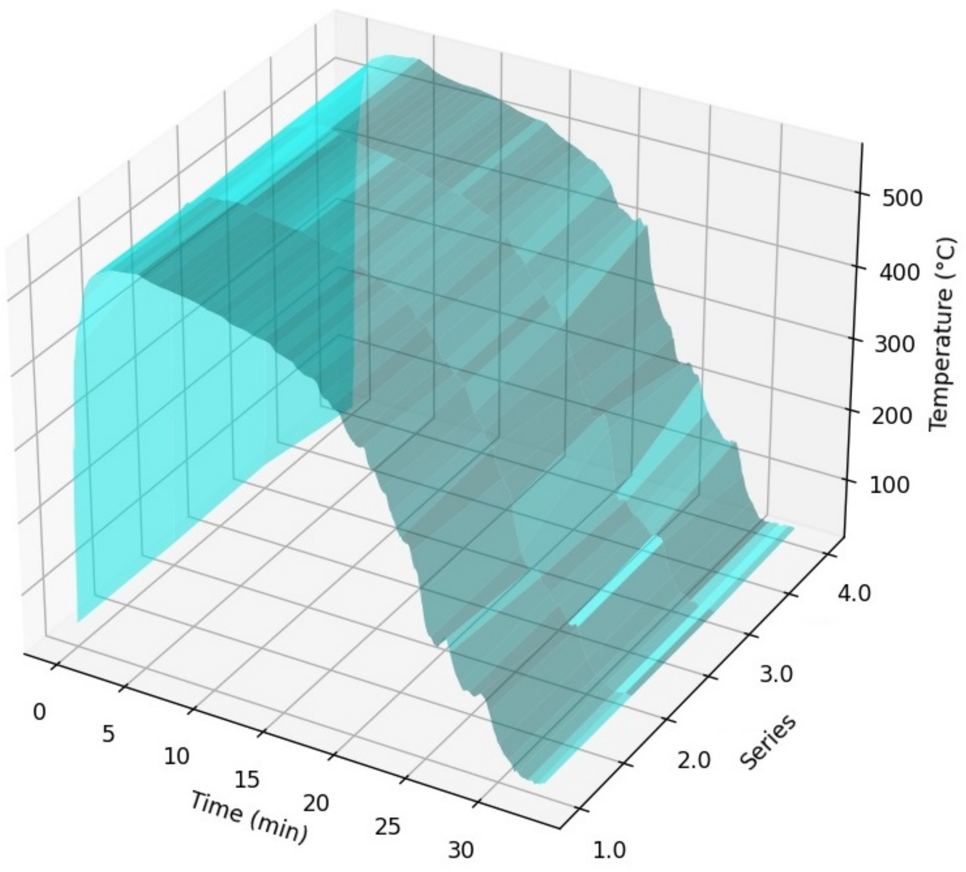

Figure 4.3: Temperature profile in 3D from experimental measurement.

The experiment's temperature data served as a valuable asset for evaluating the accuracy of the linear interpolation method employed to create the air temperature profile inside the lehr. Although this data could not validate the predicted bottle temperatures by Models 1 and 2, it could be utilized to assess the reliability of the interpolation technique.

The Mean Absolute Percentage Error (MAPE) was calculated to compare the interpolated temperature values with the corresponding actual temperature data, measured in the central position. The MAPE, which represents the average percentage difference between the predicted and actual values, served as a quantitative measure of accuracy, with a lower MAPE indicating higher precision and better alignment between the predicted and real temperatures. The MAPE of a curve fitting was also evaluated to analyse the best method for creating the temperature profile of the air inside the lehr.

The comparison between the real data and the predictive methods, including linear regression and curve fitting, can be observed in Figures 4.4 and 4.5. The location of the thermocouple chosen for the comparison is the central, as it represents the overall temperature behaviour inside the lehr.

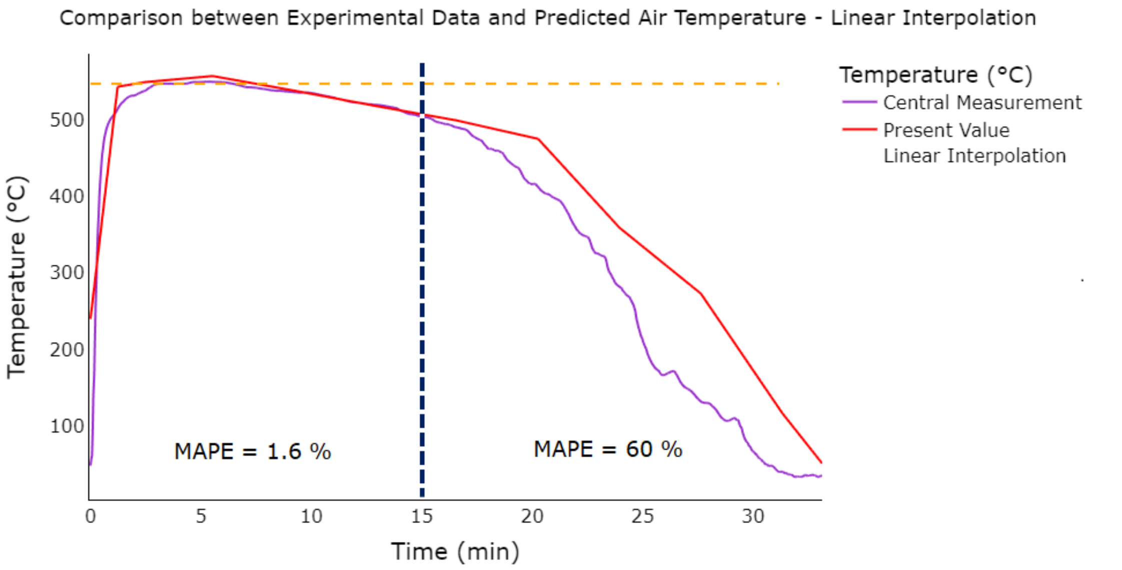

Figure 4.4: Comparison between the measured temperature and predicted temperature with linear interpolation.

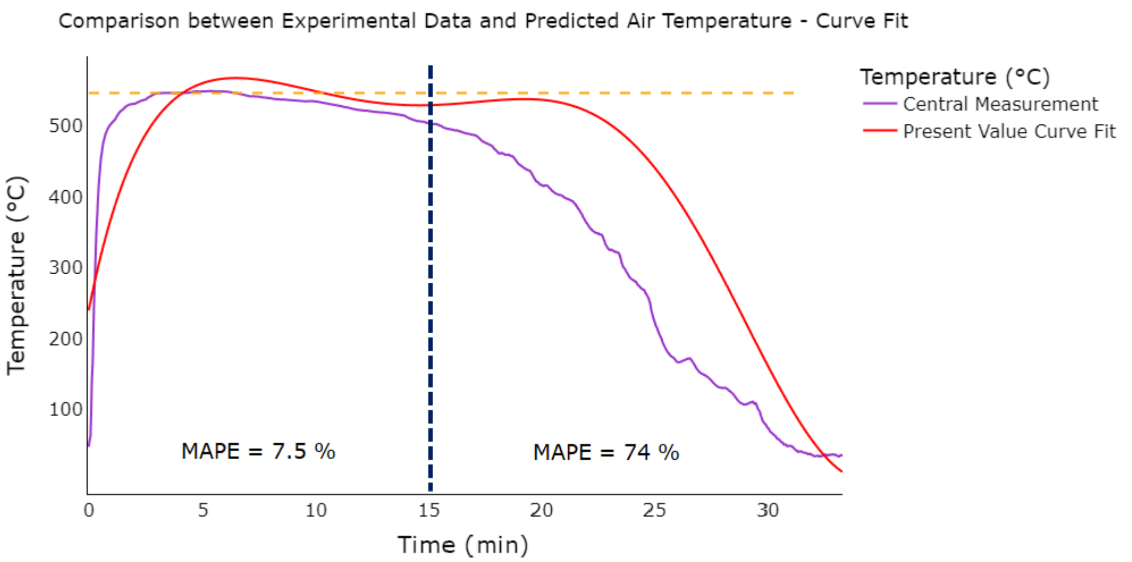

Figure 4.5: Comparison between the measured temperature and predicted temperature with curve fitting.

In Figure 4.4, the linear interpolation profile exhibited a MAPE of 34 %. However, if the temperature profiles are divided according to the heating and cooling stages of annealing presented in Section 2.1, it can be seen that the error of the linear interpolation of the heating zones indicates a low level of deviation between the predicted and actual temperature values. Considering that the heating zones are the most critical stages of the process, it validates the linear interpolation method as a reasonably accurate representation of the air temperature profile inside the lehr. The difference between the predicted and measured values in the last zones of the process can be justified by the heat loss at the outlet of the lehr or by differences between the measurements of the thermocouples located on the side walls that generate the present values temperatures and the one used in the experiment.

In Figure 4.5, the curve fit was calculated with the least square method and generated a polynomial trendline of degree 6. This method yielded a MAPE of 42 %, suggesting a greater level of deviation between the predicted temperature profile and the actual values. The error in the heating zones is 7.5 %, and in the cooling zones is 74 %, both values higher than the ones obtained with linear interpolation.

Based on the MAPE and visual comparisons, the linear interpolation method exhibits better suitability for predicting the temperature distribution inside the lehr. These findings support using linear interpolation as a reliable approach for generating the air temperature profile. It is also possible to avoid predicted air temperatures higher than the maximum measured setpoint with linear interpolation, which would not be possible with curve fitting.

The photographs taken by the infrared camera at the point where the bottles exit the lehr yielded essential insights regarding their temperature. Figure 4.6 captures the temperature at which the bottles leave the cooling zone of the annealing lehr. Appendix A presents other relevant photographs of the bottles entering and leaving the process in Figures A.1, A.2, A.3, A.4, A.5 and A.6. The bottles maintain a temperature exceeding 250 °C when they exit the lehr.

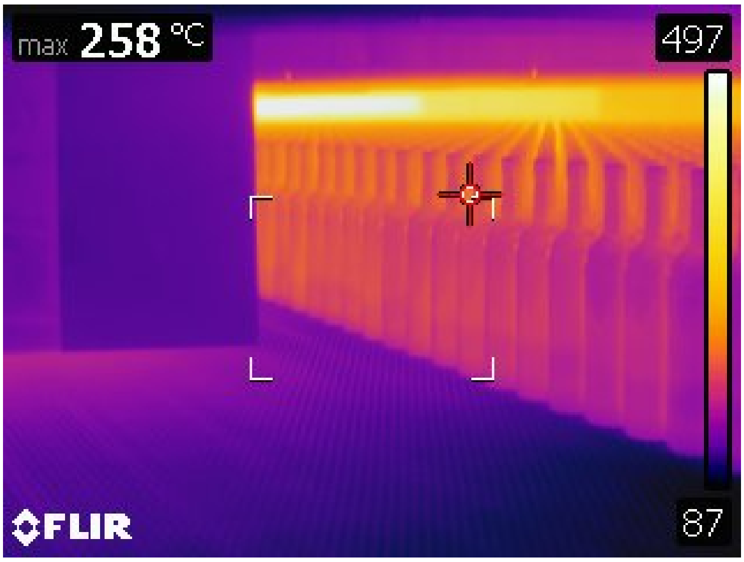

Figure 4.6: Bottles leaving the annealing lehr (a).

This observed data supports the temperature profile predicted by Model 1, demonstrating that the bottles retain the heat even in cooler air temperatures. However, the results obtained by Models 1 and 2 indicate lower temperatures than shown by the photographs. The divergence between the measured temperature by the infrared sensor and the model-predicted temperature can be attributed to the effect of radiation, which is an important form of heat transfer between the bottles and their surroundings in annealing furnaces for flat glass, according to Rantala (2019) and Altun and Başol (2022). The impact of radiation heat transfer should prolong the duration for which the bottle's temperature profile remains above the annealing point. Table 4.2 presents the amount of time, in minutes, that each thermocouple dataset stayed above the specific annealing temperature for that batch composition.

Table 4.2: Time above the annealing point for the measured air temperature and predicted bottle temperature

Position	Time above $T_{annealing}$ [min]	
	Lehr temperature	Bottle temperature
Left	-	-
Center Left	7.96	4.33
Center	6.97	3.05
Center Right	7.67	3.73
Right	6.50	0.73
Average	7.26	3.05

It can be observed that the average time spent above the annealing point regarding the air inside the lehr is approximately 8 minutes. This value is circa 3 minutes for the estimated bottle's temperature, whereas the minimum duration above the annealing point required considering the bottle's thickness is about 11 minutes. Since Equation 3.53 is an empirical equation that considers that the temperature to be reached is 5 °C above the annealing point and adopts a conservative way, it is not possible to say clearly how many minutes above the annealing point is precisely necessary to obtain a successful annealing of glass. Furthermore, it becomes not feasible to arbitrate what is the actual threshold that indicates the turning point of the success of the process. Because of that, it does not necessarily indicate that 8 minutes above the annealing point is inherently insufficient and results in unsatisfactory annealing. In addition, the model does not accommodate energy transfer due to radiation between bottles. The radiation effect should increase the duration above the annealing point of the bottle's temperature profile.

4.1.2 Model Limitations and Sensitivity Analysis

It is noteworthy to remember that key parameters such as h, k, c_p, and ρ were considered constant. In reality, radiative heat transfer is the dominant mode of heat transfer in the annealing process (Altun and Başol, 2022), and the radiative heat transfer rate is strongly temperature dependent. Assuming an overall constant h can be significantly inaccurate since it can vary considerably along the length of the lehr (Gardon, 1982).

The calculated h value falls below the expected range for forced convection in an enclosure. It is highly dependent on the air velocity, and a higher air velocity increases h since Nu can be expressed as a function of Re, which in turn is a function of the fluid velocity. It is crucial to find more accurate velocity values. Conducting experiments or simulations to determine the actual air velocity within the annealing lehr can help refine the model and enhance its predictive capabilities. The direct air velocity measurement can be done with an anemometer or a Pitot tube (Krach and Kruczkowski, 2016).

In summary, the limitations of this study can be highlighted as follows:

- **Simplified modelling assumptions**: The analysis assumes convective heat transfer as the primary mode of heat transfer, neglecting the influence of radiative heat transfer;
- **Limited consideration of material properties**: The modelling does not account for variations in physical properties such as heat transfer coefficient, thermal conductivity, specific heat, and density. Ignoring temperature-dependent material properties may introduce uncertainties and inaccuracies in the predicted temperature profiles;
- **Accuracy in forecasting air temperature**: The analysis employs linear interpolation to generate the air temperature profile inside the lehr. While it provides reasonably accurate forecasting for the first zones, there may be discrepancies in the cooling zones when compared to the real data;
- **Limitations in validating Models**: The analysis lacks direct validation of the predicted bottle temperatures, which introduces uncertainty regarding the accuracy of the digital twin in predicting the actual bottle temperatures;

A sensitivity analysis was conducted to assess the influence of specific input parameters on important output values. The analysis considered the air velocity v, thermal conductivity k, specific heat capacity c_p, and density ρ of glass as the input parameters. The one-factor-at-a-time method was employed, where each parameter was varied individually while keeping the other parameters at their base values. The lower and upper values of the glass properties are the ones corresponding to temperatures between 400 and 800 °C. The selected output parameters for evaluation were the convective heat transfer coefficient h, Biot number Bi, and thermal diffusivity α.

Tables 4.3, 4.4, 4.5, and 4.6 each relate to a different input parameter and show the results of the sensitivity analysis. The tables show the output parameter values for various input parameter values between their lower and higher bounds. These values were calculated based on the sequence diagram presented in Figure 3.1.

Table 4.3: Sensitivity analysis results for air velocity

Input Parameter			Output Parameter		
			h [$W \cdot m^{-2} \cdot K^{-1}$]	Bi	α [10^{-7} $m^2 \cdot s^{-1}$]
v	Base Value	4	11	0.036	4.91
	Lower Limit	2	6.32	0.021	4.91
	Upper Limit	8	19.16	0.063	4.91

Table 4.4: Sensitivity analysis results for glass thermal conductivity

Input Parameter			Output Parameter		
			h [$W \cdot m^{-2} \cdot K^{-1}$]	Bi	α [10^{-7} $m^2 \cdot s^{-1}$]
k	Base Value	1.51	11	0.036	4.91
	Lower Limit	1.2	11	0.046	3.53
	Upper Limit	2	11	0.028	5.88

Table 4.5: Sensitivity analysis results for glass heat capacity

Input Parameter			Output Parameter		
			h [$W \cdot m^{-2} \cdot K^{-1}$]	Bi	α [10^{-7} $m^2 \cdot s^{-1}$]
c_p	Base Value	1214	11	0.036	4.91
	Lower Limit	1100	11	0.036	4.62
	Upper Limit	1300	11	0.036	4.14

Table 4.6: Sensitivity analysis results for glass density

Input Parameter			Output Parameter		
			h [$W \cdot m^{-2} \cdot K^{-1}$]	Bi	α [10^{-7} $m^2 \cdot s^{-1}$]
ρ	Base Value	2540	11	0.036	4.91
	Lower Limit	2200	11	0.036	5.67
	Upper Limit	2800	11	0.036	4.45

Changes in the input parameters have varied effects on the output parameters. The heat transfer coefficient is primarily influenced by changes in velocity and exhibits significant variations between the lower and upper limits of velocity values. Bi is affected by variations in both the velocity and k of the glass. On the other hand, α is mainly influenced by variations in k, c_p, and ρ. Among these parameters, the glass density has the least significant effect on thermal diffusivity.

4.1.3 Interface

Figure 4.7 shows the graphical user interface created to provide insights into the transport phenomena in the glass containers throughout the annealing process. This UI enables the user to choose the setpoint temperatures, as well as the conveyor velocity, and visualize the temperature profiles. The number of times to calculate the bottle's temperature profile of the interface was also 60. If the user wants a higher number of cycles, the number should be changed in the code.

Since the Biot number is < 0.1 and it is the Model that comes closest to the values measured at the bottles at the lehr's exit, Model 1 was used to represent the bottle temperature profile in the UI.

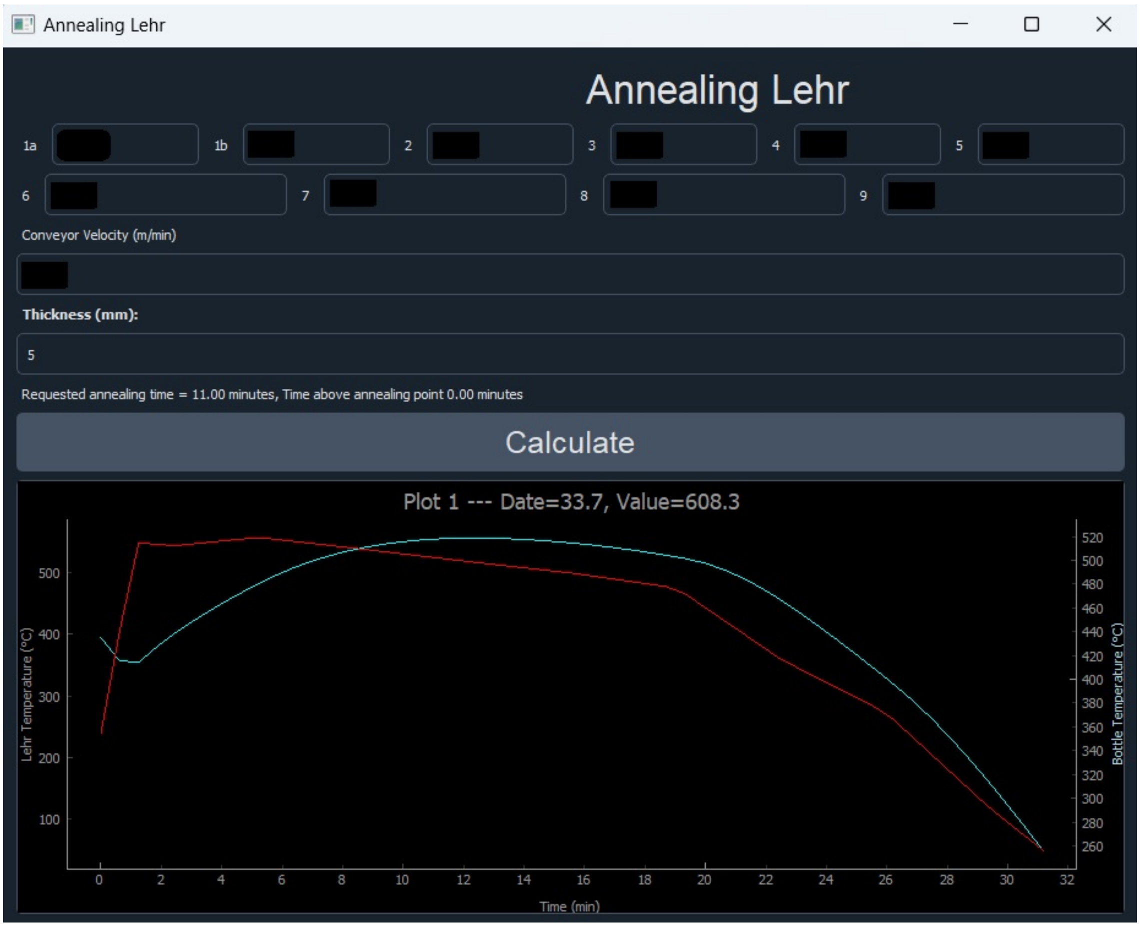

Figure 4.7: Interface for studied annealing lehr.

The interface was implemented with the PyQt5 library, and upon clicking the "Calculate" button, the application performs the necessary computations and generates a temperature graph. Additionally, the interface allows users to track their mouse movements on the graph, providing real-time temperature information at specific time points. Therefore, this UI can be a valuable tool for analysing and understanding temperature variations during the process. The setpoint temperatures, conveyor velocity, and the name of the line were omitted due to confidentiality.

In the future, data inputs should be stored in configuration files. These input data are the temperature setpoints, bottle properties, conveyor belt speed and other operational parameters. The UI is currently designed to run considering the input data from a specific annealing lehr from a line. Configuration files, such as JSON, YAML, or INI files) are a valid option to store input data and can be read within a Python script and have the required values extracted. This allows the user to modify the inputs externally without modifying the script itself.

Moreover, the algorithm can be integrated into a real-time control system, enabling automated adjustments of the annealing process parameters based on the predicted temperature profiles. Since the algorithm is implemented in Python, the interface needs to communicate with the annealing controller by using Python-based systems, such as PyPLC and pyModbus.

4.2 Heat Loss

The heat loss through the lehr's wall is estimated at 60 kW. This heat loss rate is a significant factor in its overall performance since it is already a substantial value. Furthermore, this heat loss rate mainly depends on the material thermal conductivity and the side wall's thickness. While it may not be feasible to change the material of the wall in an existing annealing lehr due to various constraints, such as cost, time, and disruption to production, it is important to consider it for future production lines.

By analysing the daily natural gas input in [Nm^3] in the annealing process between February and May, and converting it to [kW] with Equation 3.58, it was found that the average value was approximately 140 kW. This indicates the substantial impact of heat loss during annealing, as the heat loss rate accounts for about 40 % of the energy supplied to the process. Comparisons with other annealing lehrs in different BA Glass plants reveal varying patterns of natural gas input. For instance, in the Gardelegen plant with more modern lehrs, the daily natural gas input is the lowest among BA plants.

Modern lehrs are designed with improved insulation materials, thermal barriers, and energy-efficient features, resulting in reduced heat loss and enhanced overall performance. Investing in new technology can yield significant advantages in the long run. Therefore, optimising the lehr's thermal efficiency may rely on improving the lehr's design rather than solely relying on increasing the annealing time to lower the temperature setpoints. In summary, addressing heat loss through the lehr's walls, considering future possibilities for wall material, and investing in modern, energy-efficient lehr designs can lead to improved thermal efficiency and overall performance.

Chapter 5

Conclusions

5.1 Achievements

This work presented an algorithm for analysing the temperature distribution of glass containers inside an annealing lehr. The algorithm considered forced convection and one-dimensional transient conduction. The results obtained from the algorithm provided insights into the heat transfer behaviour and validated the use of Model 1 in this study. The analysis highlighted the sensitivity of Model 1 to variations in the heat transfer coefficient, which significantly influenced the temperature profile of the glass containers. Model 2, on the other hand, exhibited a different behaviour due to the interdependence of the Fourier number and the time step. The comparison between Models 1 and 2 showed that Model 2 resulted in a faster response and closer alignment with the air temperature inside the lehr.

The experimental data collected using thermocouples provided valuable information for evaluating the accuracy of the linear interpolation method employed to estimate the air temperature profile. The linear interpolation method exhibited reasonably accurate results, with a lower Mean Absolute Percentage Error (MAPE) compared to a polynomial curve fitting approach.

The limitations of this study included the simplified modelling assumptions, limited consideration of material properties, and the absence of direct validation of the predicted bottle temperatures. Furthermore, the algorithm did not account for radiation heat transfer, which is a significant factor in glass annealing processes.

The average power input for the annealing lehr is 140 kW, while the estimated heat loss through the side walls is approximately 60 kW. Nevertheless, based on the analysis conducted, it can be concluded that the studied annealing lehr is operating close to its optimal performance.

In addition, a user interface was developed to specifically accommodate the geometry and material properties of the studied annealing lehr. The integration of the digital twin and its user interface holds significant potential for aiding decision-making processes. Incorporating real-time predictions of temperature variations can be particularly valuable when considering changes in glass container types, designs, or geometric properties.

To further improve the accuracy of temperature forecasts, it is recommended to enhance the digital twin by refining its assumptions regarding transfer phenomena. Additionally, establishing a connection between the digital twin and the annealing lehr's control panel would be beneficial. This integration would facilitate seamless communication and enable more effective control and monitoring of the annealing process.

5.2 Future Work

The algorithm used to analyse heat transfer in a glass tempering furnace should incorporate radiation heat transfer to improve accuracy. The current method focuses on convection and conduction but neglects radiation, which can significantly affect temperature projections. A more thorough and realistic model can be created by including radiative heat transfer in the algorithm, allowing for a more precise assessment of the temperature distribution and energy transfer inside the annealing lehr.

The interface should be enhanced to connect with the annealing lehr's control systems, using specific communication protocols. In addition, validation of the model over extended periods is necessary, comparing predictions with actual lehr behaviour. Different glass container designs and compositions should also be tested. Therefore, the interface could be scalable to other glass tempering furnaces.

Using infrared temperature sensors on the lehr's sidewalls can measure bottle temperature without contact, which would validate the predictive models. Due to its non-contact with the bottles, potential damage or disruption in the process would be avoided.

Bibliography

Altun, G. C., & Başol, A. M. (2022). Numerical analysis of the radiant heating effectiveness of a continuous glass annealing furnace. *Applied Thermal Engineering*, *204*, 117943. https://doi.org/https://doi.org/10.1016/j.applthermaleng.2021.117943 (Cited on pages 14, 19, 56)

Alves, J. F. (2003). *Ba - marca com história no vidro de embalagem*. BA Vidro, S.A. (Cited on page 4).

Ammar, S. M., & Park, C. W. (2020). Validation of the gnielinski correlation for evaluation of heat transfer coefficient of enhanced tubes by non-linear regression model: An experimental study of absorption refrigeration system. *International Communications in Heat and Mass Transfer*, *118*, 104819. https://doi.org/https://doi.org/10.1016/j.icheatmasstransfer.2020.104819 (Cited on page 27)

Azizi, N., & Zolfaghari, S. (2004). Adaptive temperature control for simulated annealing: A comparative study. *Computers & Operations Research*, *31*(12), 2439–2451. http://www.elsevier.com/locate/dsw (Cited on pages 16, 19)

BA Glass. (2023). *Internal Documents* [BA Glass, Internal Document]. (Cited on pages 5, 12, 45).

Behera, P. (2009). *Analysis of transient heat conduction in different geometries*. (Cited on page 21).

Benbahouche, S., Roumili, F., & Sangleboeuf, J.-C. (2011). Modelling of internal stresses in sheet glass during the cooling. *World Journal of Nano Science and Engineering*, *1*, 21–26. https://doi.org/10.4236/wjnse.2011.12004 (Cited on page 17)

Bingham, P. A. (2010). Design of new energy-friendly compositions. In F. T. Wallenberger & P. A. Bingham (Eds.), *Fiberglass and glass technology: Energy-friendly compositions and applications* (pp. 286–289). Springer. https://doi.org/10.1007/978-1-4419-0736-3_11. (Cited on pages 2, 4, 38, 39)

Bird, R., Stewart, W., & Lightfoot, E. (2002). *Transport phenomena*. J. Wiley. https://books.google.pt/books?id=wYnRQwAACAAJ. (Cited on page 26)

C148 - Standard Test Methods for Polariscopic Examination of Glass Containers (2017th ed.). (2022). ASTM International. The address of the publisher. (Cited on page 13).

Çengel, Y. A. (2002). *Heat transfer; a pratical approach* (2nd). McGraw-Hill. (Cited on pages 22, 23, 25, 29, 30, 39).

Çengel, Y., & Cimbala, J. (2018). *Fluid mechanics: Fundamentals and applications*. McGraw-Hill Education. https://books.google.pt/books?id=DqFJvgAACAAJ. (Cited on pages 28, 40)

Chui, G. K. (1977). Heat transfer and temperature control in an annealing lehr for float glass. *Journal of the American Ceramic Society*, *60*(11-12) (Cited on pages 16, 19).

Churchill, S. W., & Bernstein, M. (1977). A correlating equation for forced convection from gases and liquids to a circular cylinder in crossflow. *Journal of Heat Transfer-transactions of The Asme*, *99*, 300–306 (Cited on page 28).

Das, R., & Ooi, K. (2013). Application of simulated annealing in a rectangular fin with variable heat transfer coefficient. *Inverse Problems in Science and Engineering*, *21*(8), 1352–1367. https://doi.org/10.1080/17415977.2013.764294 (Cited on pages 17, 19)

Davis, J., & Committee, A. I. H. (1998). *Metals handbook desk edition 2nd edition*. Taylor & Francis. https://books.google.pt/books?id=IpEnvBtSfPQC. (Cited on page 47)

Deissler, R. J. (1987). The convective nature of instability in plane Poiseuille flow. *The Physics of Fluids*, *30*(8), 2303–2305. https://doi.org/10.1063/1.866118 (Cited on page 29)

Dittus, F., & Boelter, L. (1985). Heat transfer in automobile radiators of the tubular type. *International Communications in Heat and Mass Transfer*, *12*(1), 3–22. https://doi.org/https://doi.org/10.1016/0735-1933(85)90003-X (Cited on page 29)

Ehrt, D., & Vogel, W. (1992). Radiation effects in glasses. *Nuclear Instruments and Methods in Physics Research Section B: Beam Interactions with Materials and Atoms*, *65*(1), IN1–8. https://doi.org/https://doi.org/10.1016/0168-583X(92)95006-D (Cited on page 31)

Endrys, J., & Turkiz, D. (1985). Die temperaturverteilung in glas bei stationärem zustand. *Internationale Baustoff- und Silikattagung Weimar*, 35–40 (Cited on page 39).

Franco, D., Zapata, N., Montoya, V., Jiménez, C., & López, E. (2018). Optimización de un proceso de recocido: Una aproximación desde la estadística y la ciencia de materiales a un caso de aplicación en la manufactura de envases de vidrio. *Revista Colombiana de Materiales*, *12*, 42–52 (Cited on page 18).

Gardon, R. (1982). Modelling annealing lehrs for flat glass. *Research staff, Ford Motor Company* (Cited on pages 48, 56).

Glass, B. (2022). Glass container production process. (Cited on pages 2, 4, 8, 9, 11).

Goldsmith, A. (1962). *Handbook of thermophysical properties of solid materials*. Pergamon Press. https://books.google.pt/books?id=FPgeAAAAMAAJ. (Cited on page 39)

Grushko, I. S. (2018). Computation of foam glass thermal field in the annealing process. *Glass Physics and Chemistry*, *44*(3), 228–233 (Cited on pages 15, 19).

Holman, J. (2010). *Heat transfer: Tenth edition*. McGraw-Hill Education. https://books.google.pt/books?id=7TGGPwAACAAJ. (Cited on pages 21, 33)

Incropera, F. P. (2006). *Introduction to heat transfer* (5th). Wiley. (Cited on pages 22, 24).

Kakaç, S., Yener, Y., & Pramuanjaroenkij, A. (2013). *Convective heat transfer, third edition*. Taylor & Francis. https://books.google.pt/books?id=PyctAgAAQBAJ. (Cited on pages 20, 22, 26, 47)

Krach, A., & Kruczkowski, J. (2016). Calibration of a system for measuring low air flow velocity in a wind tunnel. *Metrologia*, *53*(4), 1012. https://doi.org/10.1088/0026-1394/53/4/1012 (Cited on page 57)

Littleton, J. T., & Roberts, E. H. (1920). A method for determining the annealing temperature of glass. *J. Opt. Soc. Am.*, *4*(4), 224–229. https://doi.org/10.1364/JOSA.4.000224 (Cited on page 4)

Moore, J., & Sharp, D. E. (1958). Note on calculation of effect of temperature and composition on specific heat of glass. *Journal of the American Ceramic Society*, *41*, 461–463 (Cited on page 38).

Munson, B., Rothmayer, A., & Okiishi, T. (2012). *Fundamentals of fluid mechanics, 7th edition*. Wiley. https://books.google.pt/books?id=GQMcAAAAQBAJ. (Cited on pages 27, 28)

Musikant, S. (2003). Glass. In R. A. Meyers (Ed.), *Encyclopedia of physical science and technology (third edition)* (Third Edition, pp. 781–806). Academic Press. https://doi.org/https://doi.org/10.1016/B0-12-227410-5/00292-1. (Cited on page 30)

National Renewable Energy Lab., C. (, Golden. (2002). Glass industry of the future: Energy and environmental profile of the u. s. glass industry [Report documenting the partnership between DOEs Office of Industrial Technologies and the U.S. glass industry.] (Cited on page 1).

Navarro, J. (2003). *El vidrio*. Consejo Superior de Investigaciones Científicas. https://books.google.pt/books?id=4GsNCPQRaTwC. (Cited on pages 1, 3, 4, 7, 12, 23)

Rantala, M. (2015). *Heat transfer phenomena in float glass heat treatment processes* (Doctoral dissertation No. 1355) [Publication 1355]. Tampere University of Technology. Tampere, Finland. (Cited on pages 30–32, 39, 41).

Rantala, M. (2019). Thermal radiation and forced convection in flat glass tempering furnaces. *GPD 2019 Conference Proceedings* (Cited on pages 9, 15, 19, 56).

Schlichting, H., & Gersten, K. (2017). *Boundary-layer theory*. Springer. (Cited on page 28).

Schmitz, A., Kamiński, J., Maria Scalet, B., & Soria, A. (2011). Energy consumption and co2 emissions of the european glass industry. *Energy Policy*, *39*(1), 142–155. https://doi.org/https://doi.org/10.1016/j.enpol.2010.09.022 (Cited on page 5)

Schneider, P. (1955). *Conduction heat transfer*. Addison-Wesley Publishing Company. https://books.google.pt/books?id=DTBRAAAAMAAJ. (Cited on page 25)

Shah, R., & London, A. (1978). *Laminar flow forced convection in ducts: A source book for compact heat exchanger analytical data*. Academic Press. https://books.google.pt/books?id=FtNFAQAAIAAJ. (Cited on page 26)

Sharp, D. E., & Ginther, L. B. (1951). Effect of composition and temperature on the specific heat of glass. *Journal of the American Ceramic Society*, *34*, 260–271 (Cited on page 38).

Tyutyunnik, V. E., & Guloyan, Y. A. (2000). IR-Annealing Technology for Glass Products. *Glass and Ceramics*, *57*(7-8), 33–36. https://doi.org/10.1007/s10717-000-0179-2 (Cited on pages 18, 19)

Vellini, M., & Savioli, M. (2009). Energy and environmental analysis of glass container production and recycling [ECOS 2007]. *Energy*, *34*(12), 2137–2143. https://doi.org/https://doi.org/10.1016/j.energy.2008.09.017 (Cited on pages 1, 2)

Venkanna, B. (2010). *Fundamentals of heat and mass transfer*. Prentice-Hall Of India Pvt. Limited. https://books.google.pt/books?id=FGzkNIdTVC4C. (Cited on page 29)

Vidromecânica. (2019). *Arca de Recozimento* [BA Glass, Internal Document]. (Cited on page 36).

Welty, J., Rorrer, G., & Foster, D. (2014). *Fundamentals of momentum, heat, and mass transfer* (Sixth). Wiley. (Cited on page 27).

Winterton, R. (1998). Where did the dittus and boelter equation come from? *International Journal of Heat and Mass Transfer*, *41*(4), 809–810. https://doi.org/https://doi.org/10.1016/S0017-9310(97)00177-4 (Cited on page 29)

Appendix A

Figures and Tables

Table A.1: Coefficients used in the one-term approximate solution of one-dimensional transient conduction in plane walls, cylinders, and spheres

Biot	Wall - C_1	Wall - ζ_1	Cylinder - C_1	Cylinder - ζ_1	Sphere - C_1	Sphere - ζ_1
0.01	0.0998	1.0017	0.1412	1.0025	0.173	1.003
0.02	0.141	1.0033	0.1995	1.005	0.2445	1.006
0.04	0.1987	1.0066	0.2814	1.0099	0.345	1.012
0.06	0.2425	1.0098	0.3438	1.0148	0.4217	1.0179
0.08	0.2791	1.013	0.396	1.0197	0.486	1.0239
0.1	0.3111	1.0161	0.4417	1.0246	0.5423	1.0298
0.2	0.4328	1.0311	0.617	1.0483	0.7593	1.0592
0.3	0.5218	1.045	0.7465	1.0712	0.9208	1.088
0.4	0.5932	1.058	0.8516	1.0931	1.0528	1.1164
0.5	0.6533	1.0701	0.9408	1.1143	1.1656	1.1441
0.6	0.7051	1.0814	1.0184	1.1345	1.2644	1.1713
0.7	0.7506	1.0918	1.0873	1.1539	1.3525	1.1978
0.8	0.791	1.1016	1.149	1.1724	1.432	1.2236
0.9	0.8274	1.1107	1.2048	1.1902	1.5044	1.2488
1	0.8603	1.1191	1.2558	1.2071	1.5708	1.2732
2	1.0769	1.1785	1.5995	1.3384	2.0288	1.4793
3	1.1925	1.2102	1.7887	1.4191	2.2889	1.6227
4	1.2646	1.2287	1.9081	1.4698	2.4556	1.7202
5	1.3138	1.2403	1.9898	1.5029	2.5704	1.787
6	1.3496	1.2479	2.049	1.5253	2.6537	1.8338
7	1.3766	1.2532	2.0937	1.5411	2.7165	1.8673
8	1.3978	1.257	2.1286	1.5526	2.7654	1.892
9	1.4149	1.2598	2.1566	1.5611	2.8044	1.9106
10	1.4289	1.262	2.1795	1.5677	2.8363	1.9249
20	1.4961	1.2699	2.288	1.5919	2.9857	1.9781
30	1.5202	1.2717	2.3261	1.5973	3.0372	1.9898
40	1.5325	1.2723	2.3455	1.5993	3.0632	1.9942
50	1.54	1.2727	2.3572	1.6002	3.0788	1.9962
100	1.5552	1.2731	2.3809	1.6015	3.1102	1.999
∞	1.5708	1.2732	2.4048	1.6021	3.1416	2

Table A.2: Predicted temperature of Model 1 and 2

i	Time [min]	Model 1 - Bottle Temperature [°C]	Model 2 - Bottle Temperature [°C]
0	0	435	435
1	0.5	418.5	353.8
2	1.0	414.9	363.2
3	1.6	423.2	425.5
4	2.1	433.5	475.3
5	2.6	443.2	505.5
6	3.1	452.2	524.0
7	3.6	460.6	535.3
8	4.2	468.4	542.6
9	4.7	475.7	547.4
10	5.2	482.4	550.8
11	5.7	488.8	553.4
12	6.2	494.3	553.7
13	6.7	499.1	552.7
14	7.3	503.3	550.9
15	7.8	506.9	548.7
16	8.3	509.9	546.2
17	8.8	512.5	543.6
18	9.3	514.5	540.8
19	9.9	516.2	538.0
20	10.4	517.4	535.1
21	10.9	518.3	532.1
22	11.4	518.9	529.2
23	11.9	519.2	526.2
24	12.5	519.2	523.2
25	13.0	518.9	520.2
26	13.5	518.4	517.3
27	14.0	517.7	514.4
28	14.5	516.9	511.6
29	15.1	515.8	508.7
30	15.6	514.7	505.9

Table A.3: Predicted temperature of Model 1 and 2

i	Time [min]	Model 1 - Bottle Temperature [°C]	Model 2 - Bottle Temperature [°C]
31	16.1	513.3	503.0
32	16.6	511.8	499.8
33	17.1	510.1	496.5
34	17.7	508.3	493.0
35	18.2	506.3	489.5
36	18.7	504.1	486.0
37	19.2	501.9	482.4
38	19.7	499.1	476.9
39	20.2	495.1	466.4
40	20.8	489.9	453.1
41	21.3	483.8	438.1
42	21.8	476.6	422.0
43	22.3	468.6	405.4
44	22.8	459.8	388.5
45	23.4	450.6	372.6
46	23.9	441.0	358.0
47	24.4	431.1	344.1
48	24.9	421.0	330.6
49	25.4	410.7	317.3
50	26.0	400.1	304.2
51	26.5	389.3	291.2
52	27.0	377.5	273.9
53	27.5	364.7	254.0
54	28.0	351.0	232.7
55	28.6	336.4	210.5
56	29.1	321.1	187.8
57	29.6	305.2	164.8
58	30.1	288.7	142.1
59	30.6	271.9	120.5
60	31.2	254.8	99.5

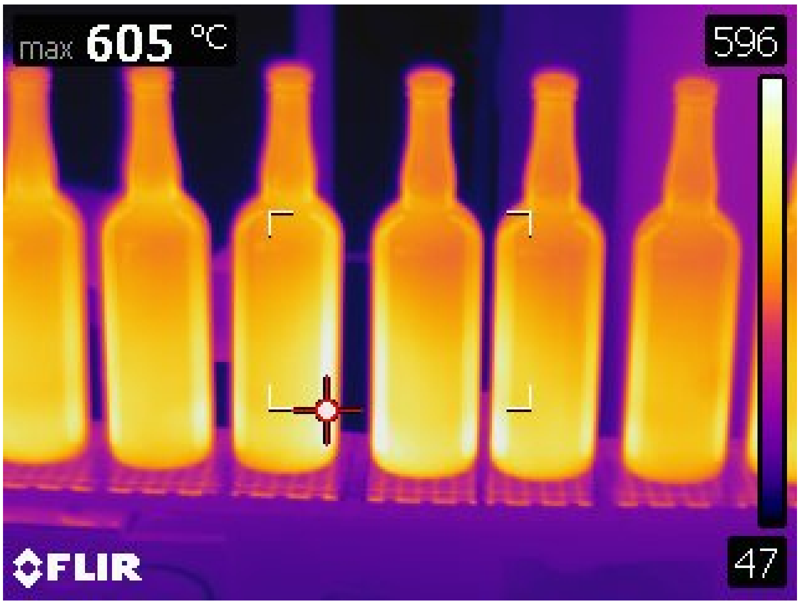

Figure A.1: Bottles between forming and annealing process (a).

Figure A.2: Bottles between forming and annealing process (b).

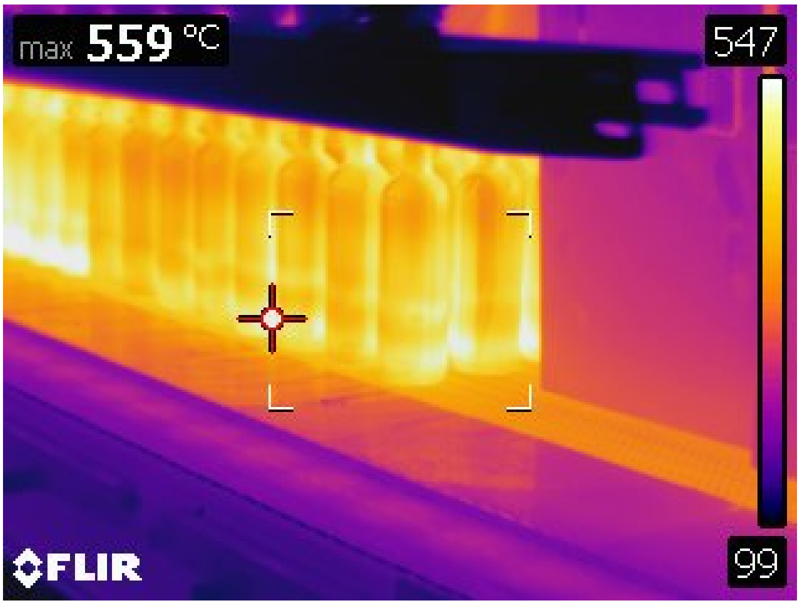

Figure A.3: Bottles entering the annealing lehr (a).

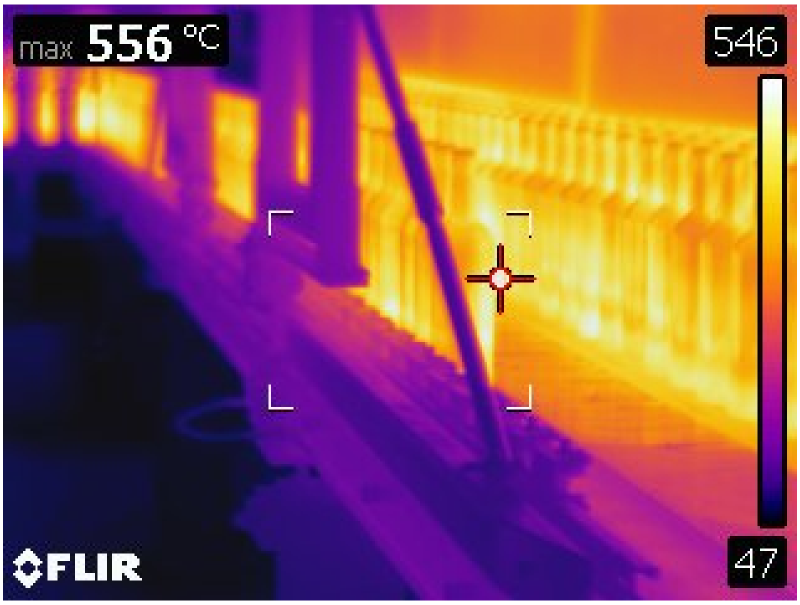

Figure A.4: Bottles entering the annealing lehr (b).

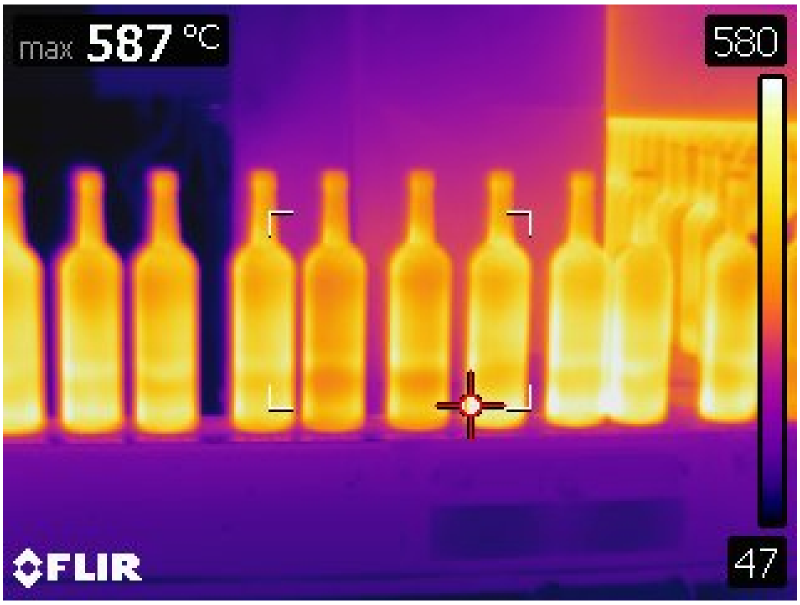

Figure A.5: Bottles entering the annealing lehr (c).

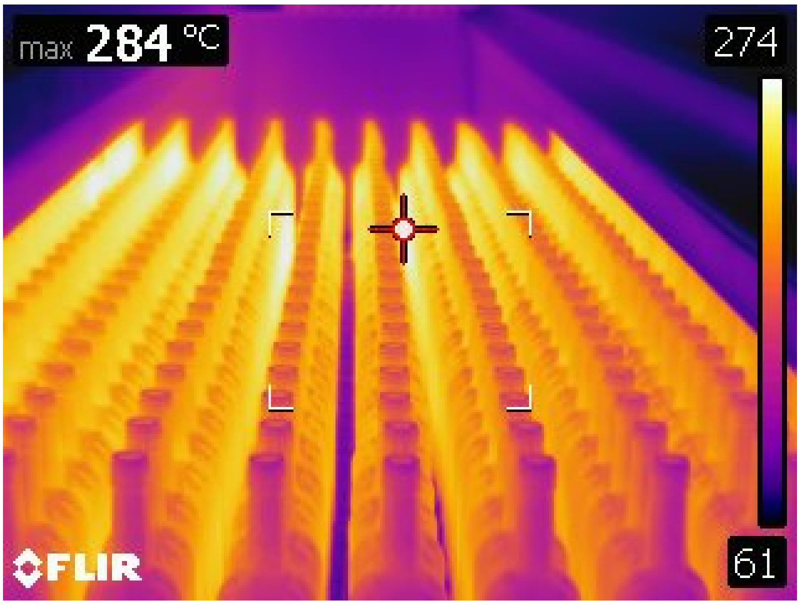

Figure A.6: Bottles leaving the annealing lehr (b).

Appendix B

Algorithm

This Appendix contains the algorithm used for the bottle temperature prediction and the UI creation. Some input data and external files were suppressed for confidentiality reasons and not all plotted graphics and auxiliary calculations are present.

```

# Importing libraries

import math as m
import pandas as pd
import numpy as np

import plotly.express as px
import plotly.io as pio
import plotly.graph_objects as go
from plotly.subplots import make_subplots
pio.templates.default = "plotly_dark"

import matplotlib.pyplot as plt
from mpl_toolkits.mplot3d import Axes3D
from matplotlib.collections import PolyCollection

from sklearn import preprocessing
from scipy.stats import linregress
from scipy.interpolate import interp1d
from scipy.integrate import solve_ivp
from scipy.optimize import curve_fit

from PyQt5.QtWidgets import QApplication, QWidget, QVBoxLayout,
    QLineEdit, QPushButton, QLabel, QHBoxLayout
from PyQt5.QtCore import Qt, QTimer
```

```
from PyQt5.QtGui import QIcon, QPixmap, QFont
from matplotlib.backends.backend_qt5agg import FigureCanvasQTAgg as
    FigureCanvas
import pyqtgraph as pg
import sys
import qdarkstyle

############### INPUT DATA ###############

' AIR '
# Input data at 500 C

density_air = 0.4565 # kg/m
velocity_air = 4 # m/s
k_air = 0.05572 # W/m. C
cp_air = 1093 # J/kg. C
viscosity_air = 3.563 * 10**-5 # kg/m.s

' GLASS '

# Defining the temperature to calculate thermal conductivity and specific
    heat
T = 500

def calculate_k_glass(T):
    k_glass = 0.7222 + 0.001583*T
    return k_glass
k_glass = calculate_k_glass(T)

def calculate_cp_glass(T, composition):
    sum_pf = 0.0
    sum_cp_i = 0.0

    for component in composition:
        component_name, percentage, f_i, cp_i = component
        sum_pf += percentage * f_i
        sum_cp_i += percentage * cp_i

    numerator = 0.00146 * T**2 * sum_pf + 2 * T * sum_pf + sum_cp_i
    denominator = (0.00146 * T + 1)**2

    cp_glass = numerator / denominator * 4187
    return cp_glass

# Composition table: (Component, pi, fi, cpi)
```

```
composition = [
    ("SiO2", 'insert the percentage', 0.000468, 0.1657),
    ("Na2O", 'insert the percentage', 0.000829, 0.2229),
    ("CaO", 'insert the percentage', 0.000410, 0.1709),
    ("Al2O3", 'insert the percentage', 0.000453, 0.1765),
    ("K2O", 'insert the percentage', 0.000445, 0.1756),
    ("MgO", 'insert the percentage', 0.000514, 0.2142),
    ("SO3", 'insert the percentage', 0.00083, 0.1890),
    ("Fe2O3", 'insert the percentage', 0.000380, 0.1449)
]

cp_glass = calculate_cp_glass(T, composition)

print(f"k: {k_glass:.2f}  W/m. C  ")
print(f"Specific heat of glass: {cp_glass:.2f} J/kg. C  ")

density_glass = 2540 # kg/m

' GLASS CONTAINER '

temperature_bottle_initial = 'insert the temperature value in  C '
bottle_weight = 0.36 # kg
d_bottle = 0.0745 # m
d_bottleneck = 0.0305 # m
r_bottle = d_bottle/2 # m
r_bottleneck = d_bottleneck/2 # m
h_bottle = 0.184 # m
h_cone = 0.044 # m
h_bottleneck = 0.073 # m
h_bottle_total = h_bottle + h_cone + h_bottleneck # m
bottle_thickness = 0.005 # m (thickness at critical point: bottom)
body_thickness = 0.003 # m
r_bottle_in = r_bottle - body_thickness # m
r_bottleneck_in = r_bottleneck - body_thickness # m
bottles_stacker_bar = 'insert the value'

' DATA - LEHR '

number_zone = 9
width_lehr = 4.35 # m
width_lehr_in = 3.6 # m
length_zone = 2.25 # m
length_lehr = length_zone*number_zone # m
height_lehr = 0.9 # m
conveyor_velocity = 'insert the value in m/s'
```

```
time_annealing = length_lehr/conveyor_velocity # s
time_zone_annealing = length_zone/conveyor_velocity # s
time_annealing_min = time_annealing/60 # min

annealing_temperature = 'insert the value in C'

lehr_pv = {
        "Entrance" : 240,
        "1a" : 'insert the temperature in  C ',
        "1b" : 'insert the temperature in  C ',
        "2" : 'insert the temperature in  C ',
        "3" : 'insert the temperature in  C ',
        "4" : 'insert the temperature in  C ',
        "5" : 'insert the temperature in  C ',
        "6" : 'insert the temperature in  C ',
        "7" : 'insert the temperature in  C ',
        "8" : 'insert the temperature in  C ',
        "9" : 'insert the temperature in  C ',
        "Exit" : 50
}

lehr_time_min = {
        "Entrance" : 0,
        "1a" : time_zone_annealing/60/3,
        "1b" : 2*time_zone_annealing/60/3,
        "2" : time_zone_annealing/60*1.5,
        "3" : time_zone_annealing/60*2.5,
        "4" : time_zone_annealing/60*3.5,
        "5" : time_zone_annealing/60*4.5,
        "6" : time_zone_annealing/60*5.5,
        "7" : time_zone_annealing/60*6.5,
        "8" : time_zone_annealing/60*7.5,
        "9" : time_zone_annealing/60*8.5,
        "Exit" : time_zone_annealing/60*9
}

' NUMBER OF BOTTLES PER ZONE '

def bottles_zone(row,column):
    n_bottles = m.ceil(row*column/(3*d_bottle/2))
    return n_bottles
n_bottles = bottles_zone(bottles_stacker_bar, length_zone)
mass_zone = n_bottles*bottle_weight

' BOTTLE VOLUME '
```

```
def volume():
    volume_cylinder_out = m.pi*r_bottle**2*h_bottle +
        m.pi*r_bottleneck**2*h_bottleneck
    volume_cylinder_in = m.pi*r_bottle_in**2*h_bottle +
        m.pi*r_bottleneck_in**2*h_bottleneck
    volume_cone_out = m.pi*h_cone*(r_bottle**2 + r_bottle*r_bottleneck +
        r_bottleneck**2)/3
    volume_cone_in = m.pi*h_cone*(r_bottle_in**2 +
        r_bottle_in*r_bottleneck_in + r_bottleneck_in**2)/3
    volume_out = volume_cylinder_out + volume_cone_out
    volume_in = volume_cylinder_in + volume_cone_in
    return volume_out, volume_in
v_out, v_in = volume()
volume_bottle = v_out - v_in

' BOTTLE SURFACE AREA'

def area():
    area_cylinder = 2*m.pi*r_bottle*h_bottle +
        2*m.pi*r_bottleneck*h_bottle
    area_cone = m.pi*(r_bottle + r_bottleneck)*m.sqrt((h_cone + (r_bottle
        - r_bottleneck)**2))
    surface_area_bottle = area_cylinder + area_cone
    return surface_area_bottle
surface_area_bottle = area()
surface_area_zone = surface_area_bottle * n_bottles

############### SPECIFIC LENGTHS AND DIAMETERS ###############

' CHARACTERISTIC LENGTH '

def characteristic_length(volume, surface_area):
    length = volume/surface_area
    return length
Lc = characteristic_length(volume_bottle, surface_area_bottle)

' EQUIVALENT DIAMETER '

def equivalent_diameter(length, width):
    de = 1.30*(length*width)**0.625/(length + width)**0.25
    return de
de = equivalent_diameter(height_lehr, length_lehr)

' HYDRAULIC DIAMETER '
```

```python

def hydraulic_diameter(a,b):
    # 4*cross-sectional area of the flow / wetted perimeter of the
        cross-section
    re = 4*(a*b)/(2*(a+b))
    return re
dh = hydraulic_diameter(height_lehr, length_lehr)

############### DIMENSIONLESS NUMBERS ###############

' REYNOLDS NUMBER '

def reynolds(density, velocity, characteristic_dimension, viscosity):
    re = density*velocity*characteristic_dimension/viscosity
    return re
re_rectangular_duct = reynolds(density_air, velocity_air, dh,
    viscosity_air)
re = re_rectangular_duct

if re >= 10**4:
    print((f'Reynolds = {re:.0f}, turbulent flow (Re > 10^4)'))
else:
    print((f'Reynolds = {re:.0f}, laminar flow (Re < 10^4)'))

' PRANDTL NUMBER '

def prandtl(viscosity, heat_capacity, conductivity):
    pr = viscosity*heat_capacity/conductivity
    return pr
pr = prandtl(viscosity_air, cp_air, k_air)

' NUSSELT NUMBER '

def nusselt(n):
    nu = 0.023*re**0.8*pr**n
    return nu
nu = nusselt(0.4)

def convection_coefficient(nu,k,L,D):
    h_inf = nu*k/L
    L_D = L/D
    if L/D < 20:
        h = (1 + (D/L)**0.7)*h_inf
    else:
        h = (1 + 6*D/L)*h_inf
```

```
    return (h_inf, h, L_D)
h_inf, h, L_D = convection_coefficient(nu,k_air,width_lehr_in/2,dh)

' BIOT NUMBER '
    # validation of an analytical analysis if Bi < 1 --> nearly uniform
        temperature fields inside the body

def biot_number(h,L,k):
    bi = h*L/k
    return bi
biot = biot_number(h, Lc, k_glass)

'conservative fashion, Lc should be associated with the length scale
    corresponding to the maximum spatial temperature difference'
biot_2 = biot_number(h, bottle_thickness, k_glass)
biot = biot_2

if biot <= 0.1:
    print(f'Bi = {biot:.3f} < 0.1, lumped capacitance method can be used')
else:
    print(f'Bi = {biot:.3f} > 0.1')

############### TRANSIENT CONDUCTION ###############

' THERMAL DIFFUSIVITY '

def thermal_diffusivity(thermal_conductivity, density, heat_capacity):
    alpha = thermal_conductivity/(density*heat_capacity)
    return alpha
alpha = thermal_diffusivity(k_glass, density_glass, cp_glass)

' FOURIER NUMBER '

def fourier(thermal_diffusivity, time, characteristic_length):
    fo = thermal_diffusivity*time/(characteristic_length)**2
    return fo

' LUMPED CAPACITANCE METHOD - CONVECTION '

def lumped_system(heat_transfer_coefficient, surface_area, time, mass,
    specific_heat, temperature_initial, temperature_inf):
    expo = m.exp(-heat_transfer_coefficient * surface_area * time / (mass
        * specific_heat))
    temperature_bottle = expo * (temperature_initial - temperature_inf) +
        temperature_inf
```

```
    return temperature_bottle

' ONE-DIMENSIONAL CONDUCTION - PLANE WALL '

def conduction_plane_wall(c, zeta, fourier, x, L, temperature_initial,
    temperature_inf):
    x_x = x/(L)
    temperature_bottle =
        c*m.exp(-zeta**2*fourier)*m.cos(zeta*x_x)*(temperature_initial -
        temperature_inf) + temperature_inf
    return temperature_bottle

############## PREDICTING AIR TEMPERATURE ##############

' DEFINING N NUMBER OF ITERATIONS '

# Creating a list of predicted temperature for n time points

def iteration_number():
    n = 1
    time_step_fourier = time_annealing/n
    fo = fourier(alpha, time_step_fourier, bottle_thickness)
    while fo >= 0.2:
        n += 1
        time_step_fourier = time_annealing/n
        fo = fourier(alpha, time_step_fourier, bottle_thickness)
    return n
n = iteration_number()

print(n)

' LINEAR INTERPOLATION '

# Creating lists for x axis (time in minutes) and y axis (temperature) of
    lehr data
lehr_time_list = [lehr_time_min['Entrance'], lehr_time_min['1a'],
    lehr_time_min['1b'], lehr_time_min['2'], lehr_time_min['3'],
    lehr_time_min['4'], lehr_time_min['5'], lehr_time_min['6'],
    lehr_time_min['7'], lehr_time_min['8'], lehr_time_min['9'],
    lehr_time_min['Exit']]
lehr_pv_list = [lehr_pv['Entrance'], lehr_pv['1a'], lehr_pv['1b'],
    lehr_pv['2'], lehr_pv['3'], lehr_pv['4'], lehr_pv['5'], lehr_pv['6'],
    lehr_pv['7'], lehr_pv['8'], lehr_pv['9'], lehr_pv['Exit']]

def interpola(times, temperatures, new_times):
```

```
    return np.interp(new_times, times, temperatures)

times = lehr_time_list
temperatures = lehr_pv_list

def defining_new_time_list(number):
    time_step_s = time_annealing/number
    time_step_min = time_annealing_min/number
    time_lehr_min_list = []
    for i in range(number + 1):
        x = time_step_min*i
        time_lehr_min_list.append(time_step_min*i)
    return time_step_s, time_lehr_min_list
# This function returns the time step of 'n' chosen iterations and a list
    of the linear interpolation results
# This time step must be the same for the following iterations

######### CURVE FITTING - POLYNOMIAL TRENDLINE #########

' LEAST-SQUARE METHOD '

lehr_temp_list = list(lehr_pv.values())
lehr_time_list = []
time_start = 0
time_zone = length_zone/conveyor_velocity

for i in range(len(lehr_temp_list)):
    lehr_time_list.append(time_start)
    time_start += time_zone

x = np.array(lehr_time_list)
y = np.array(list_temp_list)

# Choosing the polynomial degree
degree = 6

# Coefficients of the polynomial trendline and the equation
coefficients = np.polyfit(x, y, degree)
trendline_equation = np.poly1d(coefficients)

# Evaluating the trendline
y_pred = np.polyval(coefficients, x)
r_squared = 1 - (np.sum((y - y_pred) ** 2) / ((len(y) - 1) * np.var(y,
    ddof=1)))
print("R-squared:", r_squared)
```

```
def curve_fit_lehr(number):
    time_step = time_annealing/number
    lehr_curve_fit_list = []
    time = 0
    for i in range(number):
        y = trendline_equation(time)
        lehr_curve_fit_list.append(y)
        time += time_step
    return lehr_curve_fit_list

lehr_curve_fit_list = curve_fit_lehr(n)

' CHOOSING THE NUMBER OF ITERATIONS '

n = 60
time_step, time_lehr_min_list = defining_new_time_list(n)
new_times = time_lehr_min_list

' PREDICTING AIR TEMPERATURE INSIDE LEHR '

T_lehr_interpolation_list = interpola(times, temperatures, new_times)
predicted_lehr_T_list = [time_lehr_min_list, T_lehr_interpolation_list]
df_predicted_lehr_T_list =
    pd.DataFrame(predicted_lehr_T_list).transpose().rename(columns={0:
    'Time (min)', 1: 'Lehr Temperature ( C )'})
#print(df_predicted_lehr_T_list)

############### PREDICTING BOTTLE TEMPERATURE ###############

' PREDICTING BOTTLE TEMPERATURE WITH CONVECTIVE HEAT TRANSFER '

# Creating a list of predicted temperature for the bottle for the
    previous n time points
temperature_bottle_initial_convection = temperature_bottle_initial
T_bottle_convec_list = [temperature_bottle_initial_convection]

for temperature_lehr in T_lehr_interpolation_list:
        temperature_t = lumped_system(h, surface_area_bottle, time_step,
            bottle_weight, cp_glass,
            temperature_bottle_initial_convection, temperature_lehr)
        temperature_bottle_initial_convection = temperature_t
        T_bottle_convec_list.append(temperature_t)
```

```
' PREDICTING BOTTLE TEMPERATURE WITH CONDUCTIVE HEAT TRANSFER - PLANE
    WALL '

# Reading the xlsx file with the coefficients
one_term_coefficients = pd.read_excel('insert the xlsx file with the list
    of one term coefficients here')

def approximate_solution_coef():
    for i in range(len(one_term_coefficients)):
        if one_term_coefficients.loc[i, 'Biot'] >= biot:
            biot_next = one_term_coefficients.loc[i, 'Biot']
            biot_before = one_term_coefficients.loc[i - 1, 'Biot']
            c1_next = one_term_coefficients.loc[i, 'Wall - C1']
            c1_before = one_term_coefficients.loc[i - 1, 'Wall - C1']
            zeta1_next = one_term_coefficients.loc[i, 'Wall - Zeta1']
            zeta1_before = one_term_coefficients.loc[i - 1, 'Wall - Zeta1']
            break
    c1 = c1_before + (biot - biot_before)*(c1_next - c1_before /
        biot_next - biot_before)
    zeta1 = zeta1_before + (biot - biot_before)*(zeta1_next -
        zeta1_before / zeta1_next - zeta1_before)
    return c1, zeta1
c1, zeta1 = approximate_solution_coef()

# Creating a list of predicted temperature for the bottle for the
    previous n time points
temperature_bottle_initial_conduction = temperature_bottle_initial
T_bottle_cond_list = [temperature_bottle_initial]

for temperature_lehr in T_lehr_interpolation_list:
        temperature_t = conduction_plane_wall(c1, zeta1, fourier(alpha,
            time_step, bottle_thickness), h_bottle_total,
            bottle_thickness, temperature_bottle_initial_conduction,
            temperature_lehr)
        temperature_bottle_initial_conduction = temperature_t
        T_bottle_cond_list.append(temperature_t)

T_bottle_convec_list = T_bottle_convec_list[:len(time_lehr_min_list)]
T_bottle_conduc_list = T_bottle_convec_list[:len(time_lehr_min_list)]

' REQUESTED TIME FOR ANNEALING '

def time(thickness):
    t1 = 28*thickness*100 - 3 # thickness in cm
```

```
    'this formula considers 5 degrees above the upper annealing point - Corning Method'
    return t1
annealing_time = time(bottle_thickness)
print('Requested time for annealing = {:.2f} minutes'.format(annealing_time))

' PREDICTING THE RELAXATION TIME - TIME ABOVE THE UPPER ANNEALING POINT '

def time_above_temperature(temperature_list, threshold_temperature, time):

    time_above_threshold = 0
    for temperature in temperature_list:
        if temperature >= threshold_temperature:
            time_above_threshold += time
    return time_above_threshold

############### CALCULATING HEAT LOSS ###############

' HEAT LOSSES - WALL '

length_wall = time_step * conveyor_velocity
surface_area_wall = height_lehr*length_wall

h_out = 7 # W/m^2.K
wall_thickness = 0.4 # m
temperature_air = 25 #  C
k_wall = 18 # W/m.K

def thermal_conductivity_resistance(thickness, conductivity, wall_area):
    ohm = thickness/(conductivity*wall_area)
    return ohm
ohm = thermal_conductivity_resistance(wall_thickness, k_wall, surface_area_wall)

heat_loss_list = []
def heat_loss (temperature_hot_side, temperature_air_outside, surface_area, heat_transfer_coefficient_hot_side, heat_transfer_coefficient_cold_side, resistance_thermal_conductivity):
    q = (temperature_hot_side - temperature_air_outside) / (1 / (surface_area * heat_transfer_coefficient_hot_side) + 1 / (surface_area * heat_transfer_coefficient_cold_side) + resistance_thermal_conductivity)
    return (q)

```

```
heat_loss_total = 0
for temperature_lehr in T_lehr_interpolation_list:
        heat_loss_n = 2*heat_loss(temperature_lehr, temperature_air,
            surface_area_wall, h, h_out, ohm)
        heat_loss_total += heat_loss_n
        heat_loss_list.append(heat_loss_n)
        # This will return a value in W
print(f'Total heat loss = {heat_loss_total/1000:.2f} kW')

############## INTERFACE ##############

class MyWidget(QWidget):
    def __init__(self):
        super().__init__()

        self.setWindowTitle("Annealing Lehr")

        self.layout = QVBoxLayout(self)

        self.figure, self.ax = plt.subplots()
        self.plot = FigureCanvas(self.figure)

        # Logo and title
        logo_label = QLabel(self)
        pixmap = QPixmap('ba.png')
        logo_label.setPixmap(pixmap.scaled(80, 80, Qt.KeepAspectRatio))

        title_label = QLabel("Annealing Lehr", self)
        title_label.setFont(QFont('Arial', 20))

        top_layout = QHBoxLayout()
        top_layout.addWidget(logo_label)
        top_layout.addWidget(title_label)

        self.layout.addLayout(top_layout)


        # Input setup
        self.input_fields = []
        row_layouts = [QHBoxLayout(), QHBoxLayout()]  # QVBox for
            vertical display

        for i in range(1, 10):
            if i == 1:
                label_a = QLabel(f'1a')
```

```
                input_field_a = QLineEdit(self)
                input_field_a.setStyleSheet("QLineEdit { padding: 6px; border-radius: 5px; }")
                self.input_fields.append(input_field_a)

                label_b = QLabel(f'1b')
                input_field_b = QLineEdit(self)
                input_field_b.setStyleSheet("QLineEdit { padding: 6px; border-radius: 5px; }")
                self.input_fields.append(input_field_b)

                row_layouts[0].addWidget(label_a)
                row_layouts[0].addWidget(input_field_a)
                row_layouts[0].addWidget(label_b)
                row_layouts[0].addWidget(input_field_b)
            else:
                label = QLabel(f'{i}')
                input_field = QLineEdit(self)
                input_field.setStyleSheet("QLineEdit { padding: 6px; border-radius: 5px; }")
                self.input_fields.append(input_field)

                # Separating the display in two rows
                if i <= 5:
                    row_layouts[0].addWidget(label)
                    row_layouts[0].addWidget(input_field)
                else:
                    row_layouts[1].addWidget(label)
                    row_layouts[1].addWidget(input_field)

        for row_layout in row_layouts:
            self.layout.addLayout(row_layout)

        # Conveyor belt velocity input
        self.conveyor_velocity_input = QLineEdit(self)
        self.conveyor_velocity_input.setStyleSheet("QLineEdit { padding: 6px; border-radius: 5px; }")
        self.layout.addWidget(QLabel("Conveyor Velocity (m/min)"))
        self.layout.addWidget(self.conveyor_velocity_input)

        # Temperature input
        self.label = QLabel("Thickness (mm):", self)
        self.label.setStyleSheet("QLabel { font-weight: bold; }")
        self.layout.addWidget(self.label)

```

```python
        # Creating a line edit
        self.temperature_input = QLineEdit(self)
        self.temperature_input.setStyleSheet("QLineEdit { padding: 6px; border-radius: 5px; }")
        self.layout.addWidget(self.temperature_input)


        # Result Label text
        self.result_label = QLabel(self)
        self.layout.addWidget(self.result_label)

        # Setup button and plot to generate graph
        self.button = QPushButton('Calculate')
        self.button.setObjectName('Calculate')
        self.button.setFont(QFont('Arial', 15))
        self.button.setStyleSheet("QPushButton { padding: 10px; border-radius: 5px; } QPushButton:hover { background-color: #008CBA; }")
        self.button.clicked.connect(self.on_button_click)
        self.layout.addWidget(self.button)

        # Updating the result label
        self.button = self.findChild(QPushButton, 'Calculate')
        # Connect the button's clicked signal to the update_label slot
        self.button.clicked.connect(self.update_label)

        self.graphWidget = pg.PlotWidget()
        self.layout.addWidget(self.graphWidget)

        self.p1 = self.graphWidget.plotItem
        self.p2 = pg.ViewBox()
        self.p1.showAxis('right')
        self.p1.scene().addItem(self.p2)
        self.p1.getAxis('right').linkToView(self.p2)
        self.p2.setXLink(self.p1)
        self.p1.getAxis('right').setLabel('second y-axis',
            color='#ADD8E6')

        self.p1.scene().sigMouseMoved.connect(self.mouseMoved)

    def on_button_click(self):
        conveyor_velocity_new = float(self.conveyor_velocity_input.text())

        lehr_pv = {'Entrance': 240}
        keys = ['1a', '1b', '2', '3', '4', '5', '6', '7', '8', '9']
```

```python
        for key, input_field in zip(keys, self.input_fields):
            lehr_pv[key] = float(input_field.text())
        lehr_pv['Exit'] = 50

        lehr_time_list = list(lehr_time_min.values())
        lehr_pv_list = list(lehr_pv.values())

        # Time_step e new_times inside the method
        time_annealing_min = length_lehr / conveyor_velocity_new
        time_step_min = time_step/60
        new_times = np.arange(0, time_annealing_min, time_step_min)

        # Updatin T_lehr_interpolation_list
        T_lehr_interpolation_list = interpola(lehr_time_list,
            lehr_pv_list, new_times)

        # Updatin T_bottle_convec_list
        temperature_bottle_initial_convection = temperature_bottle_initial
        T_bottle_convec_list = [temperature_bottle_initial_convection]

        for temperature_lehr in T_lehr_interpolation_list:
            temperature_t = lumped_system(h, surface_area_bottle,
                time_step, bottle_weight, cp_glass,
                temperature_bottle_initial_convection, temperature_lehr)
            temperature_bottle_initial_convection = temperature_t
            T_bottle_convec_list.append(temperature_t)
        T_bottle_convec_list = T_bottle_convec_list[:len(new_times)]

        self.p1.clear()
        self.p2.clear()

        # Plotting with new data
        self.p1.plot(new_times, T_lehr_interpolation_list, pen='r')  # red
        self.p2.addItem(pg.PlotCurveItem(new_times, T_bottle_convec_list,
            pen='c'))  # cyan

        self.p1.setLabel('bottom', 'Time', units='min')
        self.p1.setLabel('left', 'Lehr Temperature', units=' C ')
        self.p1.getAxis('right').setLabel('Bottle Temperature',
            units=' C ')

        self.p1.enableAutoRange('xy', False)
        self.p2.enableAutoRange('xy', False)

    def update_label(self):
```

```
        thickness = float(self.temperature_input.text())
        annealing_time = 28*thickness/10 - 3
        time_above_annealing = 0
        for i in T_bottle_convec_list:
            if i >= annealing_temperature:
                time_above_annealing += time_step/60
        self.result_label.setText(str(annealing_time) + 'minutes' + 
            str(time_above_annealing) + 'minutes')
        self.result_label.setText("Requested annealing time = {:.2f} 
            minutes, Time above annealing point {:.2f} 
            minutes".format(annealing_time, time_above_annealing))

    def mouseMoved(self, evt):
        pos = evt
        if self.p1.sceneBoundingRect().contains(pos):
            mousePoint = self.p1.vb.mapSceneToView(pos)
            self.p1.setTitle("Plot 1 --- Date=%0.1f,   Value=%0.1f" % 
                (mousePoint.x(), mousePoint.y()))
            self.updateViews()

    def updateViews(self):
        self.p2.setGeometry(self.p1.vb.sceneBoundingRect())
        self.p2.linkedViewChanged(self.p1.vb, self.p2.XAxis)

def main():
    app = QApplication(sys.argv)

    # Window icon
    app.setWindowIcon(QIcon('ba.png'))

    # Currently in dark style, comment the line below to default one
    app.setStyleSheet(qdarkstyle.load_stylesheet_pyqt5())

    main_win = MyWidget()
    main_win.show()

    sys.exit(app.exec_())


if __name__ == '__main__':
    main()

############ CREATING A 3D GRAPH FOR THE EXPERIMENTAL DATA ############

# Creating a dataframe with each column of the csv file
```

```
lehr_dataframe = pd.read_csv('insert the csv file for the experimental
    dataset')

time = lehr_dataframe['Time (min)']
y_values = [1, 2, 3, 4]
Temperature = lehr_dataframe[['Center left', 'Center', 'Center right',
    'Right']].values.T

Time, Serie = np.meshgrid(time, y_values)

# Create a 3D figure
fig = plt.figure()
ax = fig.add_subplot(111, projection="3d")

# Plot the 3D surface
ax.plot_surface(Time, Serie, Temperature, color='cyan', alpha=0.5)

# Set axis labels
ax.set_xlabel("Time (min)")
ax.set_ylabel("Series")
ax.set_zlabel("Temperature ( C )")

# Show the plot
plt.show()

########## ANNEALING VALIDATION WITH THE EXPERIMENTAL DATA ##########

time_x = lehr_dataframe['Time (min)']
y1 = lehr_dataframe['Left']
y2 = lehr_dataframe['Center left']
y3 = lehr_dataframe['Center']
y4 = lehr_dataframe['Center right']
y5 = lehr_dataframe['Right']

# Choosing the thermocouple to be the y axis
temperature_lehr_sensor = y3

# Setting the time step in s
time_step_sensor = 2

# Creating a list of predicted temperature for the bottle for the
    previous n time points
temperature_sensor_initial = temperature_bottle_initial
T_bottle_sensor = []

```

```python
for temp_lehr in temperature_lehr_sensor:
        temperature_t = lumped_system(h, surface_area_bottle, time_step_sensor, bottle_weight, cp_glass, temperature_sensor_initial, temp_lehr)
        temperature_sensor_initial = temperature_t
        T_bottle_sensor.append(temperature_t)


# Test this for each thermocouple measurement
time_above_annealing_sensor = time_above_temperature(temperature_lehr_sensor, annealing_temperature, time_step_sensor/60)
time_above_annealing_bottle_sensor = time_above_temperature(T_bottle_sensor, annealing_temperature, time_step_sensor/60)

print('The lehr temperature stays above {} C  for {:.2f} minutes'.format(annealing_temperature, time_above_annealing_sensor))
print('The bottle temperature stays above {} C  for {:.2f} minutes'.format(annealing_temperature, time_above_annealing_bottle_sensor))

' CREATING GRAPHS AND DRAWING THE ANNEALING POINT LINE '

## Lumped Heat Capacitance ##
convection_heat_list = [T_lehr_interpolation_list, T_bottle_convec_list, time_lehr_min_list]
df_convection_heat_list = pd.DataFrame(convection_heat_list).transpose().rename(columns={0: 'Lehr', 1: 'Bottle', 2: 'Time (min)'})
convection_graph = px.line(
        df_convection_heat_list,
        x = "Time (min)",
        y = ["Bottle", 'Lehr'],
        labels = {"value" : "Temperature ( C )", "variable" : "Temperature ( C )"},
        title = 'Model 1 - PV Temperature x Bottle Temperature',
        color_discrete_map={"Bottle": "blue", "Lehr": "red"})
convection_graph.add_shape(type = 'line', x0 = time_lehr_min_list[0], y0 = annealing_temperature, x1 = time_lehr_min_list[-1], y1 = annealing_temperature,
                              line = dict(color = 'orange', width = 2, dash = 'dash'))
convection_graph.update_layout(plot_bgcolor="white")
```

```
convection_graph.update_yaxes(showgrid=False, tickfont_color='black',
    title_font_color='black')
convection_graph.update_yaxes(showline=True, linewidth=1,
    linecolor='black')
convection_graph.update_xaxes(showgrid=False, tickfont_color='black',
    title_font_color='black')
convection_graph.update_xaxes(showline=True, linewidth=1,
    linecolor='black')
convection_graph.update_layout(paper_bgcolor="white",
    title_font_color='black', title_font={'color': 'black'})
convection_graph.update_layout(legend=dict(font=dict(color='black')))
convection_graph.update_layout(margin=dict(l=50, r=50, b=50, t=50),
    height=500)
convection_graph.update_layout(width=1000)
convection_graph.update_xaxes(
    tickfont=dict(size=18),  # Change the size of the x-axis labels
    title_font=dict(size=22)  # Change the size of the x-axis title
)
convection_graph.update_yaxes(
    tickfont=dict(size=18),  # Change the size of the x-axis labels
    title_font=dict(size=22)  # Change the size of the x-axis title
)
convection_graph.update_layout(
    legend=dict(
        font=dict(size=18)  # Change the size of the legend variable
            labels
    )
)
convection_graph.update_layout(
    title_font=dict(size=22)  # Change the size of the graph title
)
convection_graph.show()

## One-term Approximate Solution ##
conduction_heat_list = [T_lehr_interpolation_list, T_bottle_cond_list,
    time_lehr_min_list]
df_conduction_heat_list =
    pd.DataFrame(conduction_heat_list).transpose().rename(columns={0:
    'Lehr', 1: 'Bottle', 2: 'Time (min)'})
conduction_plane_wall_graph = px.line(
    df_conduction_heat_list,
    x = "Time (min)",
    y = ["Bottle", 'Lehr'],
    labels = {"value" : "Temperature ( C )", "variable" : "Temperature
        ( C )"},
```

```
    title = 'Model 2 - PV Temperature x Bottle Temperature',
    color_discrete_map={"Lehr": 'red', "Bottle": "blue"})
conduction_plane_wall_graph.add_shape(type = 'line', x0 =
    time_lehr_min_list[0], y0 = annealing_temperature, x1 =
    time_lehr_min_list[-1], y1 = annealing_temperature,
                              line = dict(color = 'orange', width = 2, dash
                                  = 'dash'))
conduction_plane_wall_graph.update_layout(plot_bgcolor="white")
conduction_plane_wall_graph.update_yaxes(showgrid=False,
    tickfont_color='black', title_font_color='black')
conduction_plane_wall_graph.update_yaxes(showline=True, linewidth=1,
    linecolor='black')
conduction_plane_wall_graph.update_xaxes(showgrid=False,
    tickfont_color='black', title_font_color='black')
conduction_plane_wall_graph.update_xaxes(showline=True, linewidth=1,
    linecolor='black')
conduction_plane_wall_graph.update_layout(paper_bgcolor="white",
    title_font_color='black', title_font={'color': 'black'})
conduction_plane_wall_graph.update_layout(legend=dict(font=dict(color='black')))
conduction_plane_wall_graph.update_layout(margin=dict(l=50, r=50, b=50,
    t=50), height=500)
conduction_plane_wall_graph.update_layout(width=1000)
conduction_plane_wall_graph.update_xaxes(
    tickfont=dict(size=18),  # Change the size of the x-axis labels
    title_font=dict(size=22)  # Change the size of the x-axis title
)
conduction_plane_wall_graph.update_yaxes(
    tickfont=dict(size=18),  # Change the size of the x-axis labels
    title_font=dict(size=22)  # Change the size of the x-axis title
)
conduction_plane_wall_graph.update_layout(
    legend=dict(
        font=dict(size=18)  # Change the size of the legend variable
            labels
    )
)
conduction_plane_wall_graph.update_layout(
    title_font=dict(size=22)  # Change the size of the graph title
)
conduction_plane_wall_graph.show()

## Linear Interpolation ##
linear_interpolation_real_data_list = [T_lehr_interpolation_list_graph,
    temperature_lehr_sensor, time_x]
df_linear_interpolation_real_data_list =
```

```
pd.DataFrame(linear_interpolation_real_data_list).transpose().rename
(columns={0: 'Present Value Linear Interpolation', 1: 'Central Measurement', 2: 'Time (min)'})
df_linear_interpolation_real_data_graph = px.line(df_linear_interpolation_real_data_list,
                                                  x="Time (min)",
                                                  y=["Central Measurement", 'Present Value Linear Interpolation'],
                                                  labels={"value": "Temperature ( C )", "variable": "Temperature ( C )"},
                                                  title='Comparison between Experimental Data and Predicted Air Temperature - Linear Interpolation',
                                                  color_discrete_map={"Central Measurement": 'darkorchid', "Present Value Linear Interpolation": "red"})
df_linear_interpolation_real_data_graph.add_shape(type='line', x0=time_lehr_min_list[0], y0=annealing_temperature, x1=time_lehr_min_list[-1],
                         y1=annealing_temperature,
                         line=dict(color='orange', width=2, dash='dash'))
df_linear_interpolation_real_data_graph.update_layout(plot_bgcolor="white")
df_linear_interpolation_real_data_graph.update_yaxes(showgrid=False, tickfont_color='black', title_font_color='black')
df_linear_interpolation_real_data_graph.update_yaxes(showline=True, linewidth=1, linecolor='black')
df_linear_interpolation_real_data_graph.update_xaxes(showgrid=False, tickfont_color='black', title_font_color='black')
df_linear_interpolation_real_data_graph.update_xaxes(showline=True, linewidth=1, linecolor='black')
df_linear_interpolation_real_data_graph.update_layout(paper_bgcolor="white", title_font_color='black', title_font={'color': 'black'})
df_linear_interpolation_real_data_graph.update_layout(legend=dict
(font=dict(color='black')))
df_linear_interpolation_real_data_graph.update_layout(margin=dict(l=50, r=50, b=50, t=50), height=500)  # Adjust the margin and height as needed
df_linear_interpolation_real_data_graph.update_layout(width=1000)
df_linear_interpolation_real_data_graph.update_xaxes(
    tickfont=dict(size=16),  # Change the size of the x-axis labels
```

```
    title_font=dict(size=20)  # Change the size of the x-axis title
)
df_linear_interpolation_real_data_graph.update_yaxes(
    tickfont=dict(size=16),  # Change the size of the y-axis labels
    title_font=dict(size=20)  # Change the size of the y-axis title
)
df_linear_interpolation_real_data_graph.update_layout(
    legend=dict(
        font=dict(size=16)  # Change the size of the legend variable labels
    )
)
df_linear_interpolation_real_data_graph.update_layout(
    title_font=dict(size=18)  # Change the size of the graph title
)
df_linear_interpolation_real_data_graph.show()

## Curve Fit ##
curve_fit_real_data_list = [lehr_curve_fit_list, temperature_lehr_sensor, time_x]
df_curve_fit_real_data_list = pd.DataFrame(curve_fit_real_data_list).transpose().rename(columns=
{0: 'Present Value Curve Fit', 1: 'Central Measurement', 2: 'Time (min)'})
df_curve_fit_real_data_graph = px.line(df_curve_fit_real_data_list,
                                        x="Time (min)",
                                        y=["Central Measurement", 'Present Value Curve Fit'],
                                        labels={"value": "Temperature ( C )", "variable": "Temperature ( C )"},
                                        title='Comparison between Experimental Data and Predicted Air Temperature - Curve Fit',
                                        color_discrete_map={"Central Measurement": 'darkorchid', "Present Value Curve Fit": "red"})
df_curve_fit_real_data_graph.add_shape(type='line', x0=time_lehr_min_list[0], y0=annealing_temperature, x1=time_lehr_min_list[-1],
                y1=annealing_temperature,
                line=dict(color='orange', width=2, dash='dash'))
df_curve_fit_real_data_graph.update_layout(plot_bgcolor="white")
```

```
df_curve_fit_real_data_graph.update_yaxes(showgrid=False, tickfont_color='black', title_font_color='black')
df_curve_fit_real_data_graph.update_yaxes(showline=True, linewidth=1, linecolor='black')
df_curve_fit_real_data_graph.update_xaxes(showgrid=False, tickfont_color='black', title_font_color='black')
df_curve_fit_real_data_graph.update_xaxes(showline=True, linewidth=1, linecolor='black')
df_curve_fit_real_data_graph.update_layout(paper_bgcolor="white", title_font_color='black', title_font={'color': 'black'})
df_curve_fit_real_data_graph.update_layout(legend=dict
(font=dict(color='black')))
df_curve_fit_real_data_graph.update_layout(margin=dict(l=50, r=50, b=50, t=50), height=500)  # Adjust the margin and height as needed
df_curve_fit_real_data_graph.update_layout(width=1000)
df_curve_fit_real_data_graph.update_xaxes(
    tickfont=dict(size=16),  # Change the size of the x-axis labels
    title_font=dict(size=20)  # Change the size of the x-axis title
)
df_curve_fit_real_data_graph.update_yaxes(
    tickfont=dict(size=16),  # Change the size of the y-axis labels
    title_font=dict(size=20)  # Change the size of the y-axis title
)
df_curve_fit_real_data_graph.update_layout(
    legend=dict(
        font=dict(size=16)  # Change the size of the legend variable labels
    )
)
df_curve_fit_real_data_graph.update_layout(
    title_font=dict(size=18)  # Change the size of the graph title
)
df_curve_fit_real_data_graph.show()
```